Physikalisch Technische Bundesanstalt

CERN LIBRARIES, GENEVA
SCAN-9503183

SW9512

B. Wiegel, A. V. Alevra and B. R. L. Siebert

Calculations of the Response Functions of Bonner Spheres with a Spherical ^{3}He Proportional Counter Using a Realistic Detector Model

PTB-N-21
Braunschweig, November 1994

ISSN 0936-0492
ISBN 3-89429-563-5

Physikalisch-Technische Bundesanstalt

Neutronenphysik

PTB-Bericht N-21

Calculations of the Response Functions of Bonner Spheres with a Spherical ^{3}He Proportional Counter Using a Realistic Detector Model

by

B. Wiegel, A. V. Alevra and B. R. L. Siebert

PTB-N-21
Braunschweig, November 1994

ISSN 0936-0492
ISBN 3-89429-563-5

Calculations of the Response Functions of Bonner Spheres with a Spherical ^{3}He Proportional Counter Using a Realistic Detector Model

B. Wiegel, A.V. Alevra and B.R.L. Siebert

Physikalisch-Technische Bundesanstalt
Bundesallee 100
D-38116 Braunschweig

Abstract

A realistic geometry model of a Bonner sphere system with a spherical ^{3}He-filled proportional counter and 12 polyethylene moderating spheres with diameters ranging from 7,62 cm (3") to 45,72 cm (18") is introduced. The MCNP Monte Carlo computer code is used to calculate the responses of this Bonner sphere system to monoenergetic neutrons in the energy range between 1 meV to 20 MeV. The relative uncertainties of the responses due to the Monte Carlo calculations are less than 1 % for spheres up to 30,48 cm (12") in diameter and less than 2 % for the 15" and 18" spheres. Resonances in the carbon cross section are seen as significant structures in the response functions. Additional calculations were made to study the influence of the ^{3}He number density and the polyethylene mass density on the response as well as the angular dependence of the Bonner sphere system. The calculated responses can be adjusted to a large set of calibration measurements with only a single fit factor common to all sphere diameters and energies.

Zusammenfassung

Es wird ein realistisches Geometriemodell vorgestellt für ein Bonnerkugel-System, bestehend aus einem kugelförmigen ^{3}He-Proportionalzähler und 12 Moderatorkugeln aus Polyäthylen mit Durchmessern von 7,62 cm (3") bis 45,72 cm (18"). Mit Hilfe des Monte-Carlo-Programms MCNP werden die Ansprechfunktionen dieses Bonnerkugel-Systems für monoenergetische Neutronen im Energiebereich von 1 meV bis 20 MeV berechnet. Die relativen Unsicherheiten der Monte-Carlo-Rechnungen sind kleiner als 1 % für Kugeln mit einem Durchmesser bis 30,48 cm (12") und kleiner als 2 % für die 15"- und 18"-Kugeln. Resonanzen im Wirkungsquerschnitt von Kohlenstoff zeigen sich als signifikante Strukturen in den Ansprechfunktionen. Desweiteren wird rechnerisch der Einfluß der ^{3}He-Anzahldichte, der Polyäthylen-Massendichte auf die Ansprechfunktion und die Winkelabhängigkeit des Systems untersucht. Die gerechneten Ansprechfunktionen benötigen für die Anpassung an einen umfangreichen Satz von Kalibriermessungen nur einen einzigen Anpassungsfaktor für alle Kugeldurchmesser und Energien.

Die Serien der PTB-Berichte:

Atomphysik	PTB-APh
Dosimetrie	PTB-Dos
Elektrizität	PTB-E
Elektronische Entwicklung	PTB-EW
Fertigungsmeßtechnik	PTB-F
Informationstechnik	PTB-IT
Literaturzusammenstellungen und Veröffentlichungshinweise	PTB-L
Mechanik und Akustik	PTB-MA
Medizinische Meßtechnik	PTB-MM
Neutronenphysik	PTB-N
Internationale Organisation für Gesetzliches Meßwesen	PTB-OIML
Optik	PTB-Opt
Physikalische Grundlagen	PTB-PG
Radioaktivität	PTB-Ra
Technisch-Wissenschaftliche Dienste	PTB-TWD
Thermodynamik	PTB-W

Ausgelaufene Serien:

Akustik	(bis 1985)	PTB-Ak
Forschungs- und Meßreaktor Braunschweig	(bis 1988)	PTB-FMRB
Institut Berlin	(bis 1985)	PTB-IB
Mechanik	(bis 1985)	PTB-Me
Neutronendosimetrie	(bis 1988)	PTB-ND
Sicherstellung und Endlagerung radioaktiver Abfälle	(bis 1989)	PTB-SE

Herausgeber: Physikalisch-Technische Bundesanstalt, Braunschweig und Berlin
Referat Schrifttum, Telefon: (0531) 592-93 12

Bundesallee 100
D-38116 Braunschweig
Telefon: (0531) 592-0
Telefax: (0531) 592-92 92
Teletex: 5 31 82 09 PTB
Telex: 95 28 22 ptd d

Vertrieb:
Wirtschaftsverlag NW
Verlag für neue Wissenschaften GmbH
Am Alten Hafen 113-115
D-27568 Bremerhaven
Telefon: (0471) 460 93-95
Telefax: (0471) 427 65

Contents

List of Figures

List of Tables

1 Introduction

More than three decades have passed since the introduction of Bonner spheres [1] as a new type of neutron spectrometer. There are various other devices available to perform measurements of the spectral neutron fluence. However, Bonner spheres have the advantage of an almost isotropic response, and they cover practically the whole energy range of interest from thermal to a few hundred MeV, but one has to admit their poor energy resolution. A Bonner sphere spectrometer (BSS) consists of a detector most sensitive to thermal neutrons and a set of several moderating polyethylene spheres to cover the central counter. The fact that the energy dependence of the fluence response changes with the sphere diameter is used to determine neutron spectra, although the linear independence of their response functions is limited [2, 3, 4]. Uncertainties of the response enhance this limitation. It is therefore important to minimize the uncertainties of both measurements and calculations [5, 6].

The BSS dealt with in this report is the "PTB-C" set described in Reference [7] and its most important parameters being reviewed in Section 2. The calibration of the PTB-C system was performed by Alevra *et al.* [7] for 12 neutron energies in the range from 1,17 keV to 14,8 MeV at the PTB and in the thermal field at the National Physics Laboratory (NPL) Teddington, UK, by Thomas *et al.* [8].

There are many sets of calculated response functions available for Bonner sphere systems with LiI detectors [9]-[15], and with ^{3}He proportional counters [16]-[22]. The accuracy of the calculations depends among other things on the method of solving the radiation transport problem, on the accuracy of the cross section data, and on the adequacy of the geometry model. In Section 3 we compare two selected sets of calculated responses with the measurements of reference [7].

The degree to which the geometry of the neutron detector is known and modeled is extremely important to obtain an adequate and useful set of response functions. A description of the realistic geometry model is given in Section 4.

The calculations presented here were done with the *Monte Carlo N-Particle transport code* MCNP4.2 [23, 24, 25], which allows the treatment of a three-dimensional geometry. In Section 5 we list all parameters used in our calculations.

In Section 6, we present a complete set of response functions for the bare detector and the 12 sphere diameters of the PTB-C set. Due to a large CPU capacity, we were able to reduce the relative uncertainties of calculated responses to less than 1 % for spheres up to 30,48 cm (12") in diameter and to about 2 % for the 15" and 18" spheres. We also examined angular dependences of the Bonner sphere system, the influence of resonances of the carbon cross sections and effects of different ^{3}He number densities and polyethylene mass densities on the response functions. A comparison of our calculations with measurements [7] shows that a single fit factor can be used to adapt the calculated responses to the measured ones for all sphere diameters and all calibration energies.

An example of a MCNP input file, the complete tables of all calculated responses, the graphical comparison of calculations and calibration measurements [7] and an example of a response matrix are given in the appendices.

A response $R_d(E_\mathrm{n})$ calculated in the frame of this work is the response of a Bonner sphere with diameter d to incident *monoenergetic* neutrons, i.e. to neutrons of energy E_n. On the other hand $R_d(E_\mathrm{n})$ is understood as a continuous function of the incident neutron energy which is achieved by a *lin-log* interpolation (linear in response and logarithmic

in energy) between the calculated responses. In this context we use the term *response function* $R_d(E_n)$. In cases where the response (function) appears as an argument and if no misunderstanding is possible, $R_d(E_n)$ is abbreviated to R.

2 The Bonner sphere set

The PTB-C Bonner sphere set consists of 12 polyethylene spheres with nominal diameters d having in their center a ^{3}He-filled proportional counter of type SP90 manufactured by Centronic Ltd., UK [26]. Since all sphere diameters are multiples of one inch or half-an-inch (1 inch = 2,54 cm) they will be referred to by their outer diameter given in inches: 3", 3.5", 4", 4.5", 5", 6", 7", 8", 10", 12", 15" and 18". The sphere diameters were measured after the spheres were produced and slight deviations from the nominal values and from an ideal sphere were found. These deviations, which are discussed in appendix C, lie within ±0,2 %, the evaluated uncertainty of the diameter is thus 0,1 %.

The polyethylene density was given in reference [7] as 0,946 g/cm^3 ± 0,2 %. This value has been obtained from measurements of cylindrical samples taken from the same batch of polyethylene as the spheres. In appendix C we present the results of the determination of the polyethylene density for each individual sphere of the set. The uncertainty in determining these values is about 0,3 %. The mean polyethylene density obtained for all spheres of the set is ρ_{PE} = 0,946 g/cm^3 ± 0,7 %, i.e. the same value as given in [7], but with larger deviations from the mean. The largest deviations are seen for the 4.5" sphere (+1,5 %) and the 10" sphere (−1,3 %), but these deviations are ignored in the comparison between calculations and measurements.

The ^{3}He partial pressure in the counter of type SP90, specified by the manufacturer, is 200 kPa. Measurements with thermal neutrons [27, 8] show that counters of the same type and the same nominal pressure behave (with respect to fluence response) as if they have various pressures, the dispersion observed being about 12 %. For a better accuracy, instead of the nominal pressure, a "measured" one is needed. As a direct measurement of the pressure inside the sealed counter is not possible, the indirect determination by response measurements in well-specified thermal neutron fields is used. This can be done only in connection with calculations where the pressure, or rather the ^{3}He number density, $n^{\star}_{\mathrm{He}}$, is taken as a parameter to be "determined" (the asterisk indicates that this quantity is not directly measured but determined on certain assumptions).

The model considered, and also in this work, usually describes the proportional counter as an ideal sphere 32 mm in diameter, the whole volume being homogeneously filled with ^{3}He gas. Details such as charge collection and gas amplification are ignored, and instead it is assumed that each ^{3}He(n,p)t event is registered and contributes to the reading of the Bonner sphere. With this simple model, it is easy to deduce an analytical expression which describes the fluence response of the bare counter as a function of energy, the ^{3}He number density, $n^{\star}_{\mathrm{He}}$, being included as a parameter.

The value $4,75 \cdot 10^{19}$ cm^{-3} of the ^{3}He number density given in Reference [7] for the PTB-C counter was obtained from response measurements in the thermal field of the NPL but neglecting the influence of the 0,5 mm thick stainless steel wall of the counter. Thomas and Soochak [27] found that the wall of the counter reduces the response by about 4,7 %. Using this improved model one obtains an increased value of $n^{\star}_{\mathrm{He}} = 4,9418 \cdot 10^{19}$ cm^{-3} for the ^{3}He number density of the PTB-C counter, which corresponds to a partial pressure of the ^{3}He gas inside the counter of $p^{\star}_{\mathrm{He}} = 200\,\mathrm{kPa}$ at room temperature. Using this value for $n^{\star}_{\mathrm{He}}$ we reproduce quite well the measured responses in the NPL thermal field or in other words, the models used here and by Thomas and Soochak are consistent.

3 Comparison of calculations from literature with measured responses

The measured responses taken as references in this work are those obtained in up to 12 monoenergetic neutron fields with energies from 1,17 keV to 14,8 MeV reported by Alevra *et al.* [7], and the responses measured in a thermal neutron field reported by Thomas *et al.* [8], in every case for the PTB-C Bonner sphere set. In both references the uncertainties of the measured responses are given in terms of relative standard deviations. Most of the physical quantities determining the response are uncorrelated for all spheres at all energies. However, the measured fluences for all spheres at a given calibration energy are correlated as the same instrument (recoil telescope, proportional counter or DePangher longcounter) is used. The correlation of fluences measured at different calibration energies using the same instrument has been neglected.

Calculated responses for Bonner spheres of a similar construction to that presented in Section 2 and for a complete set of spheres in the whole energy range of interest are scarce in the literature. To our knowledge only the ANISN calculations of Thomas [19] and the MCNP calculations of Mares *et al.* [18] are complete enough to allow the establishment of a response matrix of a Bonner sphere set of the type mentioned.

3.1 The ANISN calculations of D.J. Thomas (DJT)

Applying ANISN, which is a one-dimensional neutron transport code, devices can be modeled only for spherical symmetry. The geometry model of Thomas [19] consists of a spherical shell of 32 mm inner diameter, 0,5 mm thick, made of steel with a number density of $8,50 \cdot 10^{22}\,\mathrm{cm}^{-3}$, filled with ^{3}He gas with a number density of $4,50 \cdot 10^{19}\,\mathrm{cm}^{-3}$, and placed at the center of polyethylene moderating spheres, their mass density being $0,94\,\mathrm{g/cm}^3$. Results are reported for all sphere diameters contained in the PTB-C set, as group data, in 46 energy groups covering the neutron energy range from 1 meV to 14,191 MeV.

Thomas also evaluated the influence of two important parameters on the response. R, namely the ^{3}He number density, $n^{\star}_{\mathrm{He}}$, and the polyethylene mass density, ρ_{PE}, taking into account small variations around the nominal values. He reported values of the relative derivatives

$$\frac{\mathrm{d}R/R}{\mathrm{d}n^{\star}_{\mathrm{He}}/n^{\star}_{\mathrm{He}}} \quad \text{and} \quad \frac{\mathrm{d}R/R}{\mathrm{d}\rho_{\mathrm{PE}}/\rho_{\mathrm{PE}}} \tag{3.1}$$

for each energy group and sphere diameter. These relative derivatives allowed us to obtain ANISN responses for our system ($n^{\star}_{\mathrm{He}} = 4,9418 \cdot 10^{19}\,\mathrm{cm}^{-3}$ and $\rho_{\mathrm{PE}} = 0,946\,\mathrm{g/cm}^3$) which were attributed to the logarithmic midpoints of the energy groups of [19]. The responses corresponding to the neutron energies used in measurements were obtained through spline interpolations, the values at 14,8 MeV through empirical extrapolation of Thomas' data. The calculated responses obtained in this way were fitted to the measured ones separately for each sphere and considering data at all available energies except those obtained in the thermal field. Only the uncertainties from measurements were available and taken into account; they are those reported in [7] and include the correlated contributions resulting from the fluence determinations. These uncertainties determine the weights in Equation (A.14) (see Appendix A), the fit factors and their uncertainties being determined by Equations (A.15) and (A.16), respectively.

The results of the fit for all spheres from 3" to 18" are shown in Figure 3.1 as "◆". The *reduced chi-square values*, χ^2_r, calculated according to Equation (A.17) (results not shown here) indicate that the shapes calculated by Thomas are adequate to describe the measured responses at least in the energy range between 1,17 keV and 14,8 MeV. In order to fit the absolute values from measurements, scaling factors which strongly depend on sphere diameter have to be applied ($f_{12"}/f_{3"} = 1,089/0,837 \approx 1,30$). In spite of some small fluctuations, the dependence of f of the sphere diameter d is rather smooth, indicating some systematic discrepancy between the model and reality. Moreover, a comparison of calculation and measurement made in the thermal energy region (not shown here) indicates that the DJT calculations overestimate the measured responses by factors, always dependent on sphere diameter, going up to a value of 2. The ANISN calculations of Hehn *et al.* [21], especially in the thermal energy region, show a better agreement with the measurements. Unfortunately, the results reported in [21] are limited to only three sphere diameters and are not given in numerical form. For these reasons a comparison of Hehn's calculations with the measured responses could not be made here.

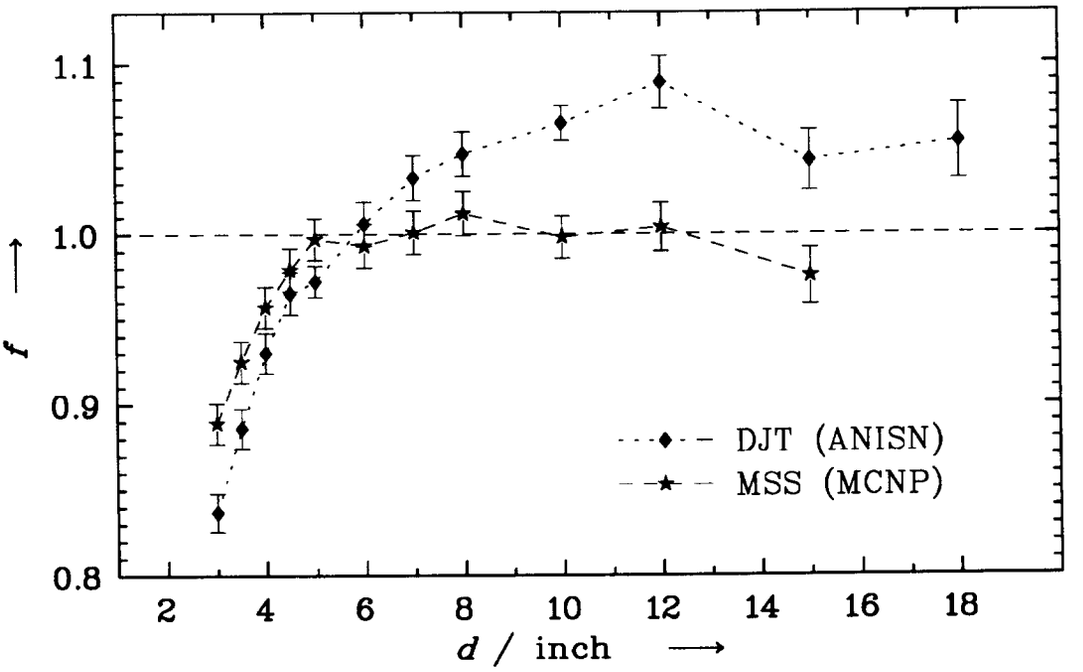

Figure 3.1: Factors f which fit calculated responses to the measured ones from Ref. [7] as a function of sphere diameter d. "◆" shows the values for the ANISN calculations from Ref. [19] (DJT); "★" shows the values for the MCNP calculations from Ref. [18] (MSS).

3.2 The MCNP calculations of Mares, Schraube and Schraube (MSS)

Although MCNP is a three-dimensional neutron transport code, the geometry model used in the calculations of Mares *et al.* [18] is point symmetrical. It consists of a spherical volume 32 mm in diameter, filled with ^{3}He gas with a number density of $4,2497 \cdot 10^{19}$ cm^{-3},

and placed at the center of polyethylene moderating spheres, the mass density of the polyethylene being 0,95 g/cm^3. The steel shell of the counter was not taken into account. Responses are reported for all sphere diameters contained in the PTB-C set except the 18" sphere, as point data at 49 logarithmic equidistant energy points with 5 energies per decade, covering the neutron energy range from 10 meV to 30 MeV.

To be consistent with the procedure applied in the previous subsection, the thermal region was excluded from the comparison with the measurements. Again, the calculated responses at experimental energies were obtained through spline interpolations, logarithmic in energy and linear in response. These values also were adapted to the values of $n^{\star}_{\mathrm{He}}$ and ρ_{PE} of our system using Thomas' derivatives, according to Equation (3.1), spline interpolated at the energies required (at 14,8 MeV the derivatives given for 14 MeV were used). Only the uncertainties from measurements as reported in [7] were considered, the uncertainties from calculations were ignored.

The fit results for all spheres, from 3" to 15", are shown in Figure 3.1 as "$\star$". The reduced chi-square values indicate that the shapes of the MSS responses are adequate to describe the measured responses. This conclusion remains valid even if the comparison is extended to the thermal energy region (not shown here), since in this case the fit factors obtained change by less than 1 %. The variation of the fit factor with sphere diameter indicates an improvement compared with the DJT responses, the largest variation being $f_{8"}/f_{3"} = 1,005/0,896 \approx 1,12$.

The shortcomings of the MSS responses are seen mainly at the boundaries of the energy range of interest. In the lower energy range there are no data in the interval from 1 meV to 10 meV which contributes about 7 % to the total thermal spectral fluence. In the high energy range, the interval from 1,2 MeV to 19 MeV contains only six calculated points which are further used for interpolations. This is insufficient as the response functions show considerable resonances in that energy region (see Section 6.1). This does not apply to the comparison of MSS with the measurements from Reference [7], because the experimental energies in the interval mentioned belong to the 6 calculated points.

The variation of the MSS fit factors with the sphere diameter which is seen practically only for diameters up to 5", looks very similar to the variation of the DJT fit factors, suggesting that the simplified spherical symmetric geometry considered in both calculations could be responsible for it. This seems obvious as the deviation of a Bonner sphere from the ideal spherical symmetry increases with decreasing sphere diameter.

4 Description of the realistic geometry model

From the discussion in Section 3 it is obvious that detailed information on the counter is necessary to correctly reproduce measured responses by calculations, especially for the small spheres. The need for a realistic description of the Bonner sphere system was also concluded from previous calculations performed at the PTB [28, 29]. At the request of the PTB, the manufacturer of the ^{3}He-filled proportional counter SP90, Centronic Ltd. (UK) [26], supplied an authorized, confidential copy of the technical drawings.

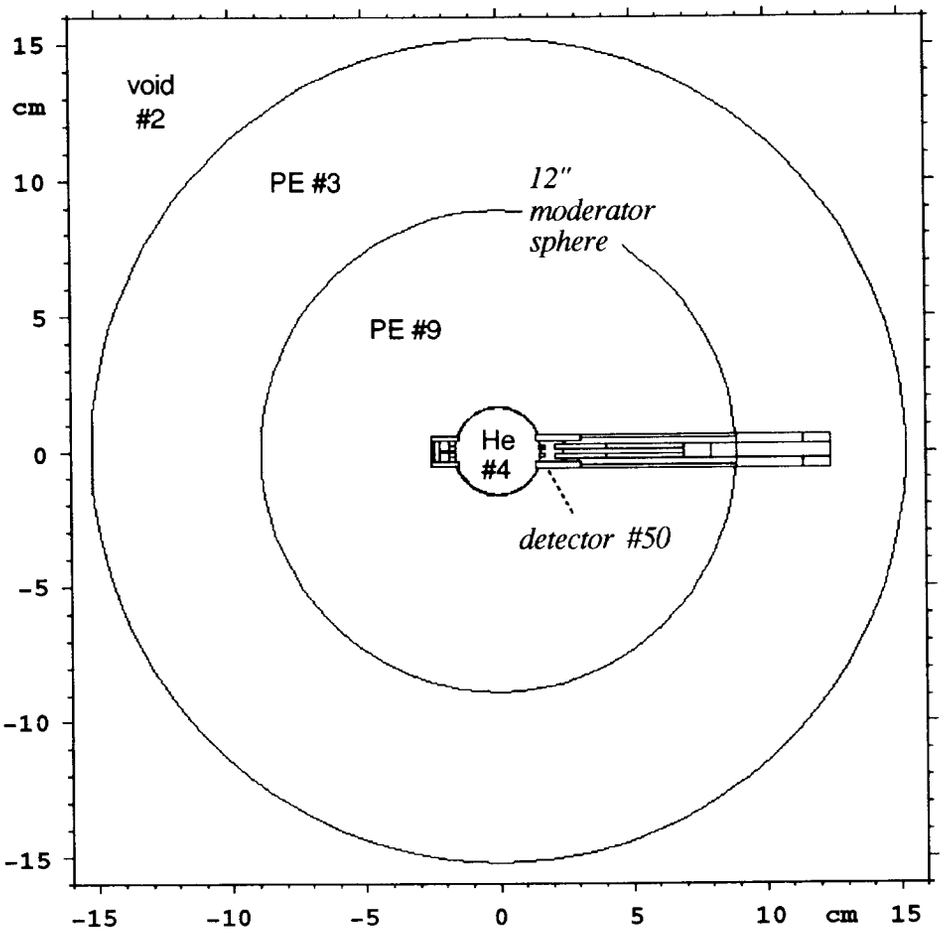

Figure 4.1: Geometry of the Bonner sphere system: ^{3}He-filled proportional counter (detector) with a 12" moderator sphere made of polyethylene (diameter d = 30,48 cm). The x-axis of the coordinate system points towards the reader, the y-axis to the right and the z-axis points upwards. The cells are indicated by materials: void*: vacuum,* PE*: polyethylene and* He*: ^{3}He, and by cell numbers "#i" from Table B.1.*

On this basis, a realistic geometry model for the Bonner sphere system was constructed, which is shown in Figures 4.1 and 4.2. The sketches are transverse sections in the $y-z$-plane at $x = 0$ cm produced by the MCNP geometry plot utility. The origin of the coordinate system is at the center of the sphere, cell #4, the x-axis points towards the reader, the y-axis points to the right and the z-axis points upwards. The geometry is

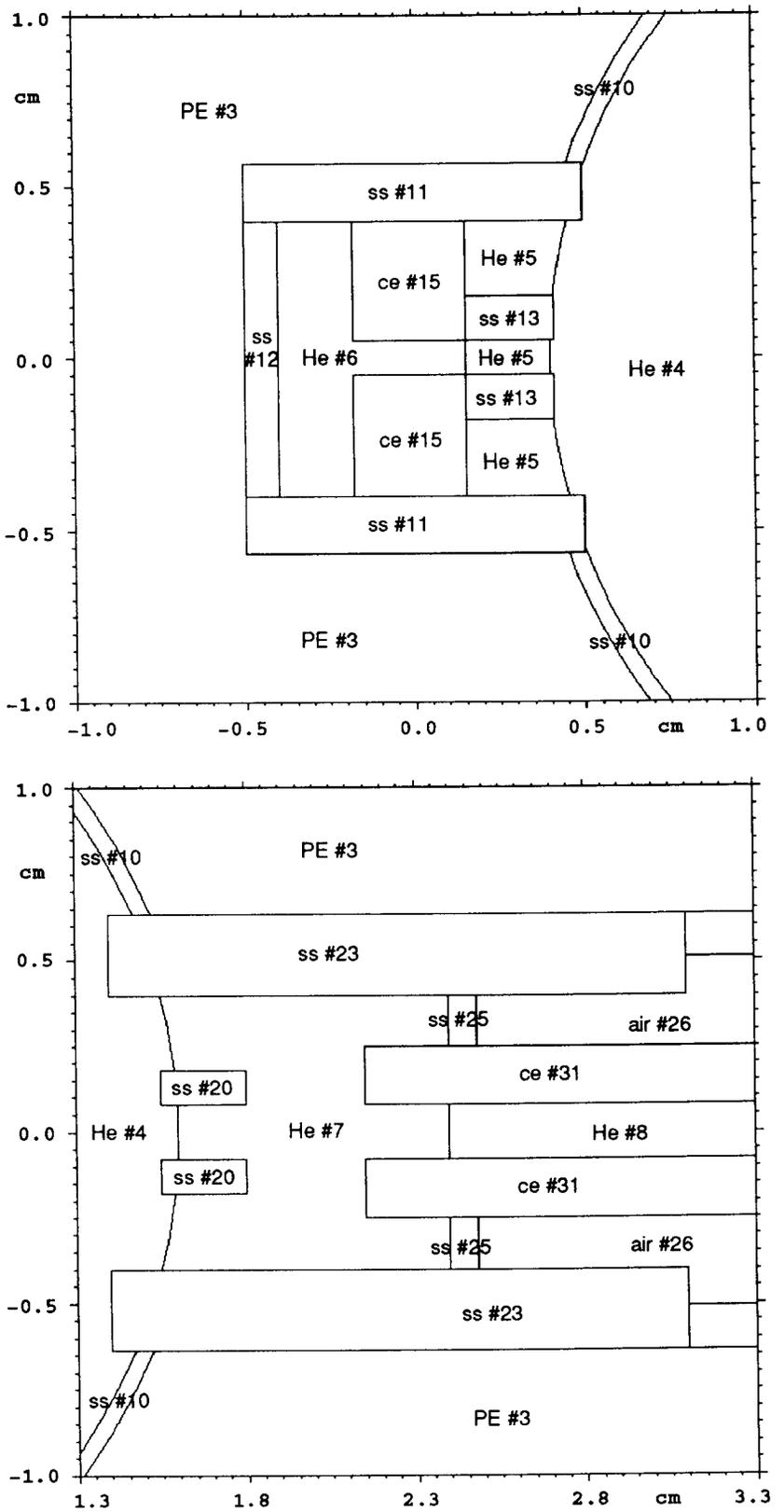

Figure 4.2: Sketch of the realistic geometry model of the ^{3}He*-filled proportional counter SP90. Top:* nose*; bottom: left part of the* stem*. The cells are indicated by materials:* PE*: polyethylene,* He*:* ^{3}He*,* ss*: stainless steel,* air*: air and* ce*: ceramic, and by cell numbers "#i" from Table B.1.*

symmetrical with respect to the y-axis. The different regions, the so-called *cells*, can be identified by their cell numbers "#i" given in the MCNP input file, Table B.1.

Figure 4.1 shows a sketch of a 12" Bonner sphere: the proportional counter SP90 (detector #50) embedded in a polyethylene ($(C_2H_4)_n$) sphere of diameter $d = 30, 48\,\text{cm}$. The cable which connects the counter with the electronic devices is not taken into account. For the purpose of *variance reduction*, i.e. special techniques used in Monte Carlo calculations (see Section 5.5), the moderator sphere is "split" in two parts, an inner sphere (cell #9) and an outer shell (cell #3).

The so-called *nose* (top sketch in Figure 4.2) is a short and the *stem* (bottom sketch in Figure 4.2) is a long cylinder placed at opposite sides of the ^{3}He-filled sphere. They are modeled as stainless steel cylinders partially filled with ^{3}He. The materials used for modeling are PE: polyethylene, He: ^{3}He, ss: stainless steel, air: air and ce: ceramic. The separation of regions with the same material is sometimes used to allow a convenient description of the geometry.

The stainless steel rings, cells #13 and #20, hold the counting wire, which has a diameter of approximately 20 μm. In the results presented here this wire was not taken into account because it is two orders of magnitude smaller than the smallest detail described in the model. The same applies to a spring which is located between the ring, cell #20, and the ceramic isolator, cell #31.

The so-called *sensitive* or *effective counter volume* is the ^{3}He-filled sphere (cell #4) with radius 1,6 mm at the center of Figure 4.1. There are additional volumes filled with ^{3}He, namely cells #5 and #6 in the nose and cells #7 and #8 in the stem. In other words, this model allows the balance of the in- and out-scattering of neutrons with respect to the effective volume to be realistically simulated. It will be seen that this is very important for the response calculation of the smaller polyethylene spheres.

5 Calculation procedure

5.1 The MCNP environment

All response calculations presented in this report were done with the "General Monte Carlo Neutron/Photon/Electron Transport Code" MCNP Version 4.2 [23, 24, 25], the value of variable `LODDAT` is `'3/5/91'`. The code is implemented on a VAXcluster and therefore available to many workstations within the cluster or for those that are connected via DECnet. We wrote a DCL (Digital Command Language) command procedure which allows an easy handling of a two-step MCNP run. In the first step, the so-called *initial run* is done for only a few (1000 to 5000) histories, i.e. the number of starting particles, or with a time limit of one to five minutes. This short run is executed in interactive mode and checks the syntax of the input file including the consistency of the geometry and the availability of the cross section data for all materials required. If it stops successfully the so-called *continue run* is executed as a batch job, so that no further action on the part of the user is required.

Table 5.1: Examples of running times needed for N starting particles (parameter `NPS`*) on a VAXstation 3100/76 for various sphere diameters d and neutron energies E_n. $R_d(E_n)$ is the response and $s(R)/R$ is its relative uncertainty due to the Monte Carlo statistics.*

d inch	E_n MeV	N	$R_d(E_n)$ cm^2	$\frac{s(R)}{R}$ %	running time min
3	$1,00 \cdot 10^{-08}$	800 000	0,822	0,5	555
3	$2,50 \cdot 10^{-06}$	500 000	2,694	0,3	562
3	$2,00 \cdot 10^{-03}$	1 000 000	1,533	0,3	96
3	$1,20 \cdot 10^{+00}$	1 000 000	0,325	0,7	551
6	$1,00 \cdot 10^{-08}$	1 000 000	0,253	1,6	897
6	$1,00 \cdot 10^{-06}$	1 000 000	1,021	0,8	2 024
6	$1,20 \cdot 10^{+00}$	800 000	2,518	0,6	1 643
6	$1,48 \cdot 10^{+01}$	1 000 000	0,499	1,1	587
12	$5,65 \cdot 10^{-01}$	1 000 000	0,657	2,0	2 627
12	$3,50 \cdot 10^{+00}$	1 000 000	1,704	1,2	2 697
12	$5,35 \cdot 10^{+00}$	1 200 000	1,940	1,1	3 381
12	$1,20 \cdot 10^{+01}$	1 000 000	1,463	1,3	1 951
18	$1,20 \cdot 10^{+00}$	6 000 000	0,137	2,6	19 261
18	$2,50 \cdot 10^{+00}$	1 800 000	0,459	2,6	6 685
18	$5,00 \cdot 10^{+00}$	1 800 000	0,898	1,8	6 195
18	$1,60 \cdot 10^{+01}$	1 800 000	1,196	1,6	4 950

There are 4 VAXstations 3100/76, 2 VAXstations 3100 and 1 VAXstation 4000/90 connected in our VAXcluster. Table 5.1 lists some examples of running times needed

for an MCNP run on a VAXstation 3100/76 for various sphere diameters d and neutron energies E_n. The energies listed for each sphere diameter are selected from the region where the response functions have their maximum. Note the number of histories N (NPS) which are necessary to reach the given relative uncertainty $s(R)/R$ of the response $R_d(E_n)$ (for uncertainties, see Section 5.4).

The increase of running time with increasing diameter is obviously not linear. Up to two weeks are needed for a single MCNP run for the 18" Bonner sphere. In fact, we had access to three further workstations of type 4000/90 and smaller, and also to two AXP DECstations 3000/400 each of which is faster by a factor of about 8,3 than a VAXstation 3100/76. Altogether, we used up to 12 VAX computers with total CPU capacity of 25 times that of a VAXstation 3100/76. The sum of all running times from 1145 MCNP runs for 12 Bonner spheres at up to 170 neutron energies is 1235 days!

5.2 Parameters for neutron transport in Bonner spheres used by MCNP

Many different material constants and parameters must be specified to realistically simulate the response of a Bonner sphere. In this section we give the complete set of parameters extracted from the input file, Table B.1. In the following, we refer to this set as the *standard parameter set.*

The history of a neutron is simulated by concatenated straight paths. The new direction of flight and the new energy is determined by reaction kinematics. The length of the path depends on the cross section density Σ_t, which is the product of the particle density of the target material and the sum over all partial cross sections of neutrons with each of the constituents of the material. If ξ is a random number ($0 \leq \xi < 1$), the distance x to the next interaction point is given by

$$x = \frac{1}{\Sigma_t} \ln(1 - \xi) \tag{5.1}$$

This relation clearly shows the importance of an exact knowledge of the density of the material, especially that of the moderator. Since the total cross sections may be assumed to be well-known, the density of the material and its stoichiometric composition mainly determines the variance of Σ_t. In selecting a particular reaction, one relies on the partial cross section and in selecting a new direction of flight for the outgoing neutrons, one relies on the angular distributions. Neither the partial cross sections nor the angular distributions are by any means as well-known as the total cross sections. Most important for this specific problem are the reaction cross sections of neutrons with carbon (C) and hydrogen (H) of the polyethylene and with ^{3}He.

At high neutron energies, the capture cross section for H, in the reaction H(n,γ)d, is negligible compared to the elastic scattering cross section $\sigma_{n,n}(E)$. The neutron (at energies considered in this report) loses, on the average, half of its initial energy. The energy loss obeys a rectangular distribution from zero to the initial energy.

In collisions with C, elastic scattering is the main reaction below about 5 MeV. The maximum energy loss in an elastic collision is only 28 %, the mean energy loss in this reaction depends on the angular distribution and consequently on neutron energy. The mean energy loss is about 14 % at low energies and decreases with increasing energies. This slowing-down (loss of energy) of the neutrons is called *moderation.*

The response of the central proportional counter is determined by the $\sigma_{n,p}(E)$ neutron cross sections in ^{3}He. The dominant reaction for moderated, i.e. low-energy neutrons is ^{3}He(n,p)t. The proton as well as the triton contributes to the detector signal, their combined energy (Q-value) is 764 keV. The elastic cross section is not important for the problem considered. As mentioned in Section 2, it is assumed that every ^{3}He(n,p)t event is counted.

5.2.1 Neutron source

The neutron source is a plane circular area of radius $r_s = (d/2 + 0,001$ cm). It is perpendicular to the symmetry axis, i.e. the y-axis in Figure 4.1, with its center at position $(x, y, z) = (0, -25$ cm, $0)$. The start positions are equally distributed within the area and the flight direction is in the positive y-direction parallel to the axis, i.e. a homogeneous uni-directional neutron beam. If the angle of incidence φ is defined as the angle between the direction of flight and the y-axis, the above configuration defines $\varphi = 0°$. Discrete values of neutron energies (*monoenergetic beam*) were used in the range from 1 meV to 20 MeV. No material constants or distribution functions are needed for the source. The environment of source and Bonner sphere is vacuum or, in terms of MCNP, is *void*, therefore neutrons reach the moderating polyethylene sphere on straight paths without any interaction.

5.2.2 Material densities

For the present calculations we use $\rho_{PE} = 0,946$ g/cm^3 for the mass density of the polyethylene spheres of the PTB-C Bonner sphere set. The densities of the individual spheres (without the embedded proportional counter) determined from the measured masses and the calculated volumes, using the volume determination feature of MCNP, are in good agreement with the mean density of the 12 Bonner spheres, for details see Appendix C. The density of commercial polyethylene varies between 0,91 and 0,98 g/cm^3. It was shown by Mares *et al.* [18] and Thomas [19] that a small variation in density can lead to a much larger change in response, i.e. $\Delta R/R \gg \Delta\rho/\rho$, and the magnitude and size of the effect varies with energy. In Section 6.3 we will discuss the influence of polyethylene density variations on the response.

The composition of the stainless steel (ss) wall of the counter is assumed to be 70,5 % Fe, 19,5 % Cr and 10 % Ni. The ceramic (ce) isolator in the nose and stem (Figure 4.2) are modeled as Al_2O_3 and air as 77,72 % N, 22,12 % O and 0,16 % H.

The most important density next to ρ_{PE} is that of the ^{3}He gas. The manufacturer of the counter states a partial gas pressure of $p_{He} = 200$ kPa for the counting gas ^{3}He and $p_{Kr} = 100$ kPa for the additional Kr gas. However, the krypton filling was not taken into account, because the neutron cross section of Kr is negligible compared with the cross section of the ^{3}He(n,p)t reaction at least for neutron energies up to 1 eV for which the counter is most sensitive. The helium number density related to the specified partial pressure was determined as $n^*_{He} = 4,9418 \cdot 10^{19}$ cm^{-3} (see Section 2). The influence of the ^{3}He gas density variation is discussed in Section 6.2.

Table 5.2 is a summary of all density values in the order of the material numbers used in the MCNP input file. The unit of n^*_{He} given here, $(10^{24}$ *atoms*$)/($cm$^{-3})$, is that requested by MCNP [23] (see also Table B.1).

Table 5.2: Standard parameter set for the presented calculations with MCNP, `M1` *to* `M5` *are the material identifiers from Table B.1.*

`M1)` $\rho_{\mathrm{PE}} = 0,946\ \mathrm{g/cm^3}$,
`M2)` $n^{\star}_{\mathrm{He}} = 4,9418 \cdot 10^{-5}\ (10^{24}\ atoms)/(\mathrm{cm^{-3}})$,
`M3)` $\rho_{\mathrm{ss}} = 7,86\ \mathrm{g/cm^3}$,
`M4)` $\rho_{\mathrm{air}} = 1,19 \cdot 10^{-3}\ \mathrm{g/cm^3}$,
`M5)` $\rho_{\mathrm{ce}} = 3,965\ \mathrm{g/cm^3}$.

5.2.3 Cross section libraries

At the time we started with the calculation of Bonner sphere responses, the neutron cross sections available in MCNP format were those distributed with the CCC-200 package by RSIC, i.e. the data libraries ENDL–85 (Lawrence Livermore National Laboratory's Evaluated Nuclear Data Library) and ENDF/B–IV (Evaluated Nuclear Data Files from Los Alamos National Laboratory). Table 5.3 lists the cross section tables used from these two libraries specified by the Z and A identifier *ZAID* for the isotopes (^{1}H, ^{3}He, ^{12}C, ^{14}N, ^{16}O and ^{27}Al) and the elements in their natural composition (Cr, Fe and Ni). In order to take into account the chemical binding of H in polyethylene at thermal neutron energies, we included the S(α, β) table `POLY.01T`. It was shown by Hehn *et al.* [21] that upscattering is seen for neutron energies up to 3 eV.

Table 5.3: Part of the MCNP output file that lists the tables (ZAIDs) selected from the available cross section data libraries for the various material components.

```
 1001.35C    1777    ZA= 1001    ENDL-85                 85/04/24    T=0K    87/12/07
 2003.35C    1268    ZA= 2003    ENDL-85                 85/04/24    T=0K    87/12/07
 6012.35C    3058    ZA= 6012    ENDL-85                 85/04/24    T=0K    86/01/31
 7014.04C   14578  N-14 ENDF/B-IV   NEW GAMMA PRODUCTION FORMAT                14 OCT 75
 8016.35C    4835    ZA= 8016    ENDL-85                 85/04/24    T=0K    86/01/31
13027.35C   22811    ZA=13027    ENDL-85                 85/04/24    T=0K    86/01/31
24000.35C    5211    ZA=24000    ENDL-85                 85/04/24    T=0K    86/02/04
26000.35C   15159    ZA=26000    ENDL-85                 85/04/24    T=0K    86/01/31
28000.11C   21651  NI ENDF/B-IV T=300.0 24 FEBRUARY 1976  POINTWISE          18 MAR 76
 POLY.01T   11544  HYDROGEN IN POLYETHYLENE AT 300 DEGREES KELVIN             010/22/85
```

5.3 Calculation of the response

The response of a Bonner sphere of diameter d to *incident* neutrons of energy E_{n} is defined in Equation (A.1), Appendix A, which is recalled here

$$R_d(E_{\mathrm{n}}) = \frac{M_d}{\Phi(E_{\mathrm{n}})} .$$

To simulate the response of the BSS on a computer, it is assumed that the number of

^{3}He(n,p)t reactions in the sensitive counter volume V_{c4} of the proportional counter is correlated to the reading M_d. This volume V_{c4} is a sphere of radius r_{c4} (cell #4 in the MCNP input file, Table B.1). We set a *tally 4* on this cell to obtain the so-called *track length estimate of fluence*, Φ_j. This quantity is calculated from the sum of those K path lengths l_k of neutrons in the counter which have an energy $\tilde{E}_j$ in the interval $(E_{j-1}, E_j]$[a]

$$\Phi_j \propto \frac{1}{K\, V_{c4}} \sum_{k=1}^{K} l_k(\tilde{E}_j)\,; \quad \tilde{E}_j \in (E_{j-1}, E_j]\,. \tag{5.2}$$

Φ_j is the area density of the *number of particles* (in cm^{-2}) normalized to one source particle in the energy range from E_{j-1} to E_j ($E_0 = 10^{-10}$ MeV). The E_j are the interval boundaries listed in Table B.1 (not to be mistaken for the midpoint energies E_i of logarithmic equidistant energy bins as defined in Equation (A.10) for incident neutrons). The response $R_d(E_n)$ (in cm^2)[b] of the detector d to incident neutrons of energy E_n is given by

$$R_d(E_n) = \sum_j \Phi_j\, a_s\, n^*_{He}\, V_{c4}\, \sigma_{n,p}(\tilde{E}_j)\,, \tag{5.3}$$

with

Φ_j particle fluence in the interval from E_{j-1} to E_j (in cm^{-2}),

a_s area of the neutron source (in cm^2),

n^*_{He} ^{3}He number density (in cm^{-3}),

V_{c4} volume of the counter, cell #4, (in cm^3),

$\sigma_{n,p}(\tilde{E}_j)$ the ^{3}He(n,p)t cross section for moderated neutrons with energy $\tilde{E}_j \in (E_{j-1}, E_j]$ (in b).

To avoid confusion in the discussion of our results (especially in Section 6.2) it should be noted that $R_d(E_n)$ is not strictly proportional to n^*_{He} as Equation (5.3) might imply. In fact, Φ_j depends in a very complicated form on n^*_{He}. However, this dependency is taken into account properly by the Monte Carlo calculations.

In Figure 5.1 we present a calculated *fluence spectrum* for the 8" sphere with incident neutron energy $E_n = 3$ MeV (dashed line with left ordinate), where E is the energy of neutrons inside the proportional counter. In this *lin-log* representation of the spectrum the expression $\Phi_E(E\,;\, d, E_n) \cdot E$ assures that the area enclosed by the histogram and the abscissa is proportional to the fluence for each bin.

The spectral fluence $\Phi_E(\tilde{E}_j\,;\, d, E_n)$ is given by $\Phi_j/\Delta E_j$ where Φ_j are the *group fluences* from Equation (5.2) and $\Delta E_j = E_j - E_{j-1}$. In formal analogy we introduce the spectral response

$$R_E(E\,;\, d, E_n) = \Phi_E(E\,;\, d, E_n)\, a_s\, n^*_{He}\, V_{c4}\, \sigma_{n,p}(\tilde{E}_j)\,; \quad \tilde{E}_j \in (E_{j-1}, E_j]\,, \tag{5.4}$$

plotted as the solid line in Figure 5.1 with the right ordinate given by $R_E(E\,;\, d, E_n) \cdot E$.

[a] In this section, the energy variables E, E_j and $\tilde{E}_j$ correspond to energies of moderated neutrons, i.e. of neutrons within the counter.

[b] The SI unit cm^2 stands for *counts* per (*neutron* per cm^2).

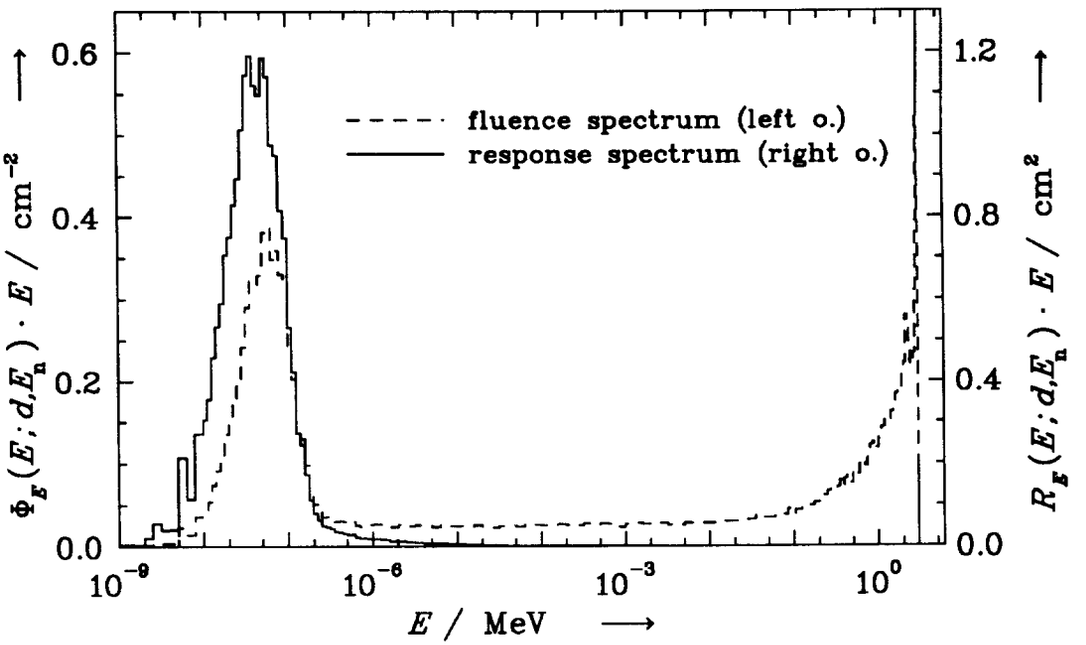

Figure 5.1: Fluence spectrum: dashed line with left ordinate, and response spectrum: solid line with right ordinate, for the 8" sphere ($d = 20,32\,cm$) and incident neutron energy $E_n = 3\,MeV$. The contents of the last fluence bin (2,999 MeV to 3 MeV) is 368 cm^{-2} whereas the contents of the last response bin is 0,2 cm^2.

Since the $\sigma_{n,p}(E)$ cross section of ^{3}He is a rapidly decreasing function of energy, only the thermal neutrons contribute to the total response. The example is shown for the 8" sphere and $E_n = 3$ MeV, the calculated response $R_d(E_n)$ is 2,419 cm^2. The contribution of neutrons with energies $E > 20$ keV to the total response is 0,26 %.

5.4 Variance of the response

Next to the responses $R_d(E_n)$ Table 5.1 lists their relative uncertainties

$$\frac{s(R)}{R} \equiv \frac{s(R_d(E_n))}{R_d(E_n)} =: u(R)\,.$$

Since the factors of Equation (5.3) are uncorrelated, they each contribute with a quadratic term to the total uncertainty.

All factors but one are either fixed, experimentally given numbers, or free parameters varying within certain ranges but well-defined for the calculations presented in this report as listed in Table 5.2. The uncertainties of the $\sigma_{n,p}(E)$ cross sections are listed in the libraries, but unfortunately the current version of MCNP does not use them.

The only non-vanishing term of the derivative of Equation (5.3) arises from the fluence Φ_j. In the MCNP output file all listed uncertainties for the responses $R_d(E_n)$ are due to the Monte Carlo statistics only.

In some cases we repeated the calculation of response $R_d(E_n)$ for a given diameter and energy but we used different ensembles of random numbers. In practice this is achieved by starting MCNP with different initial random numbers. The generated sets of pseudo

random numbers for each run are statistically independent and therefore the results can be treated as a series of independent calculations. If the calculations are made for different numbers of histories N_i, the responses $R_i = R_{d,i}(E_n)$ have uncertainties $u_i = s(R_i)/R_i$.

The response $R_d(E_n)$ is then given by the mean value of the k individual MCNP runs weighted with the inverse of the individual variances [30]

$$R_d(E_n) = \frac{\sum_{i=1}^{k} \frac{R_i}{s^2(R_i)}}{\sum_{i=1}^{k} \frac{1}{s^2(R_i)}}, \tag{5.5}$$

and its variance $s^2(R_d(E_n))$ is given by

$$s^2(R_d(E_n)) = \left(\sum_{i=1}^{k} \frac{1}{s^2(R_i)} \right)^{-1}. \tag{5.6}$$

5.5 Variance reduction

MCNP offers several methods to reduce the variance of the tallies for a fixed computer time and number of histories. We have used the *geometry splitting with russian roulette* variance reduction technique by weighting the cells with different *neutron importance* `IMP:N=1` to `IMP:N=4`. The closer the neutrons approach the counter volume, the higher is the importance. However, the effect is weak since the importance ratio of neighbouring cells is at most 3:1. The large moderator spheres (12" to 18") are "split" into two parts, an inner sphere (cell #9) with `IMP:N=3` and an outer shell (cell #3) with `IMP:N=2`. A test run with all importance values equal to unity for the 12" Bonner sphere and E_n = 7,1 MeV needed only 6,8 % more computer time to reach the same uncertainty. For this type of geometry problem it does not make sense to expend great effort on sophisticated variance reduction techniques.

6 Results and discussion

6.1 Calculated responses for the PTB-C Bonner sphere set

We calculated a total of 852 response values for the PTB-C Bonner sphere set, (3", 3.5", 4", 4.5", 5", 6", 7", 8", 10", 12", 15", 18") and the bare detector (^{3}He-filled proportional counter SP90) in homogeneous, broad parallel neutron beams using our realistic detector model (Figures 4.1 and 4.2) and the MCNP parameters listed in Table 5.2 and discussed in Section 5.2. The neutron energies E_n vary between 1 meV and 20 MeV, i.e. over more than 10 decades.

For each sphere diameter d, we calculated the response $R_d(E_n)$ at as many energies E_n as necessary to get the complete shape of the function curve rather than using a fixed set of energies for all spheres. For the 12 spheres, the calculated responses $R_d(E_n)$, in units of cm^2, and their relative uncertainties $u(R) = s(R)/R$, in percent, are listed in Appendix D, Tables D.1 to D.12, and those of the bare detector in Appendix E, Table E.1. It should be pointed out that $s(R)/R$ depends only on the number of histories N done with MCNP. Due to a large CPU capacity we were able to significantly reduce the relative uncertainty $u(R)$ compared with other published data for Bonner spheres with a spherical ^{3}He counter. In the energy region where $R_d(E_n)$ has its maximum, we usually selected N so that $u(R)$ is less than 1 % for sphere diameters up to 12" and less than 2 % for the 15" and 18" Bonner spheres.

In Figures 6.1 to 6.6 our results are presented graphically together with measured responses for the same system [7].

The responses $R_d(E_n)$ as calculated with MCNP according to Equation (5.3) are shown as small solid squares (■). In the majority of cases the uncertainty bars representing $s(R)$ are smaller than the height of the symbols. For sphere diameters 8" to 18" the inlet is a magnification of the energy range 1 MeV to 20 MeV. For the 4.5", 8", 12" and 15" spheres, we calculated the response in this range in very small steps (100 keV down to only a few keV) to study the effects of resonances in the carbon cross sections. This will be discussed later in this section.

The open squares (□) in the energy range between 1,17 keV and 14,8 MeV represent measurements performed by Alevra *et al.* [7] for calibration purposes in up to 12 monoenergetic neutron fields. The experimental data points (for the 3" to 10" sphere) attributed to the energy of 50 meV represent measurements in a field of thermal neutrons performed by Thomas *et al.* [8].

The solid lines are *lin-log* interpolations (linear in response and logarithmic in energy) between data points $(E_i, \mathcal{R}_{id})$ where $\mathcal{R}_{id}$ is the response at the 10-per-decade logarithmic equidistant energies E_i, listed in Table G.1 and discussed in Section 6.7. In energy regions where only a few responses (3 to 5 energies per decade) were calculated, the solid lines go through the data points. If there are more energies E_n than 10-per-decade, the interpolation curve represents an averaged response at energy E_i.

The figures show the well-known shapes of Bonner sphere responses, i.e. the broad shape for the small spheres which gets narrower with a shift of the maximum response to higher energies with increasing sphere diameters. Very much depending on this individual shape we selected the energy points for calculation and the required uncertainty.

It has already been reported by Bramblett *et al.* [1] that the measured responses for their 8" and 12" sphere show resonance structures between 2 MeV and 8 MeV. To see

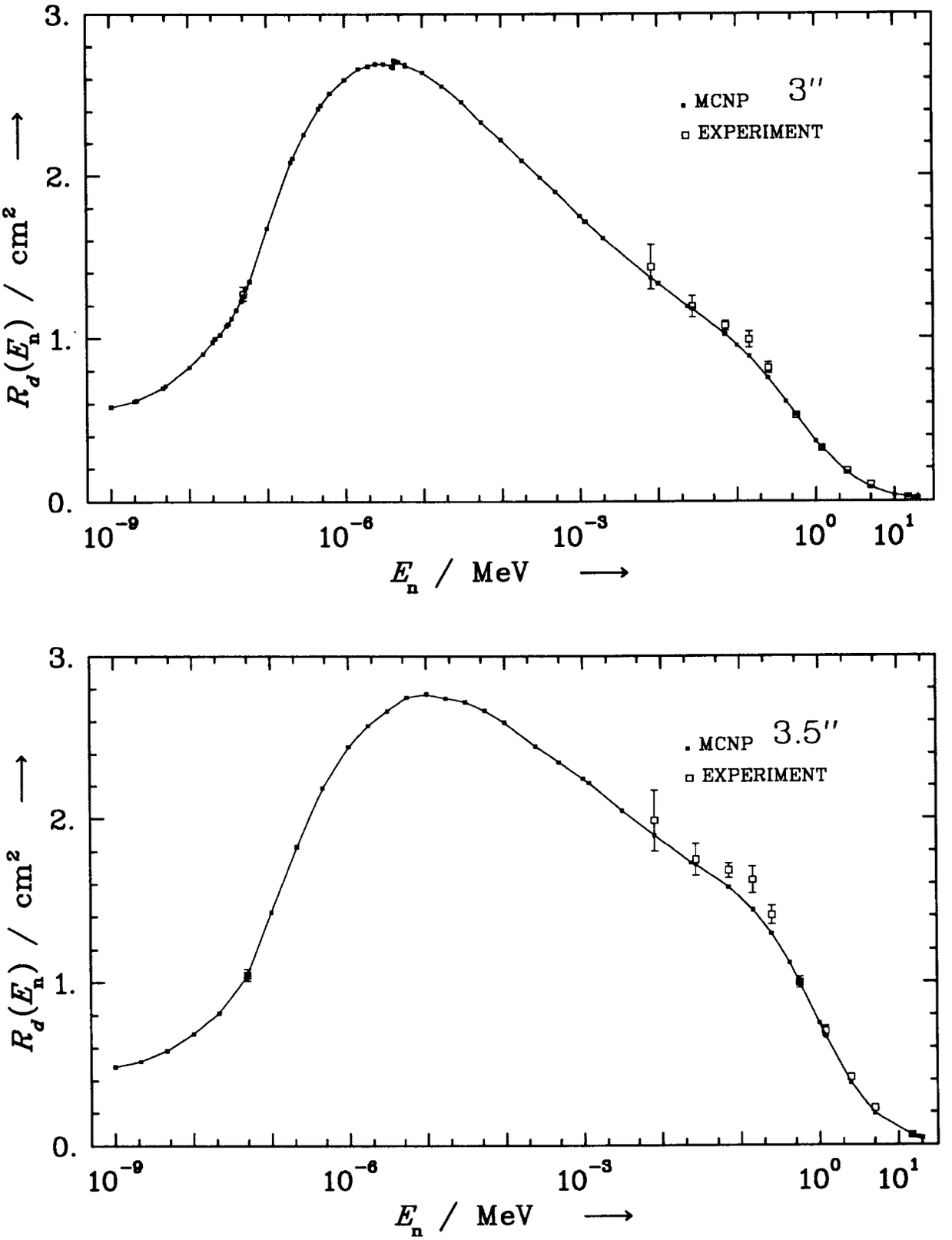

Figure 6.1: Response functions $R_d(E_n)$ for the 3" and 3.5" Bonner spheres calculated with MCNP (■), the solid lines are lin-log interpolations of the corresponding columns of matrix $\mathcal{R}$ given in Table G.1; experimental values (□) are taken from Refs. [7] and [8].

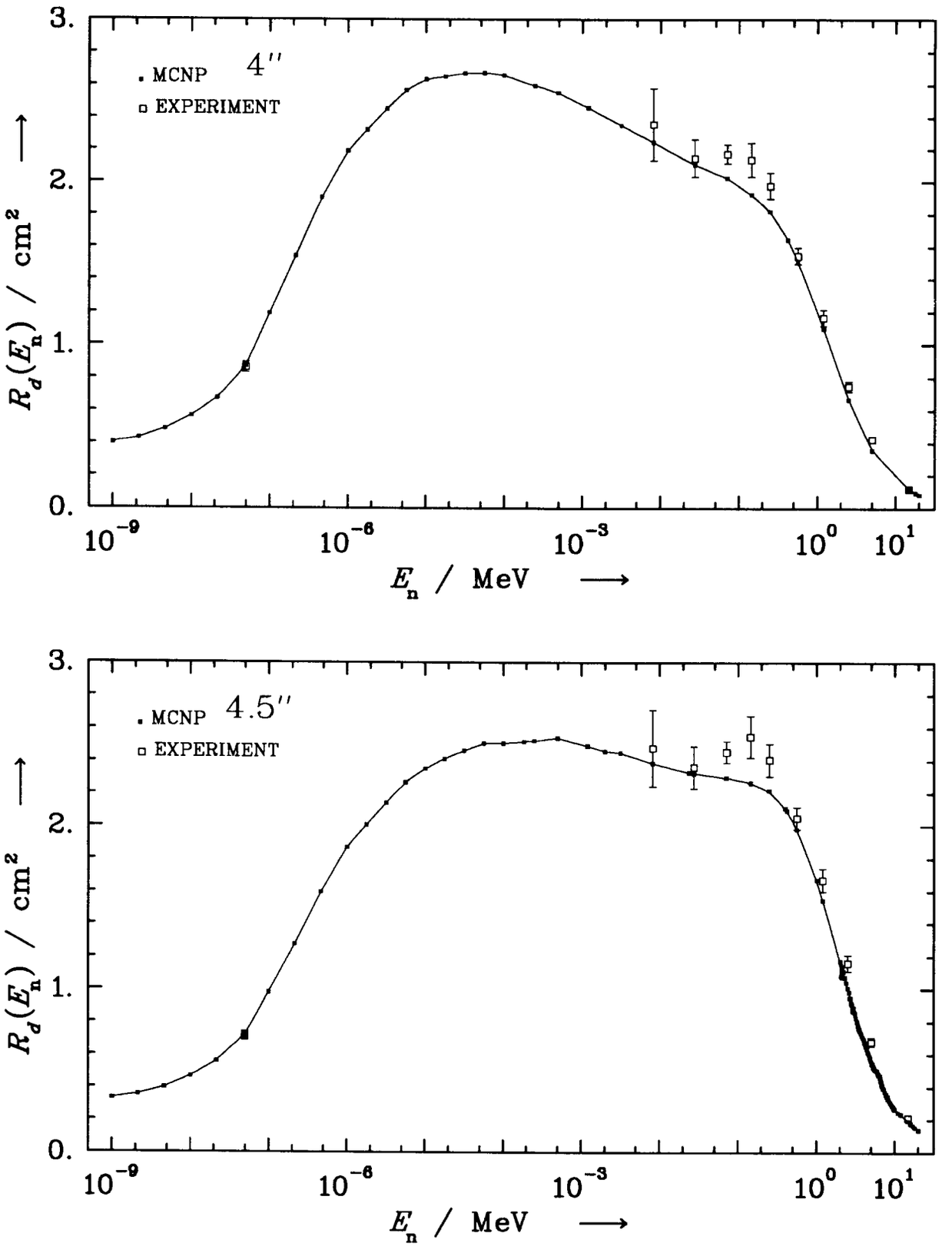

Figure 6.2: Response functions $R_d(E_n)$ for the 4" and 4.5" Bonner spheres calculated with MCNP (■), the solid lines are lin-log interpolations of the corresponding columns of matrix $\mathcal{R}$ given in Table G.1; experimental values (□) are taken from Refs. [7] and [8].

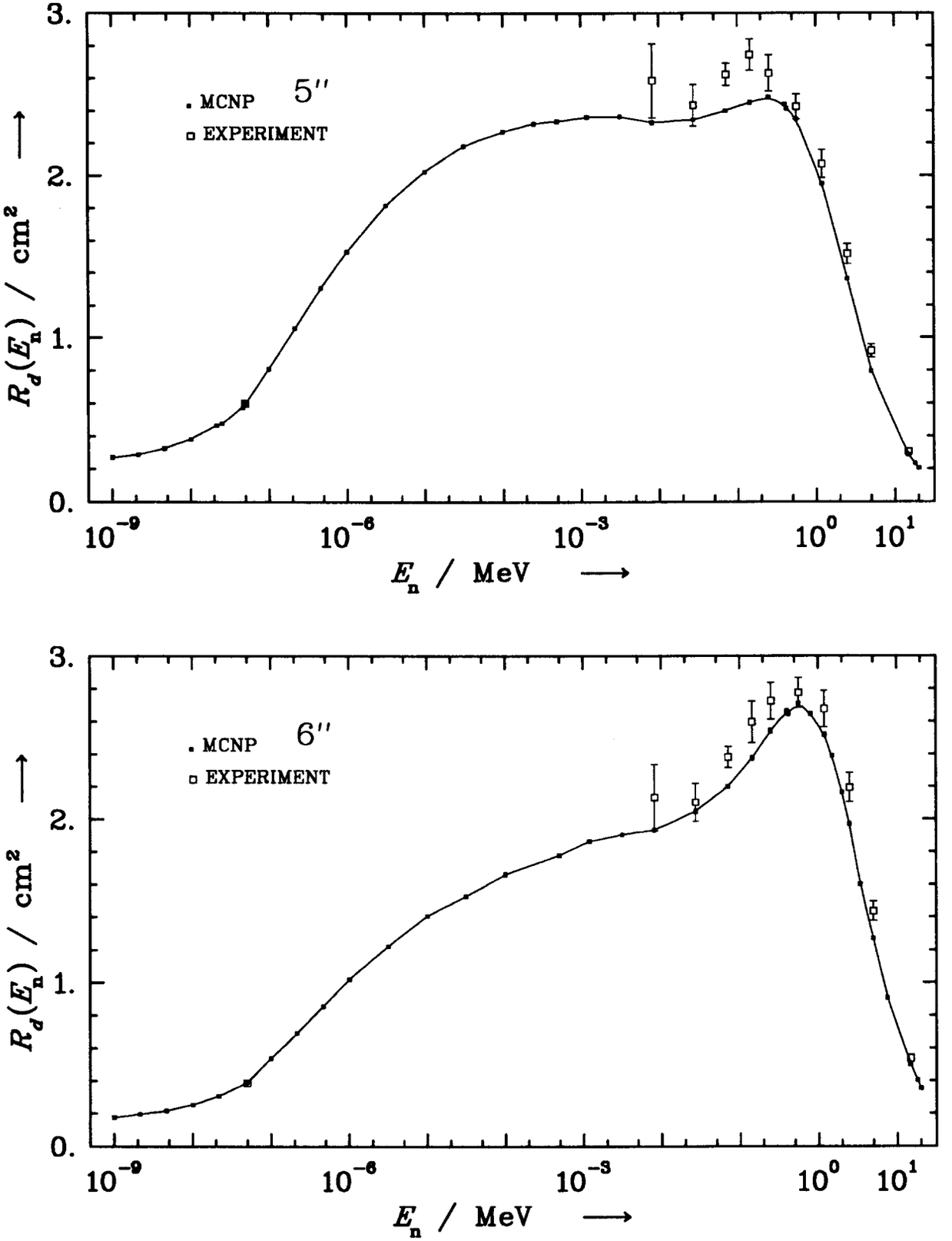

Figure 6.3: Response functions $R_d(E_n)$ for the 5" and 6" Bonner spheres calculated with MCNP (■), the solid lines are lin-log interpolations of the corresponding columns of matrix $\mathcal{R}$ given in Table G.1; experimental values (□) are taken from Refs. [7] and [8].

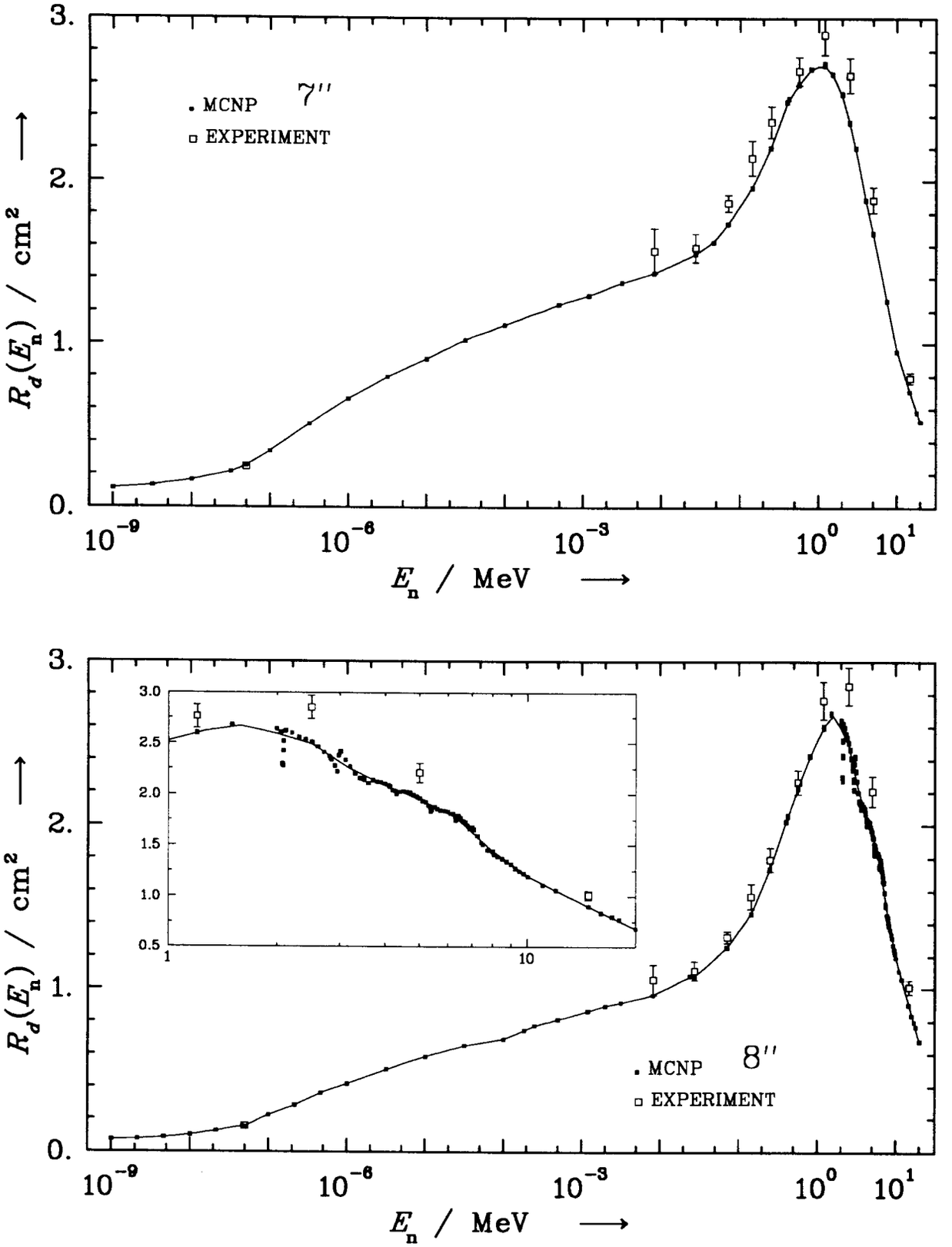

Figure 6.4: Response functions $R_d(E_n)$ for the 7" and 8" Bonner spheres calculated with MCNP (■), the solid lines are lin-log interpolations of the corresponding columns of matrix $\mathcal{R}$ given in Table G.1; experimental values (□) are taken from Refs. [7] and [8].

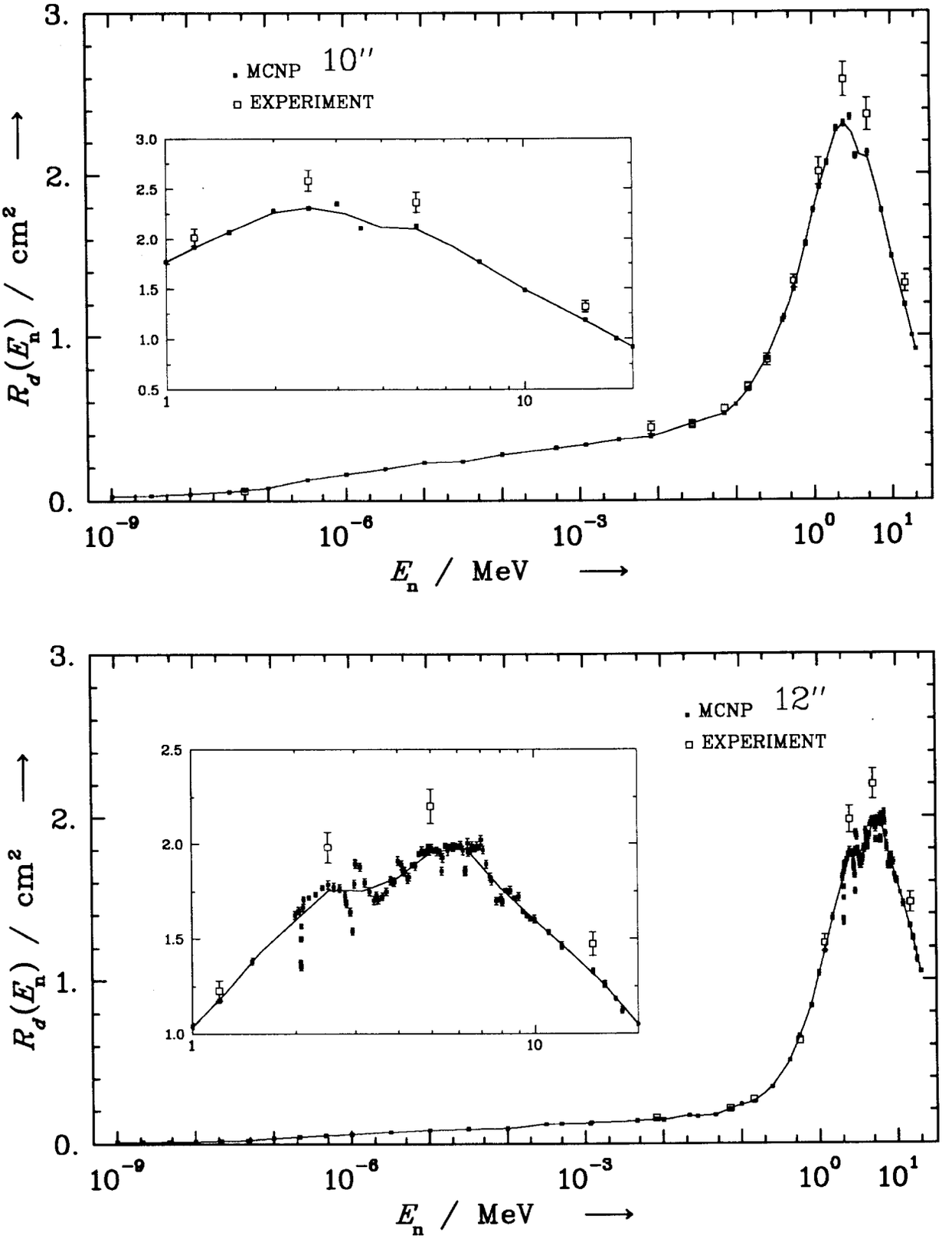

Figure 6.5: Response functions $R_d(E_n)$ for the 10" and 12" Bonner spheres calculated with MCNP (■), the solid lines are lin-log interpolations of the corresponding columns of matrix $\mathcal{R}$ given in Table G.1; experimental values (□) are taken from Refs. [7] and [8] (10" only).

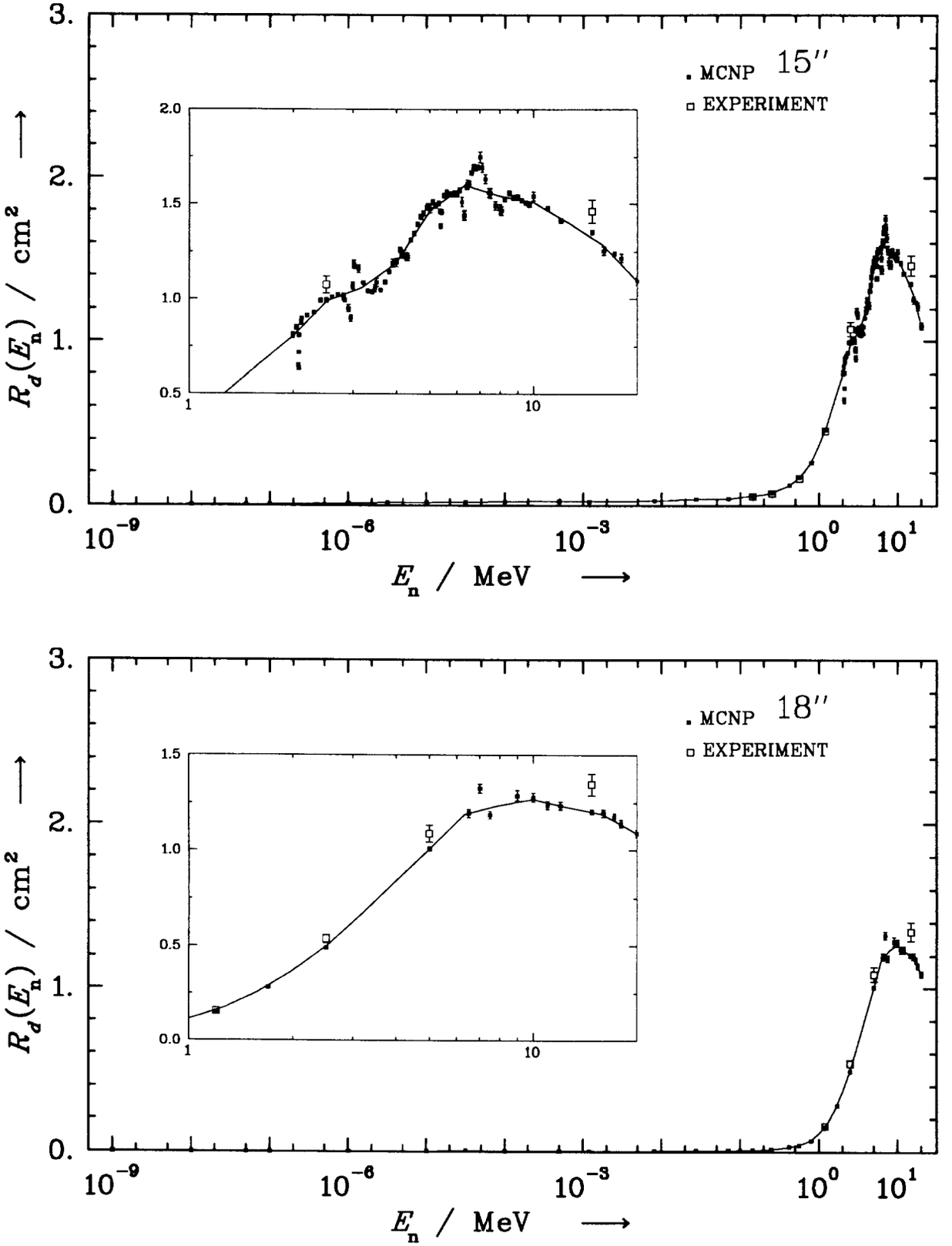

Figure 6.6: Response functions $R_d(E_n)$ for the 15" and 18" Bonner spheres calculated with MCNP (■), the solid lines are lin-log interpolations of the corresponding columns of matrix $\mathcal{R}$ given in Table G.1; experimental values (□) are taken from Ref. [7].

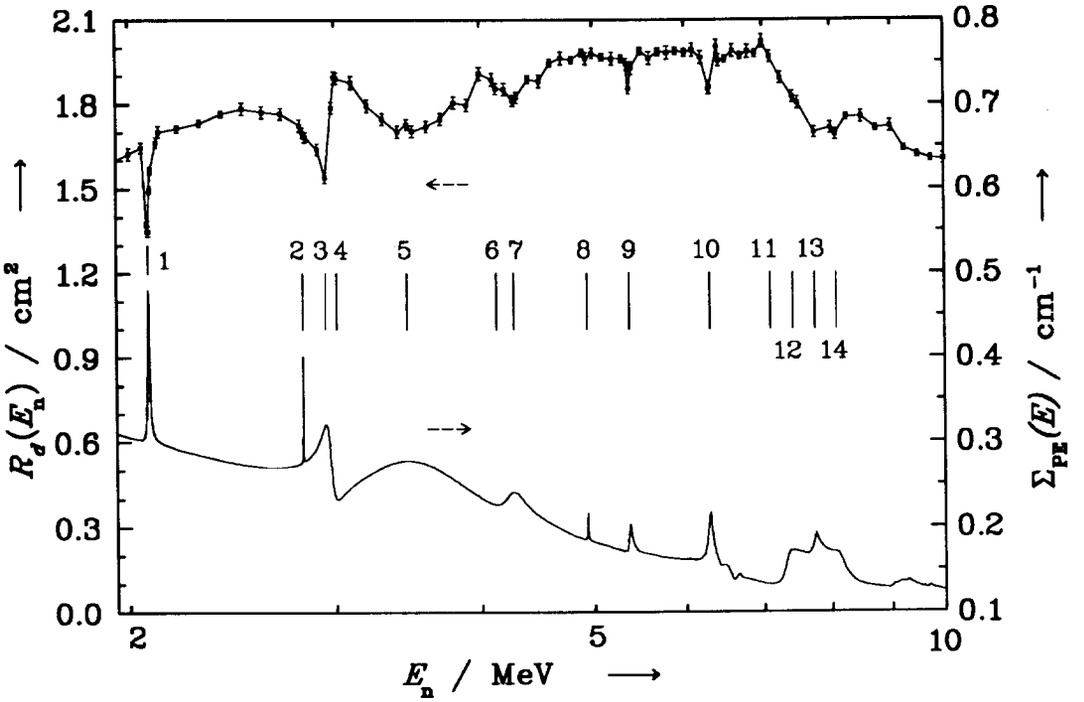

Figure 6.7: Response function $R_d(E_n)$ of the 12" Bonner sphere (upper curve and left axis) for neutron energies between 2 MeV and 10 MeV, and the neutron cross section density function of polyethylene $\Sigma_{PE}(E)$ (lower curve and right axis). The short vertical lines between the two curves indicate the position of significant maxima and minima of $\Sigma_{PE}(E)$. The numerical values (in MeV) are 1) 2,077, 2) 2,815, 3) 2,944, 4) 3,010, 5) 3,460, 6) 4,130, 7) 4,270, 8) 4,937, 9) 5,371, 10) 6,295, 11) 7,100, 12) 7,420, 13) 7,750, 14) 8,080.

whether these structures can be reproduced by the calculations, we chose the 12" sphere because its response maximum is between 1 MeV and 10 MeV. In this energy range we calculated 85 response values with a relative uncertainty of $0,7\ \% \leq u(R) \leq 1,2\ \%$. These results are shown in Figure 6.7 as the upper curve, which corresponds to the left ordinate. In this figure the line is the straight connection of the data points and only used as an eye guide. The lower curve is the cross section density of polyethylene $\Sigma_{PE}(E)$ as a function of neutron energy (right ordinate).

While the hydrogen cross section is a smooth function of energy, the peaks arise from resonances of the carbon cross section. The short vertical lines between the two curves show the position of the maxima and minima of the function $\Sigma_{PE}(E)$, the numerical values of the energies are given in the figure caption with the corresponding designations ("1", ..., "14").

Too few energy bins are given in the cross section library for the very narrow resonances at energies $E_{n,2} = 2{,}815$ MeV and $E_{n,8} = 4{,}937$ MeV, and they cannot be resolved by MCNP.

In the energy region specified we calculated the responses for three more spheres, 4.5", 8" and 15", at the same energies as for the 12" sphere. The results shown in Figure 6.8 clearly demonstrate that the structures also appear for the other three spheres. In this figure we have suppressed the symbols at each data point and marked the curves only at

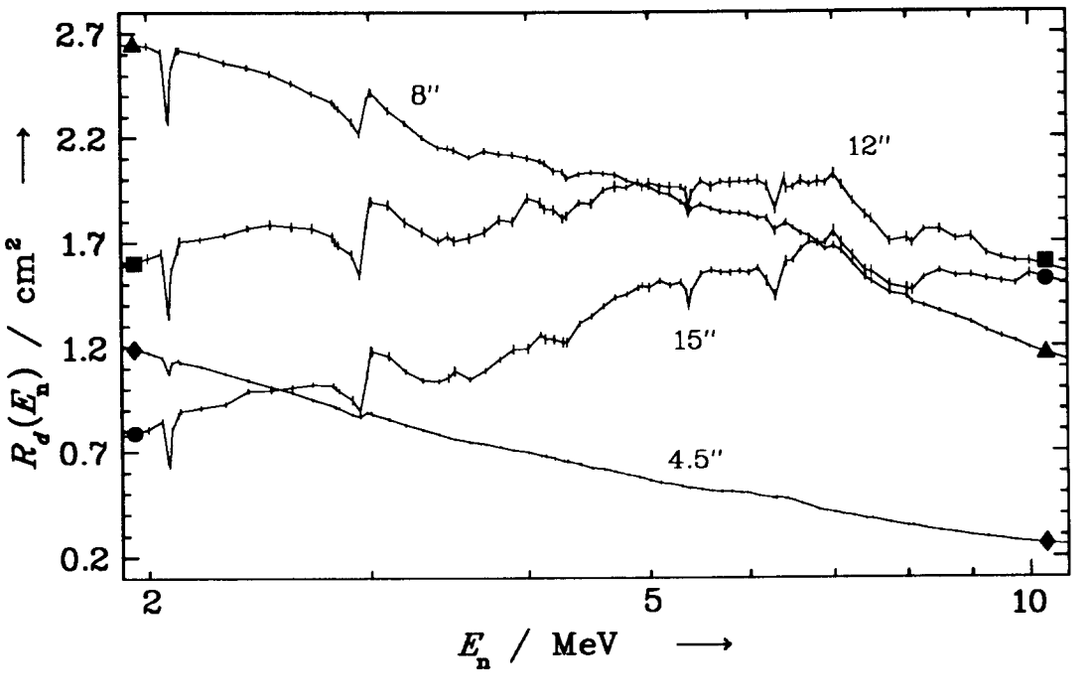

Figure 6.8: Response function $R_d(E_n)$ for the 4.5" sphere, "◆", for the 8", "▲", for the 12", "■", and for the 15" sphere, "●". At the data points only small vertical lines are drawn which represent the uncertainty bars.

both ends. At each data point the small vertical lines represent the uncertainty bars. The energy region 2 MeV to 10 MeV lies on the decreasing branches of the response curve for the 4.5" and the 8" spheres and for the other two it lies on the increasing branches. For the 4.5" sphere the effect is very weak at $E_{n,1}$ = 2,077 MeV and around 3 MeV and is insignificant at the other energies.

In Section 6.7 we discuss the effect on typical applications of calculated response functions by comparing calculated readings M_d of Bonner spheres in different types of neutron spectra if detailed information on the response function is available, for the 12" sphere for example, or if the response functions are calculated only at a few energies.

6.2 The influence of the ^{3}He number density on the response

The ^{3}He gas partial pressure, p_{He}, in the proportional counter is a parameter which may vary from detector to detector. The manufacturer of the counter states a gas filling of p_{He} = 200 kPa for the counting gas ^{3}He and p_{Kr} = 100 kPa for the additional Kr gas. However, the krypton filling was not taken into account (see Section 5.2.2). The physically important quantity is the ^{3}He number density $n^\star_{He}$, which must be determined [27]. For the PTB-C set, we use $n^\star_{He} = 4,9418 \cdot 10^{19}$ cm^{-3} (see Section 2).

Mares *et al.* [18] and Thomas [19] reported the dependence of the response on the gas pressure for their geometry model. In Reference [19] ratios $(dR/R)/(dn^\star_{He}/n^\star_{He})$ from ANISN calculations are tabulated for all 12 sphere diameters of the PTB-C system and for the 46 energy groups mentioned in Section 3.1.

To study the influence of various values of $n^\star_{He}$ or $p^\star_{He}$ on the response of our Bonner

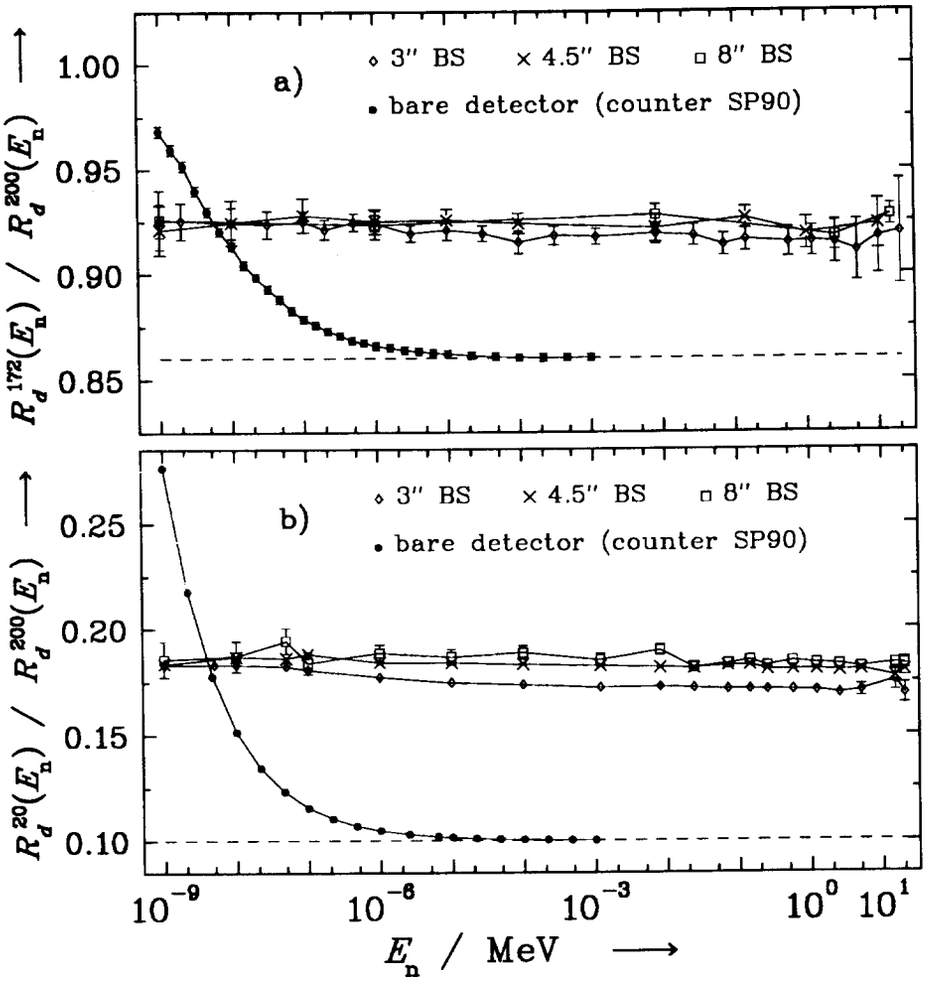

Figure 6.9: Ratios of calculated responses for proportional counters with different ^{3}He *gas pressures for the bare detector, the 3", the 4.5" and the 8" sphere, a) ratios for pressures 172 kPa to 200 kPa, b) ratios for pressures 20 kPa to 200 kPa.*

sphere set, we calculated the ratios of responses $R_d^{172}(E_n)/R_d^{200}(E_n)$, Figure 6.9a), and $R_d^{20}(E_n)/R_d^{200}(E_n)$, Figure 6.9b) for the bare detector, the 3", the 4.5" and the 8" sphere ($R_d^p(E_n)$ means the calculated response of sphere d for a partial ^{3}He gas pressure of p kPa in the counter). The responses $R_{bd}^{172}(E_n)$ and $R_{bd}^{20}(E_n)$ for the bare detector are tabulated in Table E.1 columns 4 and 6, respectively.

With increasing neutron energy, the ratio of the response for the bare detector reaches the ratio of the partial ^{3}He pressures, 0,86 (i.e. 172 kPa/200 kPa) and 0,10 (i.e. 20 kPa/200 kPa), indicated by the dashed lines in Figure 6.9 a) and b), respectively. In other words, at very low energies the bare detector is almost *black* because the probability of neutron detection is very high (78 % at E_n = 1 meV), while it becomes *gray* with increasing energy and above 100 eV it is nearly *transparent*, i.e. the response ratio is practically equal to the number density ratio.

If the counter is embedded in a moderator then the response is mainly caused by thermalized neutrons. The thermalization is incomplete for high-energy incident neutrons and small spheres. However, this results only in a small energy dependence of the response

ratio as can be seen in Figure 6.9. We find that a reduction of the gas pressure by 14 % from the nominal value of 200 kPa results in a reduction of response by about 7 %, which is in agreement with the findings of Thomas [19]. A closer look at Figure 6.9 shows that in both cases the response ratio decreases slowly with increasing neutron energy.

6.3 The influence of the polyethylene mass density on the response

The dependence of the Bonner sphere responses on the polyethylene density is also investigated in References [18] and [19], in the latter, values of $(\mathrm{d}R/R)/(\mathrm{d}\rho/\rho)$ are reported for all sphere diameters and neutron energies considered.

The whole set of calculations reported in this work up to now uses the polyethylene mass density of the PTB-C set $\rho_{\mathrm{PE}} = \rho_0 = 0{,}946\ \mathrm{g/cm^3}$ (see also Appendix C). The results for $R_d(E_\mathrm{n})$ are obtained as functions of discrete arguments d and E_n. Nevertheless, maintaining d as a discrete parameter and treating the responses as continuous functions of energy, we were able to interpolate in energy and obtain response values for any energy between 1 meV and 20 MeV that were not included in the MCNP calculations.

In a similar way, we can keep the neutron energy E_n as a discrete parameter and treat the responses as continuous functions of sphere diameter d by applying cubic spline interpolations. In Figure 6.10 such continuous response functions are shown as solid lines for 6 different neutron energies, namely 1 meV, 100 meV, 10 eV, 1,2 keV, 144 keV and 14,8 MeV, which are based on response values calculated with $\rho_0 = 0{,}946\ \mathrm{g/cm^3}$. For more clarity we denote these functions as $R(d; E_\mathrm{n}, \rho_0)$ (only in this section), where d is a *continuous argument*, E_n is a discrete argument and ρ_0 is a fixed parameter. With $R(d_0; E_\mathrm{n}, \rho_0)$ we designate MCNP calculated response values for the sphere diameters contained in the PTB-C set.

The functions $R(d; E_\mathrm{n}, \rho_0)$ can be used to obtain response values for sphere diameters which are not included in the MCNP calculations. The cubic spline interpolations in sphere diameter can be applied to any energy E_n for which MCNP calculations were done, provided that the polyethylene density remains unchanged.

In the following we will examine whether the cubic spline interpolations in sphere diameter can be used to obtain response values for Bonner spheres with a polyethylene density different to that used in our MCNP calculations.

For that purpose we repeated the MCNP calculations with our realistic geometry model for three sphere diameters, 3.5", 5" and 7", at the six neutron energies indicated in Figure 6.10, using polyethylene density values that are different to ρ_0. We obtained the following response values: $R(d_0; E_\mathrm{n}, \rho_-)$ (marked "∇" in Figure 6.10) using the smaller polyethylene density $\rho_- = 0{,}92\ \mathrm{g/cm^3}$, and $R(d_0; E_\mathrm{n}, \rho_+)$ (marked "Δ" in Figure 6.10) using the larger polyethylene density $\rho_+ = 0{,}97\ \mathrm{g/cm^3}$.

A certain modification, $\Delta\rho$, of the polyethylene density ρ keeping the sphere volume V constant implies a corresponding modification, Δm, of the sphere mass m so that

$$\left(\frac{\Delta m}{m}\right)_{V=\mathrm{const.}} = \frac{\Delta\rho}{\rho}\,.$$

Let us now produce the same modification of the mass keeping the polyethylene density

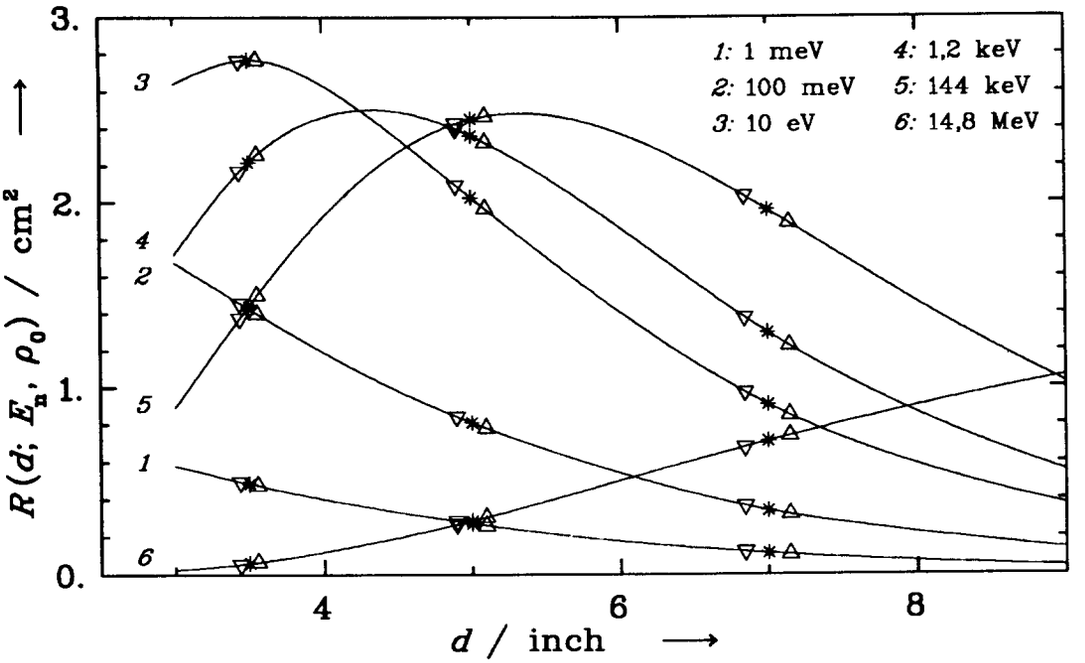

Figure 6.10: Responses $R(d; E_n, \rho_0)$ as a function of sphere diameter d for six different energies E_n using the polyethylene density $\rho_0 = \rho_{PE}$ of the PTB-C set: the solid lines are cubic spline interpolations of the point data calculated for 9 sphere diameters from 3" to 10". The points marked by ✱ indicate the data for the 3.5", 5" and 7" spheres. The symbols ∇ and Δ are explained in the text.

constant and changing the sphere volume so that

$$\left(\frac{\Delta V}{V}\right)_{\rho=\text{const.}} = \left(\frac{\Delta m}{m}\right)_{\rho=\text{const.}} \simeq \left(\frac{\Delta m}{m}\right)_{V=\text{const.}} = \frac{\Delta\rho}{\rho},$$

and consider for the moment that this modification in sphere volume has the same influence on the fluence response as the modification in polyethylene density. The modification in volume is equivalent to a modification in sphere diameter

$$\frac{\Delta d}{d} = \sqrt[3]{1+\frac{\Delta V}{V}} - 1 = \sqrt[3]{1+\frac{\Delta\rho}{\rho}} - 1\,.$$

This allows us to calculate modified sphere diameters d_+^V and d_-^V which "simulate" the modified polyethylene densities ρ_+ and ρ_-, respectively. For these modified diameters, using cubic spline interpolation in sphere diameter, we obtain the "simulated" responses $R(d_+^V; E_n, \rho_0)$ and $R(d_-^V; E_n, \rho_0)$ for each of the six energies and the three sphere diameters. The superscript V for the modified diameter indicates that the relative modification of the polyethylene density was transferred to the sphere volume. If the "simulation" is successful the ratios

$$\frac{R(d_+^V; E_n, \rho_0)}{R(d_0; E_n, \rho_+)} \quad \text{and} \quad \frac{R(d_-^V; E_n, \rho_0)}{R(d_0; E_n, \rho_-)} \tag{6.1}$$

should have values very close to unity. These ratios are shown in Figure 6.11 (as "Δ" and "∇", respectively) and their rather large deviations from unity indicate a "bad simulation".

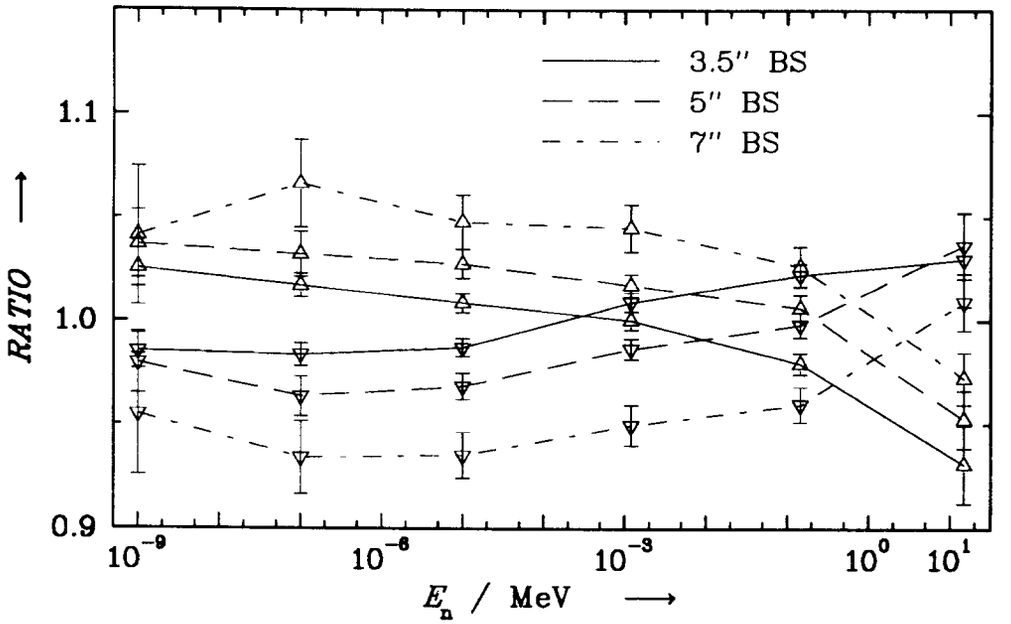

Figure 6.11: Ratios of "simulated" responses (regarding sphere volume) to calculated ones as defined in Eq. (6.1) for three different spheres. For details see text.

Let us now try another "simulation" with a modification of the *total wall thickness* of a sphere, $t = d_0 - d_c$, where $d_c = 3,3\,\mathrm{cm}$ is the outer diameter of the central counter, with

$$\left(\frac{\Delta t}{t}\right)_{\rho=\mathrm{const.}} = \frac{\Delta\rho}{\rho}.$$

This allows us to calculate modified sphere diameters d_+^t and d_-^t which "simulate" the modified polyethylene densities ρ_+ and ρ_-, respectively. For these modified diameters, using cubic spline interpolation in sphere diameter, we obtain the "simulated" responses $R(d_+^t; E_n, \rho_0)$ and $R(d_-^t; E_n, \rho_0)$ for each of the six energies and the three sphere diameters. The superscript t for the modified diameter indicates that the relative modification of the polyethylene density was transferred to the total wall thickness. If the "simulation" is successful the ratios

$$\frac{R(d_+^t; E_n, \rho_0)}{R(d_0; E_n, \rho_+)} \quad \text{and} \quad \frac{R(d_-^t; E_n, \rho_0)}{R(d_0; E_n, \rho_-)} \tag{6.2}$$

should have values very close to unity. These ratios are shown in Figure 6.12 ("▲" and "▼", respectively) together with the response ratios

$$\frac{R(d_0; E_n, \rho_+)}{R(d_0; E_n, \rho_0)} \quad \text{and} \quad \frac{R(d_0; E_n, \rho_-)}{R(d_0; E_n, \rho_0)}, \tag{6.3}$$

marked as "Δ" and "∇", respectively. While the influence of the modified polyethylene densities on the responses calculated by MCNP (ratios indicated by open triangles) can attain 11 %, the "simulated" responses remain very close to the calculated ones (ratios indicated by solid triangles).

In the literature log-normal distributions are sometimes used to fit response values [13, 18], which allow them the description of a Bonner sphere response matrix by means of only

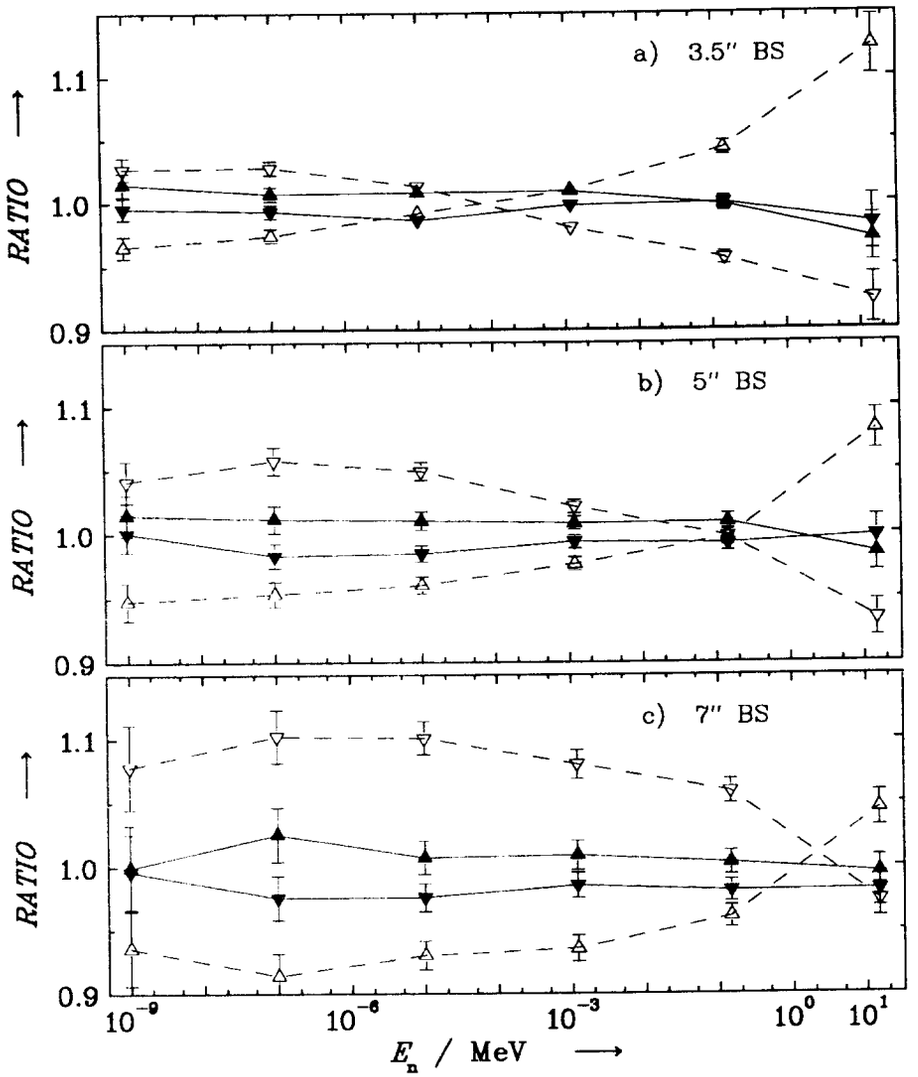

Figure 6.12: Ratios of "simulated" responses (regarding wall thickness) to calculated ones as defined in Eqs. (6.2) and (6.3) for three different spheres. For details see text.

a few parameters, usually the sphere diameter (or radius) and three further parameters that are energy dependent. If such a description of the response is used, one should keep in mind that a given set of parameters is valid only for a given polyethylene mass density, although this parameter does not appear in the given log-normal equation. The same caution is necessary if the hybrid log-normal parameterization of Mares and Schraube [15] is used. In this case the energy independent parameter d (sphere diameter) is replaced by the mass m of the sphere and four further parameters, energy dependent, are given. The fact that the analytic description obtained with these parameters succeeds to properly fit the data should not lead to the conclusion that the sphere mass m is a good parameter to replace the two independent parameters d and ρ (see the unsuccessful simulation we have illustrated in Figure 6.11).

In exchange, the use of cubic spline interpolations in sphere diameter to take into account changes in diameter, combined if necessary with simulations of type $\Delta t/t = \Delta\rho/\rho$ (as illustrated in Figure 6.12) in order to adjust the responses for changes in polyethylene density, are recommended.

6.4 Angular-dependent response of the Bonner sphere spectrometer

The characterization of Bonner spheres always includes the isotropic response as one of their major advantages. This becomes evident if one thinks of the spherical geometry of the system. Since the experiments as well as the calculations have been reduced to a homogeneous uni-directional neutron field in this section we analyze the influence of the angle of incidence on the response of the Bonner spheres.

The angle of incidence $\varphi \in [0°, 180°]$ is defined as the angle between the direction of flight of the incoming neutrons and the stem as $\varphi = 0°$, so that the neutrons move parallel to the symmetry axis from the nose to the stem, i.e. in a positive y-direction in Figure 4.1. $\varphi = 0°$ was used in the measurements with the 12 Bonner spheres reported in Reference [7].

If there is a deviation from the isotropic response, then we expect it to be largest for the smaller sphere diameters for which the relative deviation from a spherical symmetry is larger. We have performed an analysis for a) the bare detector, b) the 3" and c) the 8" and 12" Bonner spheres.

6.4.1 Angular-dependent response of the bare detector

In contrast to the setup for the irradiation of the 12 Bonner spheres, the angle φ for the irradiation of the bare detector with thermal neutrons [8], i.e. the counter without any polyethylene sphere, was 90°.

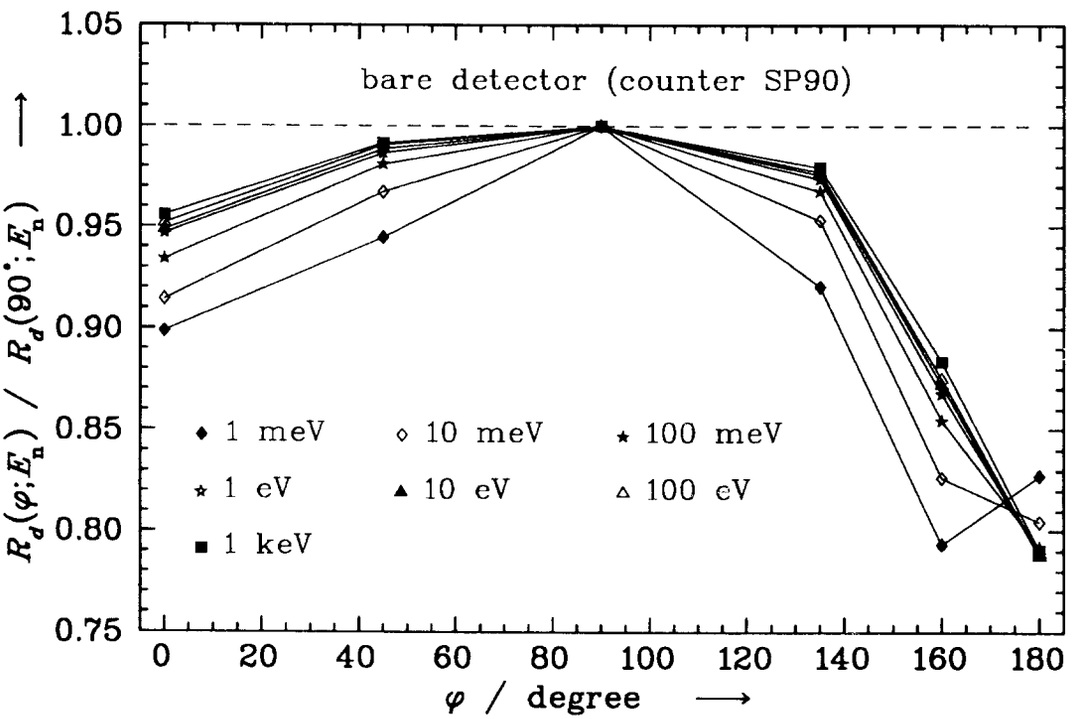

Figure 6.13: Ratios $R_d(\varphi; E_n)/R_d(90°; E_n)$ of the responses of the bare detector in a homogeneous neutron field at angles φ and 90° (used in measurements with thermal neutrons for the bare detector [8]) for various neutron energies E_n as a function of the angle.

Figure 6.13 shows the ratios of responses $R_d(\varphi; E_n)$ to $R_d(90°; E_n)$ as a function of the angle φ for the bare detector.

The bare ^{3}He-filled proportional counter is by no means an instrument with an isotropic response. The response decreases by 5 to 10 % if the neutrons impinge first on the *nose*, $\varphi = 0°$, and by about 17 to 21 % if they first have to transverse the *stem*. The anisotropy decreases systematically with increasing neutron energy.

If measurements are done in a unknown neutron field with the bare detector, one has to make sure that either a preferred neutron direction is determined, or in fields where neutrons impinge isotropic on the counter, the response must be carefully corrected by an appropriate factor.

6.4.2 Angular-dependent response of the 3" sphere

Figure 6.14 shows the ratio of responses $R_d(\varphi; E_n)$ to $R_d(0°; E_n)$ as a function of the angle φ for the 3" sphere.

These ratios are shown for five energies E_n from 1 meV to 1,2 MeV; the solid lines only connect the symbols of the same energy. If the ratios at various angles are compared, practically no systematic energy dependence is seen.

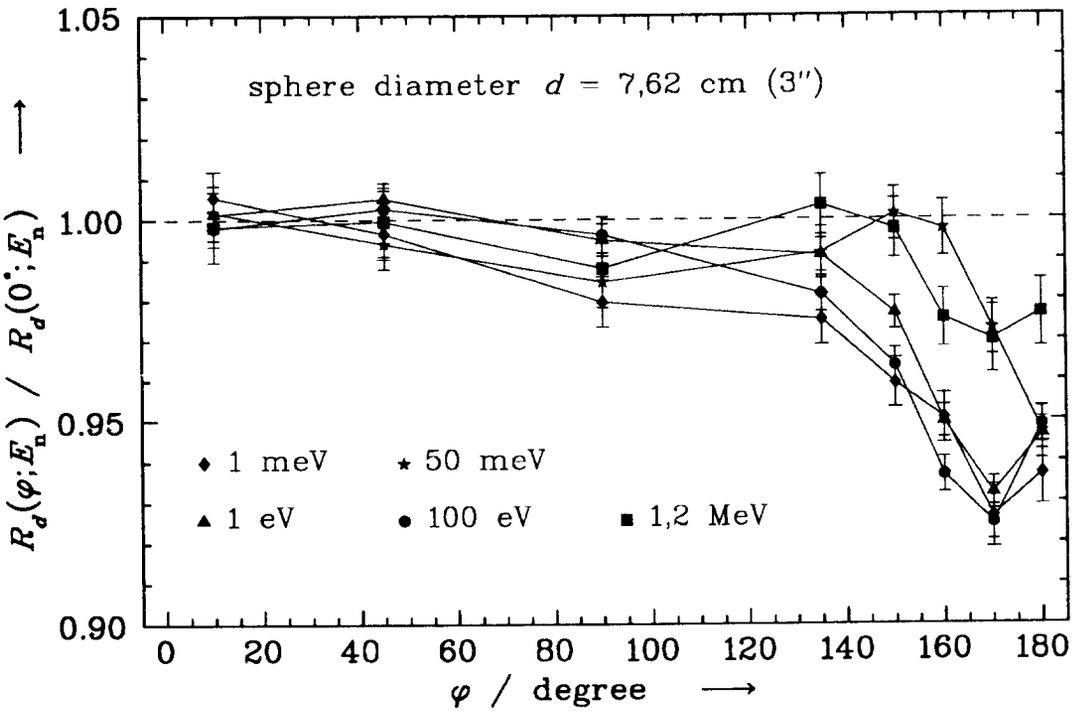

Figure 6.14: Ratios $R_d(\varphi; E_n)/R_d(0°; E_n)$ of the responses of the 3" Bonner sphere in a homogeneous neutron field at an angle φ and 0° (used in measurements [7, 8] for the spheres) for various neutron energies E_n as a function of the angle.

The response is constant within the uncertainties for angles $\varphi \leq 45°(\approx 0,15\,\Omega$, with $\Omega = 4\pi$ as the total solid angle) and then decreases slightly by about 2 % for increasing angles up to $\varphi \approx 140°(\approx 0,73\,\Omega)$. For irradiation at even larger angles that cover only 12 % of the total solid angle, the response is reduced in the mean by about 5 % compared

to the reference angle $\varphi = 0°$. From this we conclude that in an isotropic neutron field the response of the 3" Bonner sphere is at most 2 % smaller than in a directional homogeneous field with $\varphi = 0°$.

6.4.3 Angular-dependent response of the other spheres

To test the angular dependence of the response of the other 11 spheres we selected the 8" and the 12" sphere at $E_n = 1$ eV and 1,2 MeV with angles $\varphi = 90°$ and 170°. These results, as given in Table 6.1, confirm the statement that the Bonner sphere system is a spectrometer with isotropic response.

For smaller spheres the general tendency for the response to decrease with increasing angle can be explained by the increasing probability that the first interaction of the incoming neutron takes place in the stem instead in the polyethylene. This probability also depends on the neutron energy, so we get these complicated dependences on the angle for each individual energy.

Table 6.1: Ratios $R_d(\varphi; E_n)/R_d(0°; E_n)$ for the 8" and 12" Bonner spheres at two different angles φ of irradiation.

	8"		12"	
E_n	90°	170°	90°	170°
1 eV	0,997 ± 1,2%	1,011 ± 1,2%	1,023 ± 3,5%	1,023 ± 3.5%
1.2 MeV	0,994 ± 0,8%	0,999 ± 0,8%	0,991 ± 1,3%	0,993 ± 1,3%

6.5 Comparison of calculations and measured responses

Calculations of response functions allow physical insight and a basic understanding of them to be gained. Beyond this is the need for calculations as a means of appropriate interpolation between the few experimental calibration energies. The list of available experimental energies $E_x \in$ {thermal, 1,17 keV, 8,15 keV, 27,4 keV, 71 keV, 144 keV, 250 keV, 425 keV, 565 keV, 1,2 MeV, 5 MeV and 14,8 MeV} leaves a large gap between thermal neutrons and 1,17 keV neutrons, but this is the region where the small spheres are most sensitive.

At first we will consider the experimental results with monoenergetic neutrons reported in Reference [7] for the PTB-C Bonner sphere set. The parameters used in our calculations (see Table 5.2) as well as the sphere diameters and neutron energies were so selected that a direct comparison can be made.

For each measured response value $R_{d,E}^{meas}$ for sphere d at the experimental neutron energy E_x reported in [7] we calculate the ratios[c]

$$r_{d,E} = \frac{R_{d,E}^{calc}}{R_{d,E}^{meas}} \quad \text{and} \quad r_{d,E}^{-1} = \frac{R_{d,E}^{meas}}{R_{d,E}^{calc}} \tag{6.4}$$

where $R_{d,E}^{calc}$ is the value calculated in this work for the sphere d at neutron energy E_x. The corresponding relative uncertainties are given by

$$u(r_{d,E}) = u(r_{d,E}^{-1}) = \sqrt{u^2(R_{d,E}^{calc}) + u^2(R_{d,E}^{meas})}\,. \tag{6.5}$$

[c] If the experimental energy E_x is used as an index it will be abbreviated to E.

Deviations of the $r_{d,E}$ and $r_{d,E}^{-1}$ values from the ideal value of 1 are expected to be random due to their uncertainties. However, to verify this assumption, a detailed examination of these ratios will be made in the following two subsections.

6.5.1 Comparison for all spheres at a specified energy

The response ratios $r_{d,E}$ are plotted *vs.* sphere diameter in Appendix F, Figures F.1 and F.2, for each calibration energy E_x used in Reference [7] and diameters for which calibrations were performed at that energy. Only three points were excluded, namely those corresponding to the 3", 3.5" and 4" spheres at 14,8 MeV. In all these cases the response values are very low and the ratio values clearly deviate from the others, probably due to too large target-scattering corrections [7] (factors of 0,68, 0,75 and 0,80) applied at this energy for these spheres.

For each ratio, we plotted two uncertainty bars which represent standard deviations $s(r_{d,E})$. The left (thin) bar represents the contribution to the standard deviation of the ratio due to the uncertainty of uncorrelated quantities contributing to the measurements, the right (thick) bar gives the total uncertainty of the ratio, including the statistical contribution from the Monte Carlo calculation.

The weighted mean value r_E for a given experimental energy E_x was calculated from

$$r_E = \langle r_{d,E} \rangle_E = \frac{\sum_d^{n_d} r_{d,E}/s^2(r_{d,E})}{\sum_d^{n_d} 1/s^2(r_{d,E})}, \tag{6.6}$$

which is essentially Equation (A.15) if one fits "1" ($C_i \equiv 1$) to the ratios $r_{d,E} (= M_i)$. n_d indicates the number of spheres which were calibrated at the given neutron energy and taken into account for r_E. The variance of r_E is calculated by

$$s^2(r_E) = \frac{1}{\sum_d^{n_d} 1/s^2(r_{d,E})}. \tag{6.7}$$

The numerical values are printed in each diagram of Figures F.1 and F.2. All values r_E, $u(r_E) = s(r_E)/r_E$ and χ^2_r are summarized in Table 6.2. The factors f_E are defined as

$$f_E := \langle r_{d,E}^{-1} \rangle_E \neq \langle r_{d,E} \rangle_E^{-1}, \tag{6.8}$$

they fit the calculated responses to the measured ones and are also listed in Table 6.2. Since $u(f_E)$ and the corresponding reduced chi-square practically do not differ from those of r_E they are not listed. Although the values of f_E are in principle not equal to r_E^{-1} they remain very close to these (the largest deviation of 0,32 % is seen at $E_x = 5$ MeV).

As already mentioned in Section 3, the uncertainties reported in References [7] and [8] are total uncertainties, also taking into account correlations. Since we have at our disposal more detailed information than reported in these references, we were able to separate the contribution shown in the last column of Table 6.2, $u^{\mathrm{cor}}(R^m)$, which is the part of the total uncertainty of a measured fluence response due to correlations, and common to all responses measured at a given neutron energy. In most cases this correlated part of the uncertainty is mainly due to the fluence determination method, which in all cases contributes about 3 %, or even less. Nevertheless, an additional contribution in the

Table 6.2: Weighted mean values r_E of ratios $r_{d,E}$ for all diameters at a given experimental neutron energy E_x, their relative uncertainties $u(r_E)$, and the reduced chi-square χ^2_r (data correspond to Figures F.1 and F.2); n_d indicates the number of spheres which were calibrated at the given energy; f_E is the factor which fits the calculated responses to the measured ones. $u^{cor}(R^m)$ is the part from the total uncertainty of a measured fluence response due to correlations, and common to all data obtained at a given neutron energy. The data at thermal energies from the last row will be discussed in Section 6.5.3.

E_x	n_d	f_E	r_E	$u(r_E)$ %	χ^2_r	$u^{cor}(R^m)$ %
1,17 keV	2	1,0863	0,9204	3,62	0,06	8,5
8,15 keV	10	1,0916	0,9140	1,01	0,81	8,5
27,4 keV	9	1,0227	0,9774	0,82	0,29	4,8
71 keV	10	1,0707	0,9335	0,37	1,46	2,5
144 keV	11	1,0993	0,9073	0,42	4,59	4,6
250 keV	10	1,0657	0,9370	0,29	6,13	4,1
425 keV	2	1,1048	0,9050	4,29	0,02	3,3
565 keV	11	1,0204	0,9790	0,39	2,30	3,1
1,2 MeV	12	1,0509	0,9500	0,41	2,87	4,0
2,5 MeV	12	1,1140	0,8968	0,37	2,06	4,0
5 MeV	11	1,1440	0,8713	0,47	4,82	4,0
14,8 MeV	9	1,0997	0,9083	0,55	1,59	4,1
NPL-therm	10	0,9716	1,0282	0,92	0,46	2,3

experiment is due to deviations in the monitor readings during the fluence determination, and this increased the correlation part of the uncertainty especially at the lowest energies, where resonant reactions near threshold are used to produce the monoenergetic neutrons.

The values obtained for the mean response ratios r_E are indicated in Figures F.1 and F.2 by thick horizontal lines. The inner (thin) uncertainty bars plotted at both ends of these lines represent $s(r_E)$ while the outer (thick) bars represent the total uncertainty of r_E, which is obtained through quadratic summation of $u(r_E)$ and $u^{cor}(R^m)$.

An examination of Figures F.1 and F.2 reveals that there is practically no systematic tendency in the distribution of the $r_{d,E}$ values about their mean r_E, except for energies E_x = 144 keV, 250 keV and 5 MeV, where also the reduced chi-square values are large ($\chi^2_r > 4$). The systematic increase of the $r_{d,E}$ values with the sphere diameter at 144 keV and 250 keV can be partially explained if one assumes that the real neutron energies in the experiment were smaller by a few percent than the reported ones.

The dependence of the mean response ratios r_E on neutron energy which is given numerically in Table 6.2, is shown in Figure 6.15. Their uncertainties include the correlation contributions from the experiment. Furthermore, the ratios $r_{d,E}$ are considered as uncorrelated from one neutron energy to another, and the standard deviations $s(r_{d,E})$ are used to calculate the weighted mean of r_E, $\langle r_E \rangle$, the weighted mean of f_E, $\langle f_E \rangle$, and the standard deviations of these weighted mean values. As the r_E (the same being valid for f_E) are partly correlated, the value obtained for the relative uncertainty of $\langle r_E \rangle$,

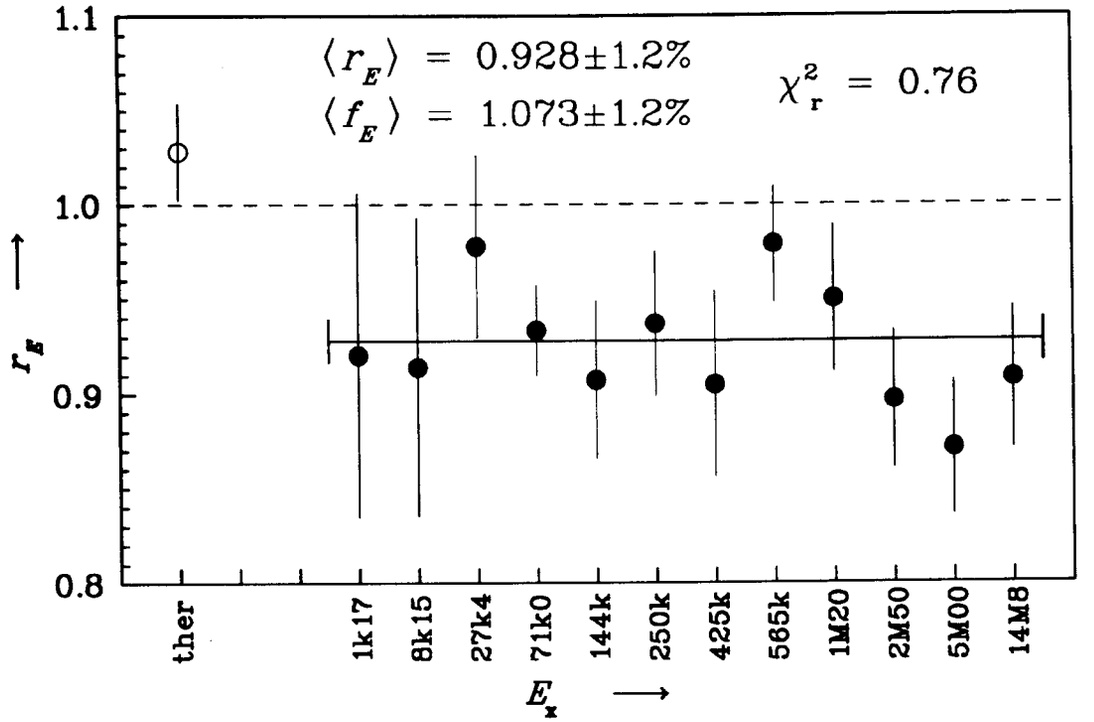

Figure 6.15: Mean ratios r_E of calculated to measured responses if all spheres at a given calibration energy E_x are considered; the bars represent their total uncertainty. The weighted mean of r_E, $\langle r_E \rangle$, and its standard deviation is plotted as a horizontal line with uncertainty bars at both ends. The weighted mean of the fit factors f_E, $\langle f_E \rangle$, is only given numerically. The point at thermal energy will be discussed in Section 6.5.3.

$u(\langle r_E \rangle) = 1.2$ %, is underrated (the same being valid for $\langle f_E \rangle$).

The data point shown in Figure 6.15 at thermal energy will be discussed in Section 6.5.3. This point was not included in $\langle r_E \rangle$ or $\langle f_E \rangle$, and is plotted here only for comparison with the other points and their mean. The spread of the points obtained with monoenergetic neutrons about their mean does not show any systematic tendency, and is generally well described by their uncertainties. The somewhat larger deviations at 565 keV and 5 MeV can be attributed to additional experimental uncertainties in the fluence determinations which could not be corrected and not reflected in the evaluated uncertainties.

6.5.2 Comparison at all energies for a specified sphere

The following analysis is very similar to that of the previous subsection.

In Figures F.3 and F.4, Appendix F, the response ratios $r_{d,E}$ are plotted for each sphere diameter used in [7] *vs.* all neutron energies for which calibrations were performed for that sphere. For reasons already mentioned, only three points were excluded, namely those corresponding to the 3", 3.5"and 4" spheres at 14,8 MeV. The data at thermal energies are not included.

The uncertainty bars shown in these figures represent: left (thin): the contribution to the standard deviation of the ratio due to the total measurement uncertainty, right (thick):

the total uncertainty of the ratio, including the statistical contribution from Monte Carlo calculations.

The weighted mean value r_d for a given sphere diameter d was calculated from

$$r_d = \langle r_{d,E} \rangle_d = \frac{\sum_E^{n_E} r_{d,E}/s^2(r_{d,E})}{\sum_E^{n_E} 1/s^2(r_{d,E})}, \tag{6.9}$$

and its variance from

$$s^2(r_d) = \frac{1}{\sum_E^{n_E} 1/s^2(r_{d,E})}, \tag{6.10}$$

Table 6.3: Weighted mean values r_d of ratios $r_{d,E}$ at all energies for a given sphere diameter d, their relative uncertainties $u(r_d)$, and the reduced chi-square χ^2_r (data correspond to Figures F.3 and F.4); n_E indicates the number of neutron energies at which the given sphere was calibrated; f_d is the factor which fits the calculated responses to the measured ones. The data for the bare detector from the last row will be explained in Section 6.5.3.

d	n_E	f_d	r_d	$u(r_d)$ %	χ^2_r
3"	11	1,0539	0,9404	1,37	1,68
3.5"	9	1,0661	0,9325	1,38	1,32
4"	10	1,0780	0,9227	1,34	1,13
4.5"	10	1,0838	0,9166	1,32	1,48
5"	10	1,0810	0,9218	1,25	0,84
6"	10	1,0737	0,9289	1,30	0,58
7"	10	1,0772	0,9257	1,31	0,60
8"	10	1,0663	0,9334	1,31	1,03
10"	10	1,0554	0,9425	1,34	1,09
12"	8	1,0500	0,9439	1,66	1,50
15"	6	1,0029	0,9875	1,86	1,88
18"	4	1,0835	0,9208	2,27	0,48
bare d.	1	0,9935	1,0065	2,88	–

The numerical results are given in Table 6.3, n_E is the number of neutron energies at which the given sphere was calibrated and taken into account for the calculation of r_d. Similar to the previous subsection the factors f_d

$$f_d := \langle r_{d,E}^{-1} \rangle_d \neq \langle r_{d,E} \rangle_d^{-1} \tag{6.11}$$

fit the calculated responses to the measured ones for the specified sphere. Here the largest deviation of f_d from r_d^{-1} is 0,97 % for the 15" sphere.

The values obtained for the mean response ratios r_d are indicated in Figures F.3 and F.4 by thick horizontal lines. The small uncertainty bars plotted at both ends of these lines represent $s(r_d)$.

As already mentioned, the results from Table 6.3 are obtained using as uncertainties of the response ratios $r_{d,E}$ the total standard deviations that include the uncertainty from the Monte Carlo calculations as well as the correlated and uncorrelated contributions of the measured quantities. The ratios $r_{d,E}$ are used here as uncorrelated. However, they are partly correlated, and for this reason the standard deviations $s(r_d)$ are underrating the theoretical standard deviations.

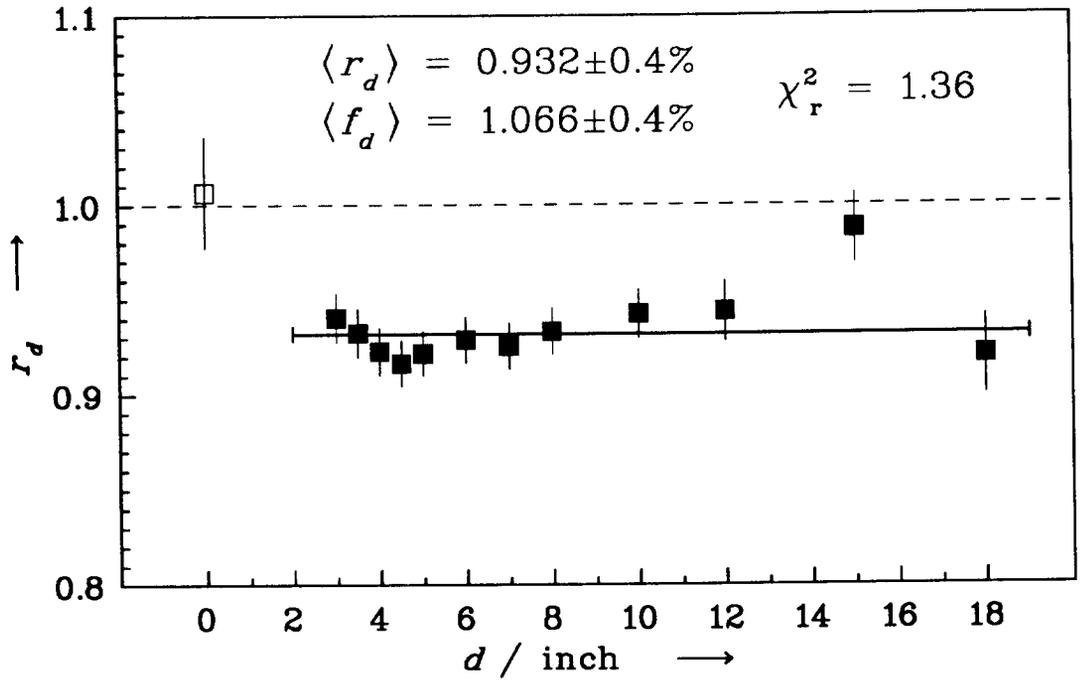

Figure 6.16: Mean ratios r_d of calculated to measured responses if all calibration energies (except thermal energy) for a given sphere diameter d are considered; the bars represent their total uncertainty. The weighted mean of r_d, $\langle r_d \rangle$, and its standard deviation are plotted as a horizontal line with uncertainty bars at both ends. The weighted mean of the fit factors f_d, $\langle f_d \rangle$, is only given numerically. The data point for the bare detector ($d = 0$) will be discussed in Section 6.5.3.

An examination of Figures F.3 and F.4 reveals some systematic tendencies in the distribution of the $r_{d,E}$ values about their mean r_d. Maxima are seen at 27,4 keV and 565 keV for practically all sphere diameters, and minima are seen at 5 MeV for small spheres up to the 6" sphere. This behavior is similar to that seen in Figure 6.15 and can be attributed to some experimental problems during the fluence determination. In spite of this, the values obtained for the reduced chi-square are relatively low. This situation can be explained by the fact that the relatively large total experimental uncertainties were used, but the possible correlation was neglected.

The dependence of the mean response ratio r_d on sphere diameter which is given numerically in Table 6.3 is shown in Figure 6.16. The r_d are considered as uncorrelated from one sphere diameter to another, and the uncertainties $s(r_d)$ are used to calculate the weighted mean of r_d, $\langle r_d \rangle$, the weighted mean of f_d, $\langle f_d \rangle$, and the standard deviations of these mean values. As mentioned before, the uncertainties of the r_d values are possibly underrated, and consequently the value obtained for the relative uncertainty of $\langle r_d \rangle$,

$u(\langle r_d \rangle) = 0.4$ %, is also underrated (the same being valid for $\langle f_d \rangle$).

The point shown in Figure 6.16 for the bare detector ($d = 0$) will be discussed in the next subsection. This point was not included in $\langle r_d \rangle$ or $\langle f_d \rangle$, and is plotted here only for comparison with the other points and their mean.

The spread of the points obtained with monoenergetic neutrons about their mean does not show any systematic tendency, and is generally well described by their uncertainties, even if they were underrated. Indeed, practically all r_d values lie close to their weighted mean $\langle r_d \rangle$ within less than ±2 %. The only exception is the r_d value for the 15" sphere which deviates from $\langle r_d \rangle$ by $3s$. No explanation was found yet for such a deviation, but examining Figures F.3 and F.4 it might be concluded that it could be pure chance: the data point at 5 MeV which should be low, is missing in the measurements. Points for the four lowest energies are also missing because the response values are very low and were not measured. On the other hand, the points at 144 keV and 250 keV where the response values are still low, are measured but they have large r_d values.

Examining Figures 6.15 and 6.16 and taking into account a possible underrating of the standard deviations obtained for the mean response ratios or fit factors, one may conclude that for the total set of data with monoenergetic neutrons for which we have determined

$$\langle r_E \rangle = 0,928 \pm 1,2\% \quad \text{and} \quad \langle f_E \rangle = 1,073 \pm 1,2\% \tag{6.12}$$

and

$$\langle r_d \rangle = 0,932 \pm 0,4\% \quad \text{and} \quad \langle f_d \rangle = 1,066 \pm 0,4\% \tag{6.13}$$

we may deduce common values

$$\langle r \rangle = 0,930 \pm 1,8\% \quad \text{and} \quad \langle f \rangle = 1,070 \pm 1,8\% \tag{6.14}$$

valid for all spheres and all energies in the range from 1,17 keV to 14,8 MeV.

6.5.3 Comparison for all spheres at thermal energies

The measurements of the fluence responses reported in Reference [8] were performed in the thermal neutron field at NPL Teddington, UK that can be described as follows:

$$\Phi_E^{\text{th}}(E) = 0,9693 \cdot \Phi_E^{\text{M}}(E) + 0,0307 \cdot \Phi_E^{\text{e}}(E) \tag{6.15}$$

where

$$\Phi_E^{\text{M}}(E) = \begin{cases} C^{\text{M}} \cdot E \cdot e^{-E/kT} & 1 \text{ meV} \leq E \leq 512 \text{ meV} \\ 0 & \text{otherwise} \end{cases} \tag{6.16}$$

is the Maxwellian component with $kT = 0,0272$ eV (for the NPL thermal field), and

$$\Phi_E^{\text{e}}(E) = \begin{cases} C^{\text{e}}/E & 100 \text{ meV} \leq E \leq 512 \text{ meV} \\ 0 & \text{otherwise} \end{cases} \tag{6.17}$$

is a slowing-down component below the cadmium cut-off. The constants C^{M} and C^{e} are chosen so that the integral fluence of each component is normalized to unity, in which case the thermal fluence given in Equation (6.15) is also normalized to unity.

The calculated responses as point values can no longer be directly compared with the measured responses in the thermal field. For a comparison, we simulate the sphere readings in the NPL thermal field using Equation (A.3) from Appendix A, with the spectral

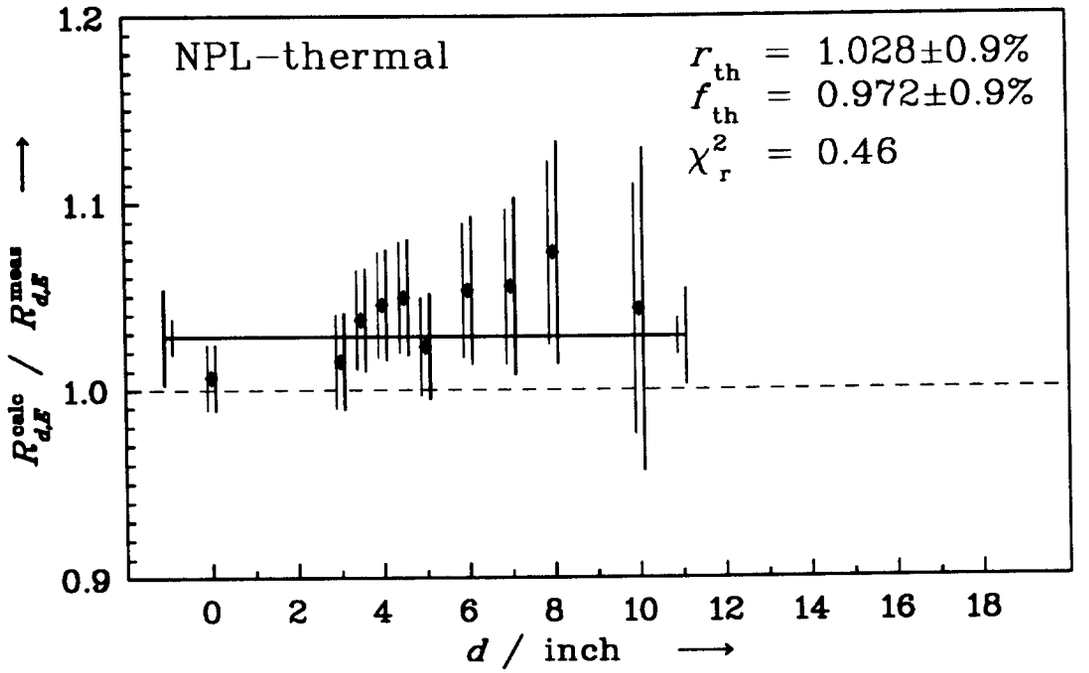

Figure 6.17: Ratios $r_{d,th}$ of calculated to measured responses in the NPL thermal field. The uncertainty bars represent: left, the contribution to the standard deviation of the ratio due to the uncertainties of uncorrelated measuring quantities; right, the total uncertainty of the ratio, including the contribution from the Monte Carlo calculations. r_{th} is the weighted mean value of $r_{d,th}$ for all diameters and f_{th} is the factor which fits the calculations to measurements. The horizontal line with uncertainty bars at both ends indicates the value of the mean ratio r_{th} and its standard deviations, taking into account the uncertainties of the uncorrelated part of the $r_{d,th}$ (small) and the total uncertainty (large).

fluence taken from Equations (6.15) to (6.17), E_{min} = 1 meV and E_{max} = 512 meV. As the calculated responses $R_d(E_n)$ are only available as point data, the integral is calculated numerically as in Equation (A.6), and in order to ensure a good numerical precision, in this interval we use 20 energy values per decade, logarithmic equidistant, the response at these energies being obtained through lin-log spline interpolations and the fluence values being calculated analytically.

The ratios of simulated responses to measured ones are shown in Figure 6.17. The treatment of the data exactly follows the procedure explained in Section 6.5.2, the relative uncertainty due to correlations of the measured fluence in the NPL thermal field is $u^{cor}(R^m) = 2,3$ %. The results for the weighted mean response ratio of all diameters, its relative uncertainty due to uncorrelated response ratios and its total relative uncertainty is:

$$r_{th} = 1,028; \quad u^{unc}(r_{th}) = 0,9\%; \quad u^{tot}(r_{th}) = 2,5\%.$$

The results obtained for the factor which fits the calculations to measurements are:

$$f_{th} = 0,972; \quad u^{unc}(f_{th}) = 0,9\%; \quad u^{tot}(f_{th}) = 2,5\%.$$

These results were included in Table 6.2 in the last row, and plotted in Figure 6.15 as a point at *thermal* energy with its total uncertainty.

For the bare detector only the experimental result in the thermal energy region is significant, so in this case (sphere diameter d=0) only a single response ratio is obtained, $r_{0,th} = 1{,}0065$, which is at the same time the mean response ratio r_0 for this detector at all energies. For this value, we calculate a relative uncertainty $u^{unc}(r_0) = 1{,}73$ % (treating the measurands as uncorrelated) and a total relative uncertainty of $u(r_0) = 2.88$ % (including the correlations from the fluence determination). These data are included for comparison in Table 6.3 and in Figure 6.16.

The mean ratios r_E and r_d from Figures 6.15 and 6.16, respectively, which were calculated here at thermal energies, are larger by 8 % to 10 % than those obtained with monoenergetic neutrons at higher energies and they were not included in the calculations of $\langle r_E \rangle$, $\langle f_E \rangle$, $\langle r_d \rangle$ and $\langle f_d \rangle$ in the previous two subsections. We have not yet been able to find an explanation for this discrepancy.

6.6 Comparison with other calculations

Such a comparison has already been prepared in section 3 where the calculations of D.J. Thomas [19] (DJT) and Mares *et al.* [18] (MSS) were compared with measured responses for our Bonner sphere set. Here we will repeat the figure from Section 3 with small modifications, and add our results from Table 6.3. The small modifications concern only the MSS calculations. We want to compare the results in absolute values, as in fact was always the case in this work. In one detail the MSS calculations differ from the others:

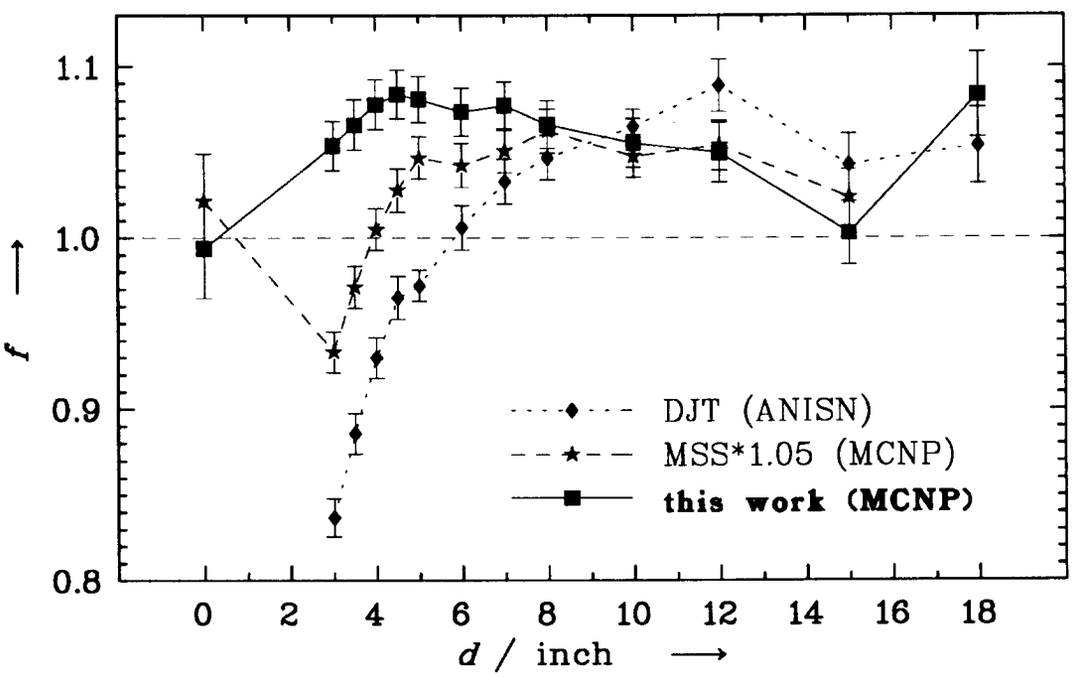

Figure 6.18: Factors f which fit calculated responses to the measured ones from Refs. [7] and [8] as a function of sphere diameter d. "◆" shows the values for the ANISN calculations from Ref. [19] (DJT); "★" shows the values for the MCNP calculations from Ref. [18] (MSS), the calculated responses being reduced for this plot by 5 %. "■" shows the fit factors obtained using the responses calculated in this work.

they do not take into account the influence of the 0,5 mm thick stainless steel (or iron) wall of the proportional counter on the response. It was estimated [27, 20] that this wall reduces practically all response values, for all spheres including the bare detector, at all energies, by about 5 %. For this reason, we plot in the new figure of the fit factor f vs. sphere diameter d, Figure 6.18, the MSS curve multiplied by 1,05.

In Figure 6.18 we were also able to introduce an MSS fit factor for the bare detector, but unfortunately it was calculated differently from ours. Instead of folding the NPL thermal spectrum with the calculated response, which is not given for energies below 10 meV, we determined a calculated response at $E_n = 40$ meV, using a lin-log spline interpolation. The response at this energy is adequate to represent the folded response of the bare detector, as we were able to prove using our more detailed calculated response. For the polyethylene spheres the behaviour of the response functions is not the same as that of the bare detector (increasing instead of decreasing with increasing energy), and the energy adequate for representing the thermal response is $E_n \simeq 50$ meV.

Figure 6.18 shows that the fit factors obtained with the three series of calculations agree all quite well within their uncertainties, even in absolute values, for sphere diameters larger than 7". With decreasing diameter they behave differently: for ANISN calculations and simplified geometry (DJT) they decrease rapidly; for MCNP calculations and simplified geometry (MSS) they decrease, but less rapidly. For MCNP calculations and realistic geometry (this work) they remain practically constant.

As far as the fit factors for the bare detector are concerned, also for thermal energies, the MSS value is in rather good agreement with the large sphere diameters, while our value makes a jump of about 8 % and cannot be consistently included in the rest of the data. We may conclude that our response value for the bare detector, and generally our computed responses, are correct at thermal energies, but for some yet unexplained reason, the calculated responses with monoenergetic neutrons with $E_n \geq 1,17\,\mathrm{keV}$ are too low by about 6 % to 8 %.

6.7 Response matrices for practical use

The need for accurate response functions and their application in few-channel unfolding procedures to determine energy spectra in unknown neutron fields has already been stated in the introduction. The various computer codes for unfolding Bonner sphere data require a variety of input formats for the response matrix [4], but they all need a certain structure of energy groups.

As an example we present in Table G.1 a 105×12 *response matrix* $\mathcal{R}$ with an energy binning of 10 per decade. Using n=10 and $E_1 = 10^{-3}$ eV in Equation (A.10) we get logarithmic equidistant energies E_i from 1 meV to 19,95 MeV which are the midpoints of energy bins of width ΔE_i as defined in Equation (A.12). We recall here Equation (A.8)

$$\mathcal{R}_{id} = \left(\int_{E_{l,i}}^{E_{u,i}} R_d(E_n)\, dE \right) / \Delta E_i$$

which is used to determine the matrix elements $\mathcal{R}_{id}$. It is assumed that $R_d(E_n)$ is a continuous function in energy. This function can be obtained by performing a lin-log interpolation (linear in response and logarithmic in energy) between the energies listed

in Tables D.1 to D.12. The columns of the response matrix $\mathcal{R}$ are shown as the solid polygons in Figures 6.1 to 6.6.

In order to check the accuracy of the response matrices we calculated the reading of all 12 Bonner spheres in five test spectra, i.e. in the field of a bare ^{252}Cf source and a D_2O moderated source, a ^{241}Am-Be source, a Maxwell type field ($kT = 4,3\,\mathrm{eV}$) whose shape is similar to the response of the 3" sphere, and finally a spectrum whose shape is equivalent to the response function of the 12" sphere.

The response function for the 5" sphere was calculated at fewer incident neutron energies E_n than all other spheres. To test if this data base is sufficient we calculated the reading of all spheres in the five test spectra using a response matrix determined only at those energies at which the 5" sphere responses had been calculated. For the soft Maxwell type spectrum, deviations of 0,1 % have been found only for the 3", 3.5", and 4" spheres. The use of the other spectra leads to deviations of up to 7 % with larger spheres, because the 5" energy set has only a few energies in the region where the response of the large spheres peak. When using the energy set of the 10" sphere, deviations of less than 2 % are seen for all spheres with all spectra.

As a final test we represented the response matrix using a logarithmic equidistant energy grid. The maximum deviation found for larger spheres (10" and greater) is less than 0,4 %, and less than 0,7 % using a grid with 20 or 10 points per decade. However, for 5 energy points per decade, deviations of up to 4,1 % for larger spheres are encountered. This must be borne in mind when using response matrices for unfolding algorithms. The details of the structure of the response functions for the large spheres cannot be achieved if one uses far fewer than 10 energy bins per decade.

Diskettes available

For convenience a DOS diskette is available from PTB upon request. It includes the `BSRC_PTB.DAT` data file with our calculated responses $R_d(E_n)$ listed in Tables D.1 to D.12 and four FORTRAN source code files `BSR_PROG.FOR`, `BSR_SUBR.FOR`, `BSR_SAMP.FOR` and `BSR_DISP.FOR`, which allow the data to be read, transposed and displayed.

The `BSR_PROG.FOR` program can be transferred to any computer with a FORTRAN 90 compiler and can be interactively used to

- extract the original values of the response functions in any form desired,
- adapt the response functions given in order to suit the user's system with respect to ρ_{PE}, and
- generate response matrices for use with unfolding codes, etc.

The `BSR_SUBR.FOR` file contains the appropriate subroutines for use in user-written programs and `BSR_SAMP.FOR` is a sample program to demonstrate the proper use of some subroutines.

The `BSR_DISP.FOR` program can be transferred to any PC with a MICROSOFT FORTRAN 90 (5.1) compiler and a graphic screen (VGA). It can be used to display the response functions and user-provided neutron spectra. The graphics library needed is also supplied on the diskette. The program source codes provide detailed comments.

7 Conclusions

We have introduced a realistic geometry model for a Bonner sphere spectrometer with a spherical ^{3}He proportional counter to calculate its response functions $R_d(E_n)$ using the three-dimensional MCNP Monte Carlo computer code. Sphere diameters d, ^{3}He number density and polyethylene mass density were selected to match the specifications of the PTB-C Bonner sphere set to allow a direct comparison of calibration measurements and our calculations. The detailed modeling of the interior of the proportional counter is necessary to obtain a common fit factor $\langle f \rangle = 1,07$ to adjust the calculated responses to the measurements for all sphere diameters in the neutron energy range between 1,17 keV and 14,8 MeV.

While there is a non-negligible angular dependence of the bare detector, it has been shown that the counter in conjunction with any polyethylene sphere greater than or equal to 7,62 cm (3" sphere) is an instrument with an isotropic response.

We have studied the influence of the variation of certain parameters (^{3}He number density and polyethylene mass density) on the response. The representation of the response $R_d(E_n)$ as a continuous function of sphere diameter d at a fixed energy E_n using a cubic spline interpolation allows a simple transformation of the response if the polyethylene density of a Bonner sphere system is slightly different to the value used in our calculations. The ratios of *diameter*-corrected responses to those calculated at the nominal diameter but with a different polyethylene density yield values of unity independent of energy with deviations of less than 2 %.

Structures in the response function in the energy range from 2 MeV to 8 MeV can clearly be attributed to resonances in the carbon cross sections.

There are still some open questions concerning the discrepancy a) between the ratio $r_{d=0}$ (Section 6.5.3) of the bare detector and the ratio r_d of the polyethylene spheres, and b) between the mean ratio r_{th} of the spheres for thermal energies and the ratios r_E at the experimental energies $E_x \geq 1,17$ keV. Since the results of all other comparisons performed in this report are consistent, it may be conjectured that measurements in additional thermal fields might help to establish whether the discrepancies have an experimental origin or are due to the cross section data libraries used in this work.

Finally, it can be stated that a full calculated response matrix, well supported by experimental calibration, allows an optimal use of Bonner spheres as a spectrometer and as a valuable tool for determining dosimetric properties at work places.

8 Acknowledgements

We gratefully acknowledge the cooperation of Centronic Ltd., UK, for supplying the technical drawings of the ^{3}He proportional counter SP90.

We thank Dr. E. Dietz for transposing the confidential drawings to a version free for publication.

We are very grateful to Dr. H. Klein for valuable discussions. This work was funded by the Commission of the European Communities under contract no. FI3P-CT920002.

References

[1] Bramblett, R.L., Ewing, R.I., and Bonner, T.W. *A New Type of Neutron Spectrometer.* Nucl. Instrum. Meth. **9**, 1–12 (1960).

[2] Routti, J.T. and Sandberg, J.V. *Unfolding Activation and Multisphere Detector Data.* Radiat. Prot. Dosim. **10**, 103–110 (1985).

[3] Weise, K. *Optimisation in Neutron Spectrometry and Dosimetry with Bonner Spheres Using a General Measure of Quality for Experiments.* Radiat. Prot. Dosim. **37**, 157–164 (1991).

[4] Alevra, A.V., Matzke, M., and Siebert, B.R.L. *Experiences from an International Unfolding Intercomparison with Bonner Spheres.* In *Proc. of the Seventh ASTM-EURATOM Symposium on Reactor Dosimetry* (EU Report 14356EN), Edited by Tsotridis, G., Diercks, R., and D'Hondt, p. 215–222, Kluwer Academic Publishers, Dortecht, 1992.

[5] Alevra, A.V. and Siebert, B.R.L. *Influence of Neutron Spectra and Fluence Response Data on the Determination of Dose Equivalent with Bonner Spheres.* PTB Bericht ND-28, Physikalisch-Technische Bundesanstalt, Braunschweig, 1986.

[6] Lowry, K.A. and Johnson, T.L. *The Effect of the Choice of Response Matrix on Neutron Spectra Unfolded from Bonner Sphere Data.* Health Phys. **50**, 543–547 (1986).

[7] Alevra, A.V., Cosack, M., Hunt, J.B., Thomas, D.J., and Schraube, H. *Experimental Determination of the Response of Four Bonner Sphere Sets to Monoenergetic Neutrons (II).* Radiat. Prot. Dosim. **40**, 91–102 (1992).

[8] Thomas, D.J., Alevra, A.V., Hunt, J.B., and Schraube, H. *Experimental Determination of the Response of Four Bonner Sphere Sets to Thermal Neutrons.* Radiat. Prot. Dosim. **54**, 25–31 (1994).

[9] Burrus, W.R. *Bonner Spheres and Threshold Detectors for Neutron Spectrometer.* Report ORNL-3360, Oak Ridge National Labortory, Tennessee, 1962.

[10] McGuire, S.A. *A Dose Monitoring Instrument for Neutrons from Thermal to 100 MeV.* Report LA-3435, Los Alamos National Laboratory, 1966.

[11] Sanna, R.S. *Thirty-one Group Response Matrices for the Multisphere Neutron Spectrometer over the Energy Range Thermal to 400 MeV.* Report HASL-267, USAEC, March 1973.

[12] Dhairyawan, M.P., Nagarajan, P.S., and Venkatarman, G. *Response Functions of Spherically Moderated Neutron Detectors.* Nucl. Instrum. Meth. **169**, 115 (1980).

[13] Zaborowski, H.L. *Dosimétrie et Spectroscopie Neutronique avec les Sphères de Bonner; Etablissement d'une Matrice Log-Normal de Référence.* In *Proc. 4th Symp. on Neutron Dosimetry*, Edited by Burger, G. and Ebert, H.G., volume 1, p. 575–587. GSF, Munich-Neuherberg, FRG, June 1981.

[14] Hertel, N.E. and Davidson, J.W. *The Response of Bonner Spheres to Neutrons from Thermal Energies to 17.3 MeV.* Nucl. Instrum. Meth. **A238**, 509–516 (1985).

[15] Mares, V. and Schraube, H. *Evaluation of the Response Matrix of a Bonner Sphere Spectrometer with LiI Detector from Thermal Energy to 100 MeV.* Nucl. Instrum. Meth. **A337**, 461–473 (1994).

[16] Vylet, V. and Kumar, A. *Energy Response Bonner Spheres to Neutrons in Parallel Beam and Point Source Geometries.* Nucl. Instrum. Meth. **A271**, 607 (1988).

[17] Caizergues, R. and Poullot, G. *Calcul de la Réponse des Sphères de Bonner pour les Détecteurs à ILi, He-3 et Mn.* Rapport CEA - R - 4400, 1972.

[18] Mares, V., Schraube, G., and Schraube, H. *Calculated Neutron Response of a Bonner Sphere Spectrometer With ^{3}He Counter.* Nucl. Instrum. Meth. **A307**, 398–412 (1991).

[19] Thomas, D.J. *Use of the Program ANISN to Calculate Response Functions for a Bonner Sphere Set with ^{3}He Detector.* NPL Report RSA(EXT)31, National Physics Laboratory, Teddington, March 1992.

[20] Perks, C.A., Thomas, D.J., Siebert, B.R.L., Jetzke, S., Hehn, G., and Schraube, H. *Comparison of Response Function Calculations for Multispheres.* Radiat. Prot. Dosim. **44**, 85–88 (1992).

[21] Hehn, G., Schweizer, M., and Haas, K. *New Calculations of Neutron Response Functions of Bonner Spheres with Helium-3 Detectors.* Kerntechnik **57**, 251–254 (1992).

[22] Aroua, A., Grecscu, M., Lanfranchi, M., Lerch, P., Prête, S., and Valley, J.-F. *Evaluation and Test of the Response Matrix of a Multisphere Neutron Spectrometer in a Wide Energy Range. Part II: Simulation.* Nucl. Instrum. Meth. **A321**, 305–311 (1992).

[23] Briesmeister (Editor), J.F. *MCNP - A General Monte Carlo Code for Neutron and Photon Transport, Version 3A.* Manual LA-7396-M, Rev. 2, Los Alamos National Laboratory, 1986.

[24] Briesmeister, J.F. and Hendricks, J.S. *MCNP4 Newsletter.* Memorandum, Los Alamos National Laboratory, April 1991.

[25] MCNP Version 4.2, RSIC Computer Code Collection CCC-200/MCNP4.

[26] Centronic Ltd. Centronic House, King Henry's Drive, New Addington, Croydon CR9 OBG, England.

[27] Thomas, D.J. and Soochak, N. *Determination of the ^{3}He Number Density for the Proportional Counter Used in the NPL Bonner Sphere System.* NPL Report RS(EXT)104, National Physics Laboratory, Teddington, July 1988.

[28] Siebert, B.R.L., Dietz, E., and Jetzke, S. *Comparison of Measured and Calculated Bonner Sphere Responses for 24 and 144 keV Incident Neutron Energies.* Radiat. Prot. Dosim. **44**, 89–92 (1992).

[29] Jetzke, S. Private communication.

[30] Brandt, S. *Datenanalyse*, p. 227. (B.I.-Wissenschaftsverlag, 1981).

A Mathematical Formalism

A.1 Reading, fluence response, spectral fluence

The *fluence response* of a spherical instrument of diameter d which is located in a broad parallel and homogeneous beam of monoenergetic neutrons with an energy E_{n} is defined as

$$R_d(E_{\mathrm{n}}) = \frac{M_d}{\Phi(E_{\mathrm{n}})} \,. \tag{A.1}$$

M_d is the *reading* of the instrument and $\Phi(E_{\mathrm{n}})$ is the *fluence* of those monoenergetic neutrons at the center of the instrument if this were removed.

The definition given in Equation (A.1) is the basis for calculations and it is adequate for most of the measurement situations encountered in neutron field spectrometry or dosimetry with spherical devices. This convention allows a single set of calculated responses to be used for interpreting different experiments. In cases where a given experiment cannot match these conditions, corrections may be needed. For instance, if inhomogeneous fields are encountered (e.g. in the vicinity of point neutron sources which is the case in most calibration situations) adequate corrections must be applied (e.g. point source geometry correction, air attenuation correction) in order to obtain full consistency with the given definition. The reduction of all measured and calculated responses to the same definition is an obvious condition, especially when a comparison is made.

If definition (A.1) is applied to an instrument having in its center an active detector (proportional counter, scintillator), then the reading M_d is obtained as *counts* and the response is expressed in *counts*/(*neutron*/cm^2) or in SI units, cm^2.

If the fluence response $R_d(E)$ of the instrument d is known as a function of energy E,* then the reading M_d of the instrument in a homogeneous field with a known *spectral fluence* $\Phi_E(E)$ (shortly termed *spectrum*)

$$\Phi_E(E) = \frac{\mathrm{d}\Phi(E)}{\mathrm{d}E} \tag{A.2}$$

can be calculated by

$$M_d = \int_{E_{\min}}^{E_{\max}} R_d(E)\, \Phi_E(E)\, \mathrm{d}E \,, \tag{A.3}$$

where $E_{\min}$ and $E_{\max}$ are the lowest and highest neutron energy present in the spectrum.

For unfolding purposes it is useful to use vector and matrix representations of the quantities implied in Equation (A.3). For this reason the energy range of interest is divided into a certain number, n_E, of adjacent energy groups (bins), the i-th group having $E_{l,i}$ and $E_{u,i}$ as the lower and the upper boundary so that $E_{u,i} = E_{l,i+1}$. The neutron fluence Φ_i pertaining to the i-th group is obtained from

$$\Phi_i = \int_{E_{l,i}}^{E_{u,i}} \Phi_E(E)\, \mathrm{d}E \,. \tag{A.4}$$

*Note that E_{n} is the energy of incident monoenergetic neutrons whereas E, $E_{l,i}$ and $E_{u,i}$ are continuous variables and also relate to the moderated neutrons inside the instrument.

The numerical representation of the spectrum (A.2) is then given by

$$\Phi_{E,i} = \frac{\Phi_i}{\Delta E_i} \quad ; \qquad \Delta E_i = E_{u,i} - E_{l,i} \tag{A.5}$$

and Equation (A.3) will take the form

$$M_d = \sum_{i=1}^{n_E} R_{d,i}\, \Phi_{E,i}\, \Delta E_i\,, \tag{A.6}$$

where $R_{d,i}$ and $\Phi_{E,i}$ approximate the mean values of $R_d(E)$ and $\Phi_E(E)$ respectively, over the i-th energy bin. The mean value $\Phi_E(E)$ is easily obtained from (A.4) and (A.5). The quantity $R_{d,i}$ should be that value which produces the same contribution to M_d in the i-th bin if (A.6) is used instead of (A.3). This can be achieved if

$$R_{d,i} = \frac{\int_{E_{l,i}}^{E_{u,i}} R_d(E)\, \Phi_E(E)\, \mathrm{d}E}{\int_{E_{l,i}}^{E_{u,i}} \Phi_E(E)\, \mathrm{d}E}\,, \tag{A.7}$$

i.e. the value $R_{d,i}$ depends on the shape of the spectral fluence. This means that the partition of the energy range of interest into energy groups depends on how many details one needs to properly describe the neutron spectral fluence. The use of one set of energy groups for all spectra encountered in practice is connected with the assumption that all these spectra are smooth enough compared with the bin widths, and do the fluence inside a bin remains practically constant. This allows us to approximate

$$R_{d,i} \approx \frac{\int_{E_{l,i}}^{E_{u,i}} R_d(E)\, \mathrm{d}E}{\Delta E_i}\,. \tag{A.8}$$

In Equation (A.8) there is no restriction concerning the variation of $R_d(E_\mathrm{n})$ inside the i-th energy group, but it is obvious that in cases where important variations occur they must be properly known.

As the energy range of interest for our instrumentation extends from 10^{-3} eV to $2 \cdot 10^7$ eV, i.e. more than 10 orders of magnitude, a logarithmic energy scale is generally used. In this case the mean values $R_{d,i}$ and $\Phi_{E,i}$ are attributed to a *midpoint energy*

$$E_i = \sqrt{E_{l,i} \cdot E_{u,i}} \tag{A.9}$$

which is the geometric or logarithmic mean of the interval between $E_{l,i}$ and $E_{u,i}$.

Often, a logarithmic equidistant subdivision of the energy scale is used with n energies per decade (usually $n = 5$ or $n = 10$). The E_i are then simply given by

$$E_i = 10^{(\frac{i-1}{n})} \cdot E_1\,, \quad 1 \le i \le n_E\,, \tag{A.10}$$

with E_1 being the lowest energy of interest and the boundaries of the i-th bin being

$$E_{l,i} = 10^{-1/(2n)} \cdot E_i\,, \quad E_{u,i} = 10^{+1/(2n)} \cdot E_i \tag{A.11}$$

giving a bin width of

$$\Delta E_i = (10^{+1/(2n)} - 10^{-1/(2n)}) \cdot E_i \tag{A.12}$$

A.2 Least-squares data fit

This section lists some basic formulas which are used to adjust the calculated responses $R_d(E_n)$ to the measured values. We do not go into the theory of the least-squares method but we recall the resulting equations.

Let us assume a set of n measured data $M_i, (i = 1, 2, \ldots, n)$ and the associated relative uncertainties $u(M_i)$, and a set of n calculated values $C_i, (i = 1, 2, \ldots, n)$ (with negligible uncertainties) which aim at simulating the measurements. The least-squares fit of the calculated to the measured data then produces a fit factor f, and the value of the *chi-square*

$$\chi^2 = \sum_{i=1}^{n} (f \cdot C_i - M_i)^2 w_i = \min. \tag{A.13}$$

reaches its minimum. The weights, w_i, to be used here are the inverse of the variances of M_i

$$w_i = 1/s^2(M_i) \tag{A.14}$$

where $s(M_i) = u(M_i) \cdot M_i$ are the standard deviations of the M_i. The result of the least-squares fit is

$$f = \frac{\sum_{i=1}^{n} C_i M_i w_i}{\sum_{i=1}^{n} C_i^2 w_i}, \tag{A.15}$$

and the variance of f is given by

$$s^2(f) = \frac{1}{\sum_{i=1}^{n} C_i^2 w_i}. \tag{A.16}$$

Finally the *reduced chi-square* obtained, defined as

$$\chi_r^2 = \frac{1}{n-1} \chi^2, \tag{A.17}$$

is a test quantity for the quality of the fit. It is a measure of the ability of the calculations to relatively reproduce the measured data. The criterion for accepting a fit is given by

$$|\chi_r^2 - 1| \leq k \sqrt{\frac{2}{n-1}}, \tag{A.18}$$

with a recommended value $k = 2$.

B The MCNP Input File

In Table B.1, we list the MCNP input file for calculating the response of the 12" Bonner sphere [1] at neutron energy $E_n = 5$ MeV. It supplies a description of the realistic geometry of the neutron detector, i.e. the ^{3}He-filled proportional counter SP90 embedded in a polyethylene sphere with an outer diameter of 30,48 cm. The reader is encouraged to refer to Figures 4.1 and 4.2 while studying this appendix.

It is not the purpose of this appendix to describe the syntax of an MCNP input file in detail but to provide the reader with all the information needed to allow an inter-institutional comparison of results. For more information on how to specify a problem to MCNP, see the MCNP manual [23]. The numbers at the beginning of each line including the character "|" do not belong to the input, and have been inserted to allow referencing to certain lines.

The first line in the `INP.DAT` file specifies the name of the problem. **`Bonnerkugel (Mod:DiWi-02/16/93)`** means Bonner sphere geometry model "DiWi", i.e. Dietz and Wiegel, created on 02/16/93. `D= 12"` is the diameter d of the moderator sphere (30,48 cm), `E= 5.00 MeV` is the energy E_n of the monoenergetic neutron beam. The character "A" in `DDK: A` stands for an index which specifies different combinations of ^{3}He gas pressure p^*_{He} and polyethylene density ρ_{PE} or irradiation at different angles φ (see below). If not otherwise specified, the calculations are made for combination "A", that is $p^*_{He} = 200$ kPa, $\rho_{PE} = 0.946$ g/cm^3 and $\varphi = 0°$.

In MCNP the geometry of a problem is given by a list of so-called *cells*, see lines 12 to 65 in Table B.1, where each cell is defined by intersections and unions of 3-dimensional *surfaces* and the complements of other cells, lines 68 to 110. The proportional counter together with a moderator sphere has a cylindrical symmetry so that only planes perpendicular to the y-axis and surfaces of spheres and cylinders are needed to describe the Bonner sphere system. The symmetry axis is the y-axis which points to the right in Figures 4.1 and 4.2.

A special feature of MCNP Version 4 is the definition of a so-called *universe cell*. In this case, cell #50 (line 64) describes the complete detector as a single complex volume (see Figure 4.1) which is filled (`FILL=1` in line 65) with all those cells that have the `U=1` identifier on their cell description card. This construction easily allows the detector to be rotated by applying the `TRCL` card to cell #50 to simulate irradiation under different angles φ, see section 6.4.

The neutron source is a circular plane of radius `RAD` $= r_s = (d/2 + 0,001$ cm). The source is placed with its center on the y-axis perpendicularly to this axis at position $y = -25,00$ cm (see lines 112 and 113). An uniform source density is used for the neutrons which move parallel to the axis in positive y-direction. The angle of irradiation, φ, is defined as the angle between the direction of the neutron beam and the stem of the detector. $\varphi = 0°$ is the irradiation from the side of the nose towards the stem (Figure 4.1).

Five different materials are used in this simulation: `M1`: polyethylene (`PE`), `M2`: ^{3}He (`He`), `M3`: stainless steel (`ss`) [*Edelstahl*], `M4`: air (`air`) [*Luft*] and `M5`: ceramic (`ce`) [*Keramik*]. In Figure 4.2 the lines between regions (cells) of the same material are a result of the description of the geometry in MCNP. In reality there is no separation between these volumes. To save computational time it is recommended in the MCNP manual to describe several simple cells instead of one continuous but complicated cell. The so-called *neutron importance* `IMP:N` of the cells indicates that we have used the *geometry splitting with*

russian roulette variance reduction techniques (see section 5.5).

The block from line 121 to 153 lists the upper energy boundaries E_j used in Equation (5.2) to define energy groups for a differential fluence spectrum of moderated neutrons in the counter. An example of such a spectrum is given in Figure 5.1.

The sensitive volume of the proportional counter is the ^{3}He-filled sphere, cell #4. The counting wire has a diameter of approximately 20 μm and is held by the two rings, cells #13 and #20. In the results presented this wire was not taken into account because it is two orders of magnitude smaller than the smallest detail described.

In order to get the neutron fluence Φ in the measuring volume (cell #4) and in two adjacent volumes which are also filled with ^{3}He (cells #5 and #7) we used the *track length estimate of particle fluence, tally 4* (`F4:N`), line 156. This tally returns the flux averaged over a cell, i.e. *particles*/cm^2 normalized to one source particle. The area `F` $= a_s = \pi r_s^2$ of the neutron source is used as a *multiplier* `FM4` (line 158) that is applied to each fluence bin Φ_j.

Tally 14, which is also a type `F4` tally is defined only for cell #4 but with three different multipliers: a) the total neutron cross section of neutrons with ^{3}He, b) the elastic cross section and c) the $\sigma_{\mathrm{n,p}}(E)$ cross section which together with the other factors `rho(3He)*V*F` $= n^*_{\mathrm{He}} \cdot V_{\mathrm{c4}} \cdot a_s$ provides the response $R_d(E_{\mathrm{n}})$ (see Equation (5.3)).

To test the syntax of an input file for a certain energy and various polyethylene spheres it is useful to run MCNP interactively for only a short time. MCNP stops the simulation if either one minute of cpu time has passed (`CTME 1.0`) or if 1000 particles have left the source (`NPS 1000`). With the `CONTINUE` option the long run is performed in a batch job.

A comment on the information given on the detector: Since the SP90 counter is a commercial product, we may not reproduce the technical drawings supplied to the PTB by the manufacturer, Centronic Ltd. [26]. The geometry shown in Figures 4.1 and 4.2 was drawn with the MCNP plot utility and defined by the instructions given in Table B.1. It contains all the relevant details with respect to the calculation of response functions, especially the presence of ^{3}He and air, but it gives no classified information. Both the figures and the table have been approved by the manufacturer.

Table B.1: Listing of the MCNP input file INP.DAT for the 12" Bonner sphere in a field of parallel neutrons with energy E_n = 5 MeV.

```
 1|Bonnerkugel (Mod:DiWi-02/16/93) D= 12.0", E= 5.00 MeV, DDK: A
 2|C
 3|C     Messvolumen gefuellt mit 3He: beachte CELL-cards 4-8
 4|C     Dichte-Druck-Kombination (DDK) A:
 5|C        - Polyethylen-Dichte rho(PE) = 0.946 g/cm^3
 6|C        - 3He Fuelldruck 200 kPa == 4.9418E-5 ( 10E24 Atome/cm^3 )
 7|C     Fuer D <= 9" : CELL 32 void,  D > 9" : CELL 32 gefuellt mit PE
 8|C     Fuer D > 10" ist die PE-Kugel in zwei Zellen aufgeteilt: 3 und 9
 9|C     Kugelradius : beachte SURFACE-card 41, SDEF-, SI1-card
10|C                   u. Tally-card FM4 ( hier der Faktor F)
11|C
12|  1   0             -1:2:-3:4:-5:6        $ Gebiet aussen
13|                        IMP:N=0
14|  2   0             +41  #1 #50           $ Gebiet innen ausserhalb BoKu
15|                        IMP:N=1
16|  3   1 -0.946       -41 +44 #50           $ aeussere PE-Kugel; i. => CELL 9
17|                        IMP:N=2
18|  4   2 4.9418E-5    -43 #11 #23 #13 #20   $ Messkugel gefuellt mit 3He
19|                        IMP:N=4 U=1
20|  5   2 4.9418E-5    +43 -52 +14 -17 #13   $ li. kugelnahes  Vol. mit 3He
21|                        IMP:N=4 U=1
22|  6   2 4.9418E-5    -52 +12 -14 #15       $  "  kugelfernes  "    "   "
23|                        IMP:N=4 U=1
24|  7   2 4.9418E-5    +43 -52 +18 -27 #20 #31  $ re. k.nahes   "    "   "
25|                        IMP:N=4 U=1
26|  8   2 4.9418E-5    -55 +27 -31           $  "  kugelfernes  "    "   "
27|                        IMP:N=4 U=1
28|  9   1 -0.946       -44 #50               $ innere PE-Kugel; a. => CELL 3
29|                        IMP:N=3
30| 10   3 -7.86        -42 +43 #5 #7 #13 #11 #20 #23  $ Messkugelwand
31|                        IMP:N=4 U=1
32| 11   3 -7.86        -51 +52 +11 -17       $ linker Stutzen
33|                        IMP:N=4 U=1
34| 12   3 -7.86        -52 +11 -12           $ linker Deckel
35|                        IMP:N=4 U=1
36| 13   3 -7.86        -53 +54 +14 -15       $ linker Drahthalter
37|                        IMP:N=4 U=1
38| 15   5 -3.965       -52 +54 +13 -14       $ linker Keramikhalter
39|                        IMP:N=4 U=1
40| 20   3 -7.86        -53 +55 +25 -26       $ rechter Drahthalter
41|                        IMP:N=4 U=1
42| 21   3 -7.86        -61 +63 -21 +22       $ rechter Ringdeckel r. St.
43|                        IMP:N=2 U=1
44| 22   3 -7.86        -61 +62 -22 +23       $ rechter Stutzen Mittelteil
45|                        IMP:N=3 U=1
46| 23   3 -7.86        -61 +52 -23 +18       $ linker Ringdeckel r. St.
```

Table B.1 continued: Listing of the MCNP input file ...

```
47|                                IMP:N=4 U=1
48| 25   3 -7.86        -52 +63 +27 -28        $ schmaler Zwischenring
49|                                IMP:N=4 U=1
50| 26   4 -1.1933E-3   -62 +63 +28 -22 #23    $ grosser Hohlraum (Luft)
51|                                IMP:N=3 U=1
52| 27   4 -1.1933E-3   -63 +32 -22            $ kleiner Hohlraum (Luft)
53|                                IMP:N=3 U=1
54| 28   1 -0.946       -63 +22 -33            $ Teflon-Ausfuehrleitung (PE)
55|                                IMP:N=2 U=1
56| 29   3 -7.86        -63 +31 -32            $ Deckel Innenstutzen
57|                                IMP:N=3 U=1
58| 30   3 -7.86        -63 +55 +30 -31        $ Innenstutzen
59|                                IMP:N=3 U=1
60| 31   5 -3.965       -63 +55 +29 -30        $ rechter Keramikhalter
61|                                IMP:N=3 U=1
62| 32   1 -0.946       -61 +63 +21 -33        $ Leerraum (0) / PE (1 -0.946)
63|                                IMP:N=2 U=1
64| 50   0              -40:(-50 +10 -7):(-60 -20 +7)  $ Detektor
65|                                IMP:N=1 FILL=1   $ ATTENTION FILL-Parameter
66|
67|C     1-39: Ebenen, 40-49: Kugeln, 50-79: Zylinder
68|  1   PX -25.000           $ hintere Kastenflaeche
69|  2   PX +25.000           $ vordere     "
70|  3   PY -25.000           $ linke       "
71|  4   PY +25.000           $ rechte      "
72|  5   PZ -25.000           $ untere      "
73|  6   PZ +25.000           $ obere       "
74|  7   PY   0.000           $ Hilfsebene zur Unterscheidung links-rechts
75| 10   PY  -2.499999        $ linke Begrenzung Universum 1
76| 11   PY  -2.500           $ Aussenseite linker Deckel
77| 12   PY  -2.400           $ Innenseite    "       "
78| 13   PY  -2.180           $ linke  Seite linker Keramikisolator
79| 14   PY  -1.850           $ rechte Seite " " & 1. S. linker Drahthalter
80| 15   PY  -1.588           $ rechte Seite linker Drahthalter
81| 17   PY  -1.500           $ rechte Seite linker Hilfsring
82| 18   PY  +1.400           $ linke Seite rechter   "
83| 20   PY +12.399999        $ rechte Begrenzung Universum 1
84| 21   PY +11.400           $ Aussenseite rechter Stutzenring
85| 22   PY  +8.900           $ Innenseite    "       "
86| 23   PY  +3.100           $ Innenseite  linker    "
87| 25   PY  +1.550           $ linke  Seite rechter Keramikhalter
88| 26   PY  +1.800           $ rechte   "     "       "
89| 27   PY  +2.400           $ linke  Seite Halterungsring
90| 28   PY  +2.480           $ rechte   "     "
91| 29   PY  +2.150           $ linke  Seite rechter Keramikisolator
92| 30   PY  +4.050           $ rechte   "     "       "
93| 31   PY  +6.950           $ Hilfsebene
```

Table B.1 continued: Listing of the MCNP input file ...

```
 94| 32   PY  +7.950          $ Hilfsebene
 95| 33   PY +12.400          $ rechtes Ende Ausfuehrleitung
 96| 40   SO   1.649999       $ Kugel zur Begrenzung Universum 1
 97| 41   SO  15.240          $ Polyethylen Kugel => SI1 (Radius=NAME*1.27)
 98| 42   SO   1.650          $ Messkugelwand aussen
 99| 43   SO   1.600          $    "          innen
100| 44   SO   8.900          $ Unterscheidung der IMP innerhalb PE-Kugel
101| 50   CY   0.569999       $ linker Zylinder Begrenzung Universum 1
102| 51   CY   0.570          $ aussen linker Stutzen
103| 52   CY   0.400          $ innen linker / innen_1 rechter Stutzen
104| 53   CY   0.180          $ aussen linker/rechter Drahthalter
105| 54   CY   0.050          $ innen linker Drahthalter
106| 55   CY   0.080          $ innen  rechter Drahthalter
107| 60   CY   0.634999       $ rechter Zylinder Begrenzung Universum 1
108| 61   CY   0.635          $ aussen rechter Stutzen
109| 62   CY   0.510          $ innen_2   "       "
110| 63   CY   0.250          $ aussen innerer Edelstahlblock
111|
112| SDEF SUR=3 POS=0 -25. 0 RAD=D1 DIR=1 VEC=0 1 0 ERG=5.000E+00
113|  SI1 0 15.241                                  $ Zentrum bis Kugelradius
114|   M1 1001 .66666667 6012 .33333333             $ Poly-Ethylen == (C2H4)n
115|  MT1 POLY.01                                   $ S(alpha,beta) identifier
116|   M2 2003 1.                                   $ 3He
117|   M3 24000 -.195 26000 -.705 28000 -.1         $ Edelstahl
118|   M4 1001 -.0016 7014 -.7772 6012 -.2212       $ Luft
119|   M5 13027 .40 8016 .60                        $ Keramik (Al2O3)
120|C
121|   E0  1.000E-09   1.259E-09   1.585E-09   1.995E-09   2.512E-09
122|       3.162E-09   3.981E-09   5.012E-09   6.310E-09   7.943E-09
123|       1.000E-08   1.122E-08   1.259E-08   1.413E-08   1.585E-08
124|       1.778E-08   1.995E-08   2.239E-08   2.512E-08   2.818E-08
125|       3.162E-08   3.548E-08   3.981E-08   4.467E-08   5.012E-08
126|       5.623E-08   6.310E-08   7.079E-08   7.943E-08   8.913E-08
127|       1.000E-07   1.122E-07   1.259E-07   1.413E-07   1.585E-07
128|       1.778E-07   1.995E-07   2.239E-07   2.512E-07   2.818E-07
129|       3.162E-07   3.548E-07   3.981E-07   4.467E-07   5.012E-07
130|       5.623E-07   6.310E-07   7.079E-07   7.943E-07   8.913E-07
131|       1.000E-06   1.259E-06   1.585E-06   1.995E-06   2.512E-06
132|       3.162E-06   3.981E-06   5.012E-06   6.310E-06   7.943E-06
133|       1.000E-05   1.259E-05   1.585E-05   1.995E-05   2.512E-05
134|       3.162E-05   3.981E-05   5.012E-05   6.310E-05   7.943E-05
135|       1.000E-04   1.259E-04   1.585E-04   1.995E-04   2.512E-04
136|       3.162E-04   3.981E-04   5.012E-04   6.310E-04   7.943E-04
137|       1.000E-03   1.259E-03   1.585E-03   1.995E-03   2.512E-03
138|       3.162E-03   3.981E-03   5.012E-03   6.310E-03   7.943E-03
139|       1.000E-02   1.500E-02   2.000E-02   2.500E-02   3.000E-02
140|       3.500E-02   4.000E-02   4.500E-02   5.000E-02   5.500E-02
```

Table B.1 continued: Listing of the MCNP input file ...

```
141|        6.000E-02   6.500E-02   7.000E-02   7.500E-02   8.000E-02
142|        8.500E-02   9.000E-02   9.500E-02   1.000E-01   1.250E-01
143|        1.500E-01   1.750E-01   2.000E-01   2.250E-01   2.500E-01
144|        2.750E-01   3.000E-01   3.250E-01   3.500E-01   3.750E-01
145|        4.000E-01   4.250E-01   4.500E-01   4.750E-01   5.000E-01
146|        5.500E-01   6.000E-01   6.500E-01   7.000E-01   7.500E-01
147|        8.000E-01   8.500E-01   9.000E-01   9.500E-01   1.000E+00
148|        1.100E+00   1.200E+00   1.300E+00   1.400E+00   1.500E+00
149|        1.600E+00   1.700E+00   1.800E+00   1.900E+00   2.000E+00
150|        2.100E+00   2.200E+00   2.300E+00   2.400E+00   2.500E+00
151|        2.600E+00   2.700E+00   2.800E+00   2.900E+00   3.000E+00
152|        3.250E+00   3.500E+00   3.750E+00   4.000E+00   4.250E+00
153|        4.500E+00   4.750E+00   4.999E+00   5.000E+00   5.250E+00
154|C
155|  FC4 "Neutron fluence per incident fluence" in Gebiet 4,5 u. 7
156| F4:N 4 5 7
157|  FQ4 E F
158|  FM4 729.755                                          $ F = SI1^2*Pi
159|C
160| FC14 Response des Detektors (Gebiet 4) in cm^2
161|F14:N 4
162| FQ14 E M   $ rho(3He)*V*F=4.9418E-5*1.70579E+1*7.29755E+2 = 0.61516
163| FM14 (0.61516 2 1) (0.61516 2 2) (0.61516 2 103)
164|C
165|PHYS:N 20. 1.E-6
166|PRDMP -1000000 -120
167|C
168|CUT:N 100000
169| CTME 1.0
170|  NPS 1000
171|PRINT 120
172|
```

C Mass densities of the polyethylene spheres

The polyethylene mass density $\rho_{PE} = 0{,}946$ g/cm^3 $\pm$ 0,2 % reported in [7] for the PTB-C Bonner sphere set has been determined from measurements of cylindrical samples taken from the same batch of polyethylene as the spheres.

MCNP has the ability to calculate the volume of an object from the given geometry, here it is cell #3 for sphere diameters of 3" to 10" and cells #3 plus #9 for diameters of 12" to 18" (see Figure 4.1 and Table B.1). In other words, the volume of a polyethylene sphere is that of a sphere with a nominal diameter d^{nom} (column 1 in inches, column 2 in cm in Table C.1) reduced by the volume of the central detector. The connector and the cable attached to the detector and the air layers possibly between internal parts were neglected, the corresponding space inside the sphere being considered as filled with polyethylene. The remaining deviations of this geometry from the reality will be reflected in the values obtained for the polyethylene mass densities of the spheres. The values of these MCNP volumes, V_d^{MCNP}, are given in column 5 of Table C.1.

Table C.1: The polyethylene mass density of the PTB-C Bonner sphere system determined from the measured sphere diameters and masses, and the volumes calculated by the MCNP code using a realistic geometry of the central detector.

1	2	3	4	5	6	7	8
d^{nom} inch	d^{nom} cm	d^{meas} cm	$\delta d/d$ %	V_d^{MCNP} cm^3	m_d^{meas} g	$\rho_{PE,d}$ g/cm^3	$\delta\rho/\rho$ %
3	7,620	7,625	+0,066	209,149	197,58	0,9426	−0,380
3.5	8,890	8,893	+0,034	344,551	326,07	0,9453	−0,095
4	10,160	10,182	+0,217	525,001	499,73	0,9454	−0,008
4.5	11,430	11,425	−0,044	756,933	726,06	0,9605	+1,511
5	12,700	12,700	0,0	1 046,78	988,50	0,9443	−0,200
6	15,240	15,202	−0,249	1 825,97	1 712,7	0,9451	−0,116
7	17,780	17,82	+0,225	2 914,05	2 776,1	0,9462	0,0
8	20,320	20,30	−0,098	4 362,50	4 136,8	0,9511	+0,518
10	25,400	25,40	0,0	8 546,81	7 985,6	0,9343	−1,258
12	30,480	30,50	+0,066	14 793,3	13 930,7	0,9398	−0,676
15	38,100	38,01	−0,236	28 924,9	27 282,3	0,9500	+0,402
18	45,720	45,64	−0,175	50 006,6	47 220,3	0,9493	+0,328
mean polyethylene mass density $\rho_{PE} = (0{,}9462 \pm 0{,}0062)$ g/cm^3							

The measured diameters d^{meas} of the spheres are given in column 3 of Table C.1 and their relative deviations from the nominal diameters, $\delta d/d$, in column 4. The relative uncertainty in the determination of sphere diameters is estimated to be 0,2 % taking into account that slight deviations of the sphere surfaces from ideal spherical shapes were found. Column 4 shows that most deviations of the measured diameters from the nominal ones remain below the uncertainty of the measurement. Nevertheless, the MCNP volumes

were corrected for these deviations by adding a volume

$$\delta V_d = \frac{\pi}{2} \cdot d^2 \cdot \delta d\,.$$

The masses of the spheres, m_d^{meas} (column 6), were measured with small uncertainties of 0,01 %. The polyethylene mass density for each sphere, $\rho_{\text{PE},d}$, is then given by

$$\rho_{\text{PE},d} = \frac{m_d^{\text{meas}}}{V_d^{\text{MCNP}} + \delta V_d}\,,$$

listed in column 7 of Table C.1.

The uncertainty for these values is $u(\rho_{\text{PE},d}) = 0{,}3$ %, taking into account the uncertainty of the measured sphere diameters and the slightly simplified geometry model used to calculate the MCNP volumes. As the mean polyethylene density for all 12 spheres of the PTB-C set we obtained the value $\rho_{\text{PE}} = (0{,}9462 \pm 0{,}0062)$ g/cm^3, which should be taken as $\rho_{\text{PE}} = 0{,}946$ g/cm^3 $\pm 0{,}7$ %, i.e. the same value as reported in reference [7] but with a considerably larger uncertainty. This situation is reflected by the relative deviations $\delta\rho/\rho$ of the individual polyethylene density values from their mean shown in column 8.

D Calculated responses

Table D.1: Calculated responses $R_d(E_n) = R$ and their relative uncertainty $s(R)/R$ at energy E_n for the 3" Bonner sphere (BS).

E_n	$R_d(E_n)$	$s(R)/R$
MeV	cm^2	%
$1,000 \cdot 10^{-09}$	,5799	0,4
$2,000 \cdot 10^{-09}$	,6137	0,6
$2,150 \cdot 10^{-09}$	,6188	0,5
$4,640 \cdot 10^{-09}$	,6955	0,5
$5,000 \cdot 10^{-09}$	,7057	0,6
$1,000 \cdot 10^{-08}$	,8218	0,5
$1,500 \cdot 10^{-08}$	,9029	0,5
$2,000 \cdot 10^{-08}$	,9767	0,5
$2,150 \cdot 10^{-08}$	,9948	0,4
$2,500 \cdot 10^{-08}$	1,021	0,5
$3,000 \cdot 10^{-08}$	1,075	0,5
$3,160 \cdot 10^{-08}$	1,084	0,5
$3,500 \cdot 10^{-08}$	1,120	0,5
$4,000 \cdot 10^{-08}$	1,170	0,5
$4,640 \cdot 10^{-08}$	1,224	0,4
$4,700 \cdot 10^{-08}$	1,230	0,5
$5,000 \cdot 10^{-08}$	1,258	0,5
$5,500 \cdot 10^{-08}$	1,309	0,5
$6,000 \cdot 10^{-08}$	1,346	0,4
$1,000 \cdot 10^{-07}$	1,674	0,3
$2,000 \cdot 10^{-07}$	2,080	0,3
$2,150 \cdot 10^{-07}$	2,108	0,3
$3,000 \cdot 10^{-07}$	2,255	0,3
$4,640 \cdot 10^{-07}$	2,415	0,2
$5,000 \cdot 10^{-07}$	2,436	0,3
$6,500 \cdot 10^{-07}$	2,510	0,2
$1,000 \cdot 10^{-06}$	2,593	0,2
$1,500 \cdot 10^{-06}$	2,661	0,3
$2,000 \cdot 10^{-06}$	2,679	0,3
$2,500 \cdot 10^{-06}$	2,694	0,3
$3,160 \cdot 10^{-06}$	2,692	0,3
$4,000 \cdot 10^{-06}$	2,679	0,3
$4,250 \cdot 10^{-06}$	2,670	0,3
$4,310 \cdot 10^{-06}$	2,714	0,2
$4,370 \cdot 10^{-06}$	2,709	0,2
$4,500 \cdot 10^{-06}$	2,709	0,3
$4,750 \cdot 10^{-06}$	2,707	0,3
$5,000 \cdot 10^{-06}$	2,704	0,3
$6,000 \cdot 10^{-06}$	2,685	0,5
$1,000 \cdot 10^{-05}$	2,641	0,3
$1,780 \cdot 10^{-05}$	2,557	0,2
$3,160 \cdot 10^{-05}$	2,457	0,3

Table D.1 continued: ... for the 3" BS

E_n	$R_d(E_n)$	$s(R)/R$
MeV	cm^2	%
$5,620 \cdot 10^{-05}$	2,330	0,2
$1,000 \cdot 10^{-04}$	2,221	0,3
$1,860 \cdot 10^{-04}$	2,092	0,3
$3,160 \cdot 10^{-04}$	1,987	0,3
$5,000 \cdot 10^{-04}$	1,899	0,3
$1,000 \cdot 10^{-03}$	1,749	0,3
$1,170 \cdot 10^{-03}$	1,713	0,4
$1,200 \cdot 10^{-03}$	1,716	0,3
$2,000 \cdot 10^{-03}$	1,613	0,3
$8,150 \cdot 10^{-03}$	1,365	0,4
$1,000 \cdot 10^{-02}$	1,333	0,3
$2,400 \cdot 10^{-02}$	1,189	0,3
$2,740 \cdot 10^{-02}$	1,174	0,4
$7,100 \cdot 10^{-02}$	1,021	0,4
$1,000 \cdot 10^{-01}$	,9546	0,4
$1,440 \cdot 10^{-01}$	,8859	0,4
$2,500 \cdot 10^{-01}$	,7516	0,4
$4,250 \cdot 10^{-01}$	,6092	0,5
$5,650 \cdot 10^{-01}$	,5261	0,5
$1,000 \cdot 10^{+00}$	,3637	0,5
$1,200 \cdot 10^{+00}$	,3253	0,7
$2,500 \cdot 10^{+00}$	,1709	0,9
$5,000 \cdot 10^{+00}$	,0804	1,3
$1,000 \cdot 10^{+01}$	,0335	1,4
$1,480 \cdot 10^{+01}$	,0243	2,4
$1,800 \cdot 10^{+01}$	,0199	1,9
$2,000 \cdot 10^{+01}$	,0177	2,0

Table D.2: Calculated responses $R_d(E_n) = R$ and their relative uncertainty $s(R)/R$ at energy E_n for the 3.5" Bonner sphere (BS).

E_n	$R_d(E_n)$	$s(R)/R$
MeV	cm^2	%
$1,000 \cdot 10^{-09}$	,4846	0,7
$2,150 \cdot 10^{-09}$	,5176	0,7
$4,640 \cdot 10^{-09}$	,5826	0,6
$1,000 \cdot 10^{-08}$	,6858	0,6
$2,150 \cdot 10^{-08}$	,8141	0,5
$4,640 \cdot 10^{-08}$	1,022	0,5
$5,000 \cdot 10^{-08}$	1,046	0,6
$1,000 \cdot 10^{-07}$	1,427	0,4
$2,150 \cdot 10^{-07}$	1,829	0,3
$4,640 \cdot 10^{-07}$	2,187	0,3
$1,000 \cdot 10^{-06}$	2,442	0,3
$1,780 \cdot 10^{-06}$	2,572	0,3

Table D.2 continued: ... for the 3.5" BS

E_n	$R_d(E_n)$	$s(R)/R$
MeV	cm^2	%
$3,160 \cdot 10^{-06}$	2,662	0,3
$5,620 \cdot 10^{-06}$	2,747	0,3
$1,000 \cdot 10^{-05}$	2,768	0,3
$1,780 \cdot 10^{-05}$	2,740	0,2
$3,160 \cdot 10^{-05}$	2,719	0,3
$5,620 \cdot 10^{-05}$	2,664	0,2
$1,000 \cdot 10^{-04}$	2,591	0,3
$2,500 \cdot 10^{-04}$	2,447	0,3
$5,000 \cdot 10^{-04}$	2,348	0,3
$1,200 \cdot 10^{-03}$	2,218	0,3
$3,160 \cdot 10^{-03}$	2,047	0,3
$8,150 \cdot 10^{-03}$	1,896	0,3
$2,740 \cdot 10^{-02}$	1,716	0,3
$7,100 \cdot 10^{-02}$	1,580	0,4
$1,440 \cdot 10^{-01}$	1,440	0,4
$2,500 \cdot 10^{-01}$	1,295	0,5
$4,250 \cdot 10^{-01}$	1,115	0,4
$5,650 \cdot 10^{-01}$	,9950	0,5
$1,200 \cdot 10^{+00}$	,6671	0,6
$2,500 \cdot 10^{+00}$	,3810	0,7
$5,000 \cdot 10^{+00}$	,1928	0,7
$1,480 \cdot 10^{+01}$	,0597	1,8
$1,800 \cdot 10^{+01}$	,0489	1,5
$2,000 \cdot 10^{+01}$	,0426	1,5

Table D.3: Calculated responses $R_d(E_n) = R$ and their relative uncertainty $s(R)/R$ at energy E_n for the 4" Bonner sphere (BS).

E_n	$R_d(E_n)$	$s(R)/R$
MeV	cm^2	%
$1,000 \cdot 10^{-09}$	,4020	0,9
$2,150 \cdot 10^{-09}$	,4279	0,8
$4,640 \cdot 10^{-09}$	,4835	0,8
$1,000 \cdot 10^{-08}$	,5639	0,7
$2,150 \cdot 10^{-08}$	,6735	0,7
$4,640 \cdot 10^{-08}$	,8486	0,6
$5,000 \cdot 10^{-08}$	,8685	0,8
$1,000 \cdot 10^{-07}$	1,189	0,5
$2,150 \cdot 10^{-07}$	1,543	0,4
$4,640 \cdot 10^{-07}$	1,901	0,4
$1,000 \cdot 10^{-06}$	2,190	0,4
$1,780 \cdot 10^{-06}$	2,323	0,3
$3,160 \cdot 10^{-06}$	2,450	0,3
$5,620 \cdot 10^{-06}$	2,567	0,3
$1,000 \cdot 10^{-05}$	2,633	0,3

Table D.3 continued: ... for the 4" BS

E_n	$R_d(E_n)$	$s(R)/R$
MeV	cm^2	%
$1,780 \cdot 10^{-05}$	2,650	0,3
$3,160 \cdot 10^{-05}$	2,671	0,3
$5,620 \cdot 10^{-05}$	2,674	0,3
$1,000 \cdot 10^{-04}$	2,659	0,3
$2,500 \cdot 10^{-04}$	2,596	0,3
$5,000 \cdot 10^{-04}$	2,551	0,3
$1,200 \cdot 10^{-03}$	2,460	0,3
$3,160 \cdot 10^{-03}$	2,352	0,3
$8,150 \cdot 10^{-03}$	2,246	0,4
$2,740 \cdot 10^{-02}$	2,107	0,4
$7,100 \cdot 10^{-02}$	2,022	0,4
$1,440 \cdot 10^{-01}$	1,920	0,4
$2,500 \cdot 10^{-01}$	1,818	0,4
$4,250 \cdot 10^{-01}$	1,643	0,4
$5,650 \cdot 10^{-01}$	1,510	0,4
$1,200 \cdot 10^{+00}$	1,098	0,6
$2,500 \cdot 10^{+00}$	,6678	0,6
$5,000 \cdot 10^{+00}$	,3569	0,6
$1,480 \cdot 10^{+01}$	,1204	1,5
$1,800 \cdot 10^{+01}$	,0962	1,2
$2,000 \cdot 10^{+01}$	,0837	1,3

Table D.4: Calculated responses $R_d(E_n) = R$ and their relative uncertainty $s(R)/R$ at energy E_n for the 4.5" Bonner sphere (BS).

E_n	$R_d(E_n)$	$s(R)/R$
MeV	cm^2	%
$1,000 \cdot 10^{-09}$	,3317	1,1
$2,150 \cdot 10^{-09}$	,3549	1,0
$4,640 \cdot 10^{-09}$	,3957	1,0
$1,000 \cdot 10^{-08}$	,4655	0,9
$2,150 \cdot 10^{-08}$	,5575	0,8
$4,640 \cdot 10^{-08}$	,7051	0,7
$4,700 \cdot 10^{-08}$	,7010	0,8
$5,000 \cdot 10^{-08}$	,7140	0,7
$1,000 \cdot 10^{-07}$	,9790	0,6
$2,150 \cdot 10^{-07}$	1,272	0,5
$4,640 \cdot 10^{-07}$	1,593	0,5
$1,000 \cdot 10^{-06}$	1,867	0,4
$1,780 \cdot 10^{-06}$	2,005	0,4
$3,160 \cdot 10^{-06}$	2,139	0,4
$5,620 \cdot 10^{-06}$	2,267	0,4
$1,000 \cdot 10^{-05}$	2,351	0,4
$1,780 \cdot 10^{-05}$	2,411	0,4
$3,160 \cdot 10^{-05}$	2,460	0,4

Table D.4 continued: ... for the 4.5" BS

E_n	$R_d(E_n)$	$s(R)/R$
MeV	cm^2	%
$5,620 \cdot 10^{-05}$	2,505	0,3
$1,000 \cdot 10^{-04}$	2,506	0,4
$1,860 \cdot 10^{-04}$	2,516	0,4
$2,500 \cdot 10^{-04}$	2,521	0,3
$5,000 \cdot 10^{-04}$	2,538	0,4
$1,200 \cdot 10^{-03}$	2,491	0,4
$2,000 \cdot 10^{-03}$	2,458	0,4
$3,160 \cdot 10^{-03}$	2,448	0,4
$8,150 \cdot 10^{-03}$	2,385	0,4
$2,400 \cdot 10^{-02}$	2,329	0,4
$2,740 \cdot 10^{-02}$	2,324	0,4
$7,100 \cdot 10^{-02}$	2,297	0,4
$1,440 \cdot 10^{-01}$	2,267	0,4
$2,500 \cdot 10^{-01}$	2,218	0,2
$4,000 \cdot 10^{-01}$	2,109	0,4
$4,250 \cdot 10^{-01}$	2,096	0,4
$5,650 \cdot 10^{-01}$	1,981	0,4
$1,000 \cdot 10^{+00}$	1,671	0,5
$1,200 \cdot 10^{+00}$	1,546	0,5
$2,000 \cdot 10^{+00}$	1,174	0,5
$2,050 \cdot 10^{+00}$	1,152	0,5
$2,072 \cdot 10^{+00}$	1,084	0,4
$2,077 \cdot 10^{+00}$	1,077	0,5
$2,082 \cdot 10^{+00}$	1,108	0,5
$2,086 \cdot 10^{+00}$	1,124	0,4
$2,110 \cdot 10^{+00}$	1,138	0,5
$2,120 \cdot 10^{+00}$	1,128	0,4
$2,200 \cdot 10^{+00}$	1,110	0,5
$2,300 \cdot 10^{+00}$	1,073	0,4
$2,400 \cdot 10^{+00}$	1,043	0,5
$2,500 \cdot 10^{+00}$	1,010	0,6
$2,600 \cdot 10^{+00}$	,9840	0,5
$2,700 \cdot 10^{+00}$	,9489	0,5
$2,800 \cdot 10^{+00}$	,9203	0,5
$2,815 \cdot 10^{+00}$	,9143	0,5
$2,830 \cdot 10^{+00}$	,9098	0,5
$2,900 \cdot 10^{+00}$	,8783	0,6
$2,944 \cdot 10^{+00}$	,8654	0,6
$2,980 \cdot 10^{+00}$	,8888	0,6
$3,000 \cdot 10^{+00}$	,8853	0,6
$3,010 \cdot 10^{+00}$	,8783	0,6
$3,100 \cdot 10^{+00}$	,8561	0,5
$3,200 \cdot 10^{+00}$	,8281	0,5
$3,300 \cdot 10^{+00}$	,8054	0,5
$3,400 \cdot 10^{+00}$	,7836	0,5
$3,460 \cdot 10^{+00}$	,7694	0,6

Table D.4 continued: ... for the 4.5" BS

E_n	$R_d(E_n)$	$s(R)/R$
MeV	cm^2	%
$3,500 \cdot 10^{+00}$	,7593	0,5
$3,600 \cdot 10^{+00}$	,7450	0,5
$3,700 \cdot 10^{+00}$	,7345	0,5
$3,800 \cdot 10^{+00}$	,7214	0,5
$3,900 \cdot 10^{+00}$	,7064	0,5
$4,000 \cdot 10^{+00}$	,6987	0,7
$4,100 \cdot 10^{+00}$	,6801	0,5
$4,130 \cdot 10^{+00}$	,6786	0,7
$4,200 \cdot 10^{+00}$	,6668	0,7
$4,270 \cdot 10^{+00}$	,6538	0,7
$4,300 \cdot 10^{+00}$	,6531	0,7
$4,400 \cdot 10^{+00}$	,6387	0,5
$4,500 \cdot 10^{+00}$	,6198	0,5
$4,600 \cdot 10^{+00}$	,6142	0,6
$4,700 \cdot 10^{+00}$	,6029	0,5
$4,800 \cdot 10^{+00}$	,5892	0,6
$4,900 \cdot 10^{+00}$	,5786	0,6
$4,937 \cdot 10^{+00}$	,5717	0,6
$5,000 \cdot 10^{+00}$	,5628	0,6
$5,100 \cdot 10^{+00}$	,5508	0,6
$5,200 \cdot 10^{+00}$	,5452	0,6
$5,300 \cdot 10^{+00}$	,5338	0,6
$5,350 \cdot 10^{+00}$	,5279	0,6
$5,371 \cdot 10^{+00}$	,5242	0,8
$5,400 \cdot 10^{+00}$	,5246	0,6
$5,500 \cdot 10^{+00}$	,5171	0,6
$5,600 \cdot 10^{+00}$	,5110	0,6
$5,700 \cdot 10^{+00}$	,5064	0,6
$5,800 \cdot 10^{+00}$	,5066	0,6
$5,900 \cdot 10^{+00}$	,5013	0,6
$6,000 \cdot 10^{+00}$	,4996	0,6
$6,100 \cdot 10^{+00}$	,4871	0,6
$6,200 \cdot 10^{+00}$	,4822	0,6
$6,295 \cdot 10^{+00}$	,4757	0,8
$6,300 \cdot 10^{+00}$	,4803	0,6
$6,400 \cdot 10^{+00}$	,4751	0,6
$6,420 \cdot 10^{+00}$	,4727	0,8
$6,500 \cdot 10^{+00}$	,4645	0,6
$6,600 \cdot 10^{+00}$	,4498	0,6
$6,700 \cdot 10^{+00}$	,4364	0,6
$6,800 \cdot 10^{+00}$	,4229	0,6
$6,900 \cdot 10^{+00}$	,4138	0,6
$7,000 \cdot 10^{+00}$	,4086	0,9
$7,100 \cdot 10^{+00}$	,3992	0,9
$7,250 \cdot 10^{+00}$	,3915	0,9
$7,420 \cdot 10^{+00}$	,3770	0,9

Table D.4 continued: ... for the 4.5" BS

E_n	$R_d(E_n)$	$s(R)/R$
MeV	cm^2	%
$7,500 \cdot 10^{+00}$	,3760	0,7
$7,750 \cdot 10^{+00}$	,3589	0,9
$8,000 \cdot 10^{+00}$	,3449	0,7
$8,080 \cdot 10^{+00}$	,3438	0,9
$8,250 \cdot 10^{+00}$	,3317	0,7
$8,500 \cdot 10^{+00}$	,3184	0,7
$8,750 \cdot 10^{+00}$	,3093	0,7
$9,000 \cdot 10^{+00}$	,2963	0,7
$9,250 \cdot 10^{+00}$	,2884	0,7
$9,500 \cdot 10^{+00}$	,2813	0,7
$9,750 \cdot 10^{+00}$	,2727	0,7
$1,000 \cdot 10^{+01}$	,2653	1,1
$1,100 \cdot 10^{+01}$	,2458	0,8
$1,200 \cdot 10^{+01}$	,2349	0,8
$1,480 \cdot 10^{+01}$	,1961	1,3
$1,600 \cdot 10^{+01}$	,1785	0,8
$1,720 \cdot 10^{+01}$	,1668	0,8
$1,800 \cdot 10^{+01}$	,1576	1,0
$2,000 \cdot 10^{+01}$	,1397	1,1

Table D.5: Calculated responses $R_d(E_n) = R$ and their relative uncertainty $s(R)/R$ at energy E_n for the 5" Bonner sphere (BS).

E_n	$R_d(E_n)$	$s(R)/R$
MeV	cm^2	%
$1,000 \cdot 10^{-09}$	,2714	1,3
$2,150 \cdot 10^{-09}$	,2897	1,3
$4,640 \cdot 10^{-09}$	,3252	1,2
$1,000 \cdot 10^{-08}$	,3820	1,1
$2,150 \cdot 10^{-08}$	,4659	1,0
$2,530 \cdot 10^{-08}$	,4772	1,0
$4,640 \cdot 10^{-08}$	,5754	0,9
$5,000 \cdot 10^{-08}$	,5942	0,9
$1,000 \cdot 10^{-07}$	,8084	0,8
$2,150 \cdot 10^{-07}$	1,056	0,7
$4,640 \cdot 10^{-07}$	1,306	0,6
$1,000 \cdot 10^{-06}$	1,528	0,5
$3,160 \cdot 10^{-06}$	1,816	0,5
$1,000 \cdot 10^{-05}$	2,026	0,5
$3,160 \cdot 10^{-05}$	2,183	0,4
$1,000 \cdot 10^{-04}$	2,271	0,4
$2,500 \cdot 10^{-04}$	2,321	0,4
$5,000 \cdot 10^{-04}$	2,336	0,4
$1,200 \cdot 10^{-03}$	2,362	0,3
$3,160 \cdot 10^{-03}$	2,364	0,4

Table D.5 continued: ... for the 5" BS

E_n	$R_d(E_n)$	$s(R)/R$
MeV	cm^2	%
$8,150 \cdot 10^{-03}$	2,327	0,4
$2,740 \cdot 10^{-02}$	2,345	0,4
$7,100 \cdot 10^{-02}$	2,399	0,4
$1,440 \cdot 10^{-01}$	2,450	0,4
$2,500 \cdot 10^{-01}$	2,480	0,5
$4,000 \cdot 10^{-01}$	2,437	0,4
$4,250 \cdot 10^{-01}$	2,413	0,4
$5,650 \cdot 10^{-01}$	2,349	0,4
$1,200 \cdot 10^{+00}$	1,949	0,5
$2,500 \cdot 10^{+00}$	1,364	0,6
$5,000 \cdot 10^{+00}$	,7937	0,8
$1,480 \cdot 10^{+01}$	,2854	1,3
$1,800 \cdot 10^{+01}$	,2320	1,0
$2,000 \cdot 10^{+01}$	,2039	1,0

Table D.6: Calculated responses $R_d(E_n) = R$ and their relative uncertainty $s(R)/R$ at energy E_n for the 6" Bonner sphere (BS).

E_n	$R_d(E_n)$	$s(R)/R$
MeV	cm^2	%
$1,000 \cdot 10^{-09}$	,1760	1,9
$2,150 \cdot 10^{-09}$	,1955	1,8
$4,640 \cdot 10^{-09}$	,2161	1,8
$1,000 \cdot 10^{-08}$	,2530	1,6
$2,150 \cdot 10^{-08}$	,3062	1,5
$4,640 \cdot 10^{-08}$	,3795	1,3
$5,000 \cdot 10^{-08}$	,3885	1,3
$1,000 \cdot 10^{-07}$	,5397	1,1
$2,150 \cdot 10^{-07}$	,6916	1,0
$4,640 \cdot 10^{-07}$	,8564	0,9
$1,000 \cdot 10^{-06}$	1,021	0,8
$3,160 \cdot 10^{-06}$	1,222	0,7
$1,000 \cdot 10^{-05}$	1,408	0,7
$3,160 \cdot 10^{-05}$	1,528	0,6
$1,000 \cdot 10^{-04}$	1,662	0,6
$5,000 \cdot 10^{-04}$	1,778	0,6
$1,200 \cdot 10^{-03}$	1,864	0,6
$3,160 \cdot 10^{-03}$	1,905	0,5
$8,150 \cdot 10^{-03}$	1,933	0,6
$2,740 \cdot 10^{-02}$	2,048	0,6
$7,100 \cdot 10^{-02}$	2,200	0,5
$1,440 \cdot 10^{-01}$	2,374	0,5
$2,500 \cdot 10^{-01}$	2,540	0,6
$4,000 \cdot 10^{-01}$	2,662	0,4
$4,250 \cdot 10^{-01}$	2,645	0,4

Table D.6 continued: ... for the 6" BS

E_n	$R_d(E_n)$	$s(R)/R$
MeV	cm^2	%
$5,650 \cdot 10^{-01}$	2,707	0,5
$8,000 \cdot 10^{-01}$	2,646	0,5
$1,200 \cdot 10^{+00}$	2,519	0,6
$1,500 \cdot 10^{+00}$	2,389	0,5
$2,000 \cdot 10^{+00}$	2,164	0,5
$2,500 \cdot 10^{+00}$	1,972	0,6
$3,400 \cdot 10^{+00}$	1,602	0,6
$5,000 \cdot 10^{+00}$	1,270	0,8
$7,500 \cdot 10^{+00}$	,9057	0,8
$1,480 \cdot 10^{+01}$	,4989	1,1
$1,800 \cdot 10^{+01}$	,4033	0,9
$2,000 \cdot 10^{+01}$	,3528	0,9

Table D.7: Calculated responses $R_d(E_n) = R$ and their relative uncertainty $s(R)/R$ at energy E_n for the 7" Bonner sphere (BS).

E_n	$R_d(E_n)$	$s(R)/R$
MeV	cm^2	%
$1,000 \cdot 10^{-09}$	,1127	2,8
$3,160 \cdot 10^{-09}$	,1296	2,6
$1,000 \cdot 10^{-08}$	,1635	2,3
$3,160 \cdot 10^{-08}$	,2126	2,0
$5,000 \cdot 10^{-08}$	,2517	1,9
$1,000 \cdot 10^{-07}$	,3396	1,6
$3,160 \cdot 10^{-07}$	,5076	1,4
$1,000 \cdot 10^{-06}$	,6603	1,2
$3,160 \cdot 10^{-06}$	,7924	1,1
$1,000 \cdot 10^{-05}$	,9038	1,0
$3,160 \cdot 10^{-05}$	1,022	0,9
$1,000 \cdot 10^{-04}$	1,113	0,9
$5,000 \cdot 10^{-04}$	1,238	0,9
$1,200 \cdot 10^{-03}$	1,295	0,8
$3,160 \cdot 10^{-03}$	1,373	0,7
$8,150 \cdot 10^{-03}$	1,433	0,8
$2,740 \cdot 10^{-02}$	1,551	0,8
$4,640 \cdot 10^{-02}$	1,624	0,7
$7,100 \cdot 10^{-02}$	1,735	0,7
$1,440 \cdot 10^{-01}$	1,958	0,7
$2,500 \cdot 10^{-01}$	2,205	0,6
$4,000 \cdot 10^{-01}$	2,486	0,5
$4,250 \cdot 10^{-01}$	2,509	0,6
$5,650 \cdot 10^{-01}$	2,598	0,6
$8,000 \cdot 10^{-01}$	2,692	0,5
$1,200 \cdot 10^{+00}$	2,719	0,6
$1,500 \cdot 10^{+00}$	2,660	0,5

Table D.7 continued: ... for the 7" BS

E_n	$R_d(E_n)$	$s(R)/R$
MeV	cm^2	%
$2,000 \cdot 10^{+00}$	2,538	0,5
$2,500 \cdot 10^{+00}$	2,359	0,6
$3,000 \cdot 10^{+00}$	2,206	0,6
$4,000 \cdot 10^{+00}$	1,884	0,6
$5,000 \cdot 10^{+00}$	1,678	0,8
$7,500 \cdot 10^{+00}$	1,261	0,8
$1,000 \cdot 10^{+01}$	,9503	0,9
$1,480 \cdot 10^{+01}$	,7078	1,1
$1,800 \cdot 10^{+01}$	,5806	0,9
$2,000 \cdot 10^{+01}$	,5245	0,9

Table D.8: Calculated responses $R_d(E_n) = R$ and their relative uncertainty $s(R)/R$ at energy E_n for the 8" Bonner sphere (BS).

E_n	$R_d(E_n)$	$s(R)/R$
MeV	cm^2	%
$1,000 \cdot 10^{-09}$	,0718	1,1
$2,150 \cdot 10^{-09}$	,0747	3,9
$4,640 \cdot 10^{-09}$	,0861	3,7
$1,000 \cdot 10^{-08}$	,1013	3,4
$2,150 \cdot 10^{-08}$	,1253	3,1
$4,640 \cdot 10^{-08}$	,1558	2,7
$5,000 \cdot 10^{-08}$	,1519	2,7
$1,000 \cdot 10^{-07}$	,2230	2,3
$2,150 \cdot 10^{-07}$	,2821	2,0
$4,640 \cdot 10^{-07}$	,3597	1,9
$1,000 \cdot 10^{-06}$	,4160	0,5
$3,160 \cdot 10^{-06}$	,5049	1,5
$1,000 \cdot 10^{-05}$	,5846	1,4
$3,160 \cdot 10^{-05}$	,6496	1,4
$1,000 \cdot 10^{-04}$	,6912	1,3
$1,860 \cdot 10^{-04}$	,7437	1,0
$2,500 \cdot 10^{-04}$	,7727	1,1
$5,000 \cdot 10^{-04}$	,8109	1,2
$1,200 \cdot 10^{-03}$	,8606	1,2
$2,000 \cdot 10^{-03}$	,8932	1,0
$3,160 \cdot 10^{-03}$	,9140	1,0
$8,150 \cdot 10^{-03}$	,9596	0,4
$2,400 \cdot 10^{-02}$	1,077	0,9
$2,740 \cdot 10^{-02}$	1,072	1,0
$7,100 \cdot 10^{-02}$	1,254	1,0
$1,440 \cdot 10^{-01}$	1,461	0,9
$2,500 \cdot 10^{-01}$	1,733	0,8
$4,000 \cdot 10^{-01}$	2,024	0,7
$4,250 \cdot 10^{-01}$	2,057	0,7

Table D.8 continued: ... for the 8" BS

E_n	$R_d(E_n)$	$s(R)/R$
MeV	cm^2	%
$5,650 \cdot 10^{-01}$	2,228	0,7
$8,000 \cdot 10^{-01}$	2,422	0,6
$1,200 \cdot 10^{+00}$	2,600	0,8
$1,500 \cdot 10^{+00}$	2,681	0,6
$2,000 \cdot 10^{+00}$	2,640	0,5
$2,050 \cdot 10^{+00}$	2,609	0,6
$2,072 \cdot 10^{+00}$	2,296	0,7
$2,077 \cdot 10^{+00}$	2,277	0,7
$2,082 \cdot 10^{+00}$	2,425	0,6
$2,086 \cdot 10^{+00}$	2,518	0,6
$2,110 \cdot 10^{+00}$	2,618	0,6
$2,120 \cdot 10^{+00}$	2,620	0,5
$2,200 \cdot 10^{+00}$	2,599	0,5
$2,300 \cdot 10^{+00}$	2,560	0,5
$2,400 \cdot 10^{+00}$	2,537	0,5
$2,500 \cdot 10^{+00}$	2,507	0,6
$2,600 \cdot 10^{+00}$	2,462	0,5
$2,700 \cdot 10^{+00}$	2,410	0,5
$2,800 \cdot 10^{+00}$	2,371	0,5
$2,815 \cdot 10^{+00}$	2,356	0,5
$2,830 \cdot 10^{+00}$	2,339	0,5
$2,900 \cdot 10^{+00}$	2,276	0,7
$2,944 \cdot 10^{+00}$	2,218	0,7
$2,980 \cdot 10^{+00}$	2,377	0,6
$3,000 \cdot 10^{+00}$	2,419	0,7
$3,010 \cdot 10^{+00}$	2,417	0,6
$3,100 \cdot 10^{+00}$	2,330	0,6
$3,200 \cdot 10^{+00}$	2,270	0,5
$3,300 \cdot 10^{+00}$	2,201	0,5
$3,400 \cdot 10^{+00}$	2,153	0,5
$3,460 \cdot 10^{+00}$	2,149	0,7
$3,500 \cdot 10^{+00}$	2,140	0,7
$3,600 \cdot 10^{+00}$	2,104	0,6
$3,700 \cdot 10^{+00}$	2,135	0,5
$3,800 \cdot 10^{+00}$	2,121	0,5
$3,900 \cdot 10^{+00}$	2,115	0,7
$4,000 \cdot 10^{+00}$	2,100	0,7
$4,100 \cdot 10^{+00}$	2,084	0,5
$4,130 \cdot 10^{+00}$	2,075	0,7
$4,200 \cdot 10^{+00}$	2,037	0,7
$4,270 \cdot 10^{+00}$	2,034	0,7
$4,300 \cdot 10^{+00}$	2,002	0,7
$4,400 \cdot 10^{+00}$	2,023	0,6
$4,500 \cdot 10^{+00}$	2,030	0,5
$4,600 \cdot 10^{+00}$	2,025	0,5
$4,700 \cdot 10^{+00}$	2,020	0,5

Table D.8 continued: ... for the 8" BS

E_n	$R_d(E_n)$	$s(R)/R$
MeV	cm^2	%
$4,800 \cdot 10^{+00}$	1,992	0,5
$4,900 \cdot 10^{+00}$	1,977	0,5
$4,937 \cdot 10^{+00}$	1,971	0,6
$5,000 \cdot 10^{+00}$	1,962	0,6
$5,100 \cdot 10^{+00}$	1,935	0,5
$5,200 \cdot 10^{+00}$	1,924	0,5
$5,300 \cdot 10^{+00}$	1,890	0,6
$5,350 \cdot 10^{+00}$	1,875	0,6
$5,371 \cdot 10^{+00}$	1,828	0,7
$5,400 \cdot 10^{+00}$	1,853	0,6
$5,500 \cdot 10^{+00}$	1,877	0,6
$5,600 \cdot 10^{+00}$	1,857	0,6
$5,700 \cdot 10^{+00}$	1,841	0,5
$5,800 \cdot 10^{+00}$	1,836	0,6
$5,900 \cdot 10^{+00}$	1,836	0,5
$6,000 \cdot 10^{+00}$	1,828	0,6
$6,100 \cdot 10^{+00}$	1,811	0,5
$6,200 \cdot 10^{+00}$	1,811	0,8
$6,295 \cdot 10^{+00}$	1,744	0,8
$6,300 \cdot 10^{+00}$	1,756	0,8
$6,400 \cdot 10^{+00}$	1,785	0,5
$6,420 \cdot 10^{+00}$	1,790	0,7
$6,500 \cdot 10^{+00}$	1,765	0,5
$6,600 \cdot 10^{+00}$	1,739	0,6
$6,700 \cdot 10^{+00}$	1,725	0,6
$6,800 \cdot 10^{+00}$	1,696	0,6
$6,900 \cdot 10^{+00}$	1,662	0,6
$7,000 \cdot 10^{+00}$	1,677	0,8
$7,100 \cdot 10^{+00}$	1,655	0,8
$7,250 \cdot 10^{+00}$	1,593	0,8
$7,420 \cdot 10^{+00}$	1,525	0,8
$7,500 \cdot 10^{+00}$	1,509	0,9
$7,750 \cdot 10^{+00}$	1,454	0,8
$8,000 \cdot 10^{+00}$	1,439	0,9
$8,080 \cdot 10^{+00}$	1,407	0,8
$8,250 \cdot 10^{+00}$	1,392	0,6
$8,500 \cdot 10^{+00}$	1,365	0,6
$8,750 \cdot 10^{+00}$	1,338	0,6
$9,000 \cdot 10^{+00}$	1,313	0,6
$9,250 \cdot 10^{+00}$	1,271	0,6
$9,500 \cdot 10^{+00}$	1,246	0,6
$9,750 \cdot 10^{+00}$	1,221	0,6
$1,000 \cdot 10^{+01}$	1,191	0,7
$1,100 \cdot 10^{+01}$	1,108	0,6
$1,200 \cdot 10^{+01}$	1,059	1,0
$1,480 \cdot 10^{+01}$	,9005	0,4

Table D.8 continued: ... for the 8" BS

E_n	$R_d(E_n)$	$s(R)/R$
MeV	cm^2	%
$1,600 \cdot 10^{+01}$	,8359	1,2
$1,720 \cdot 10^{+01}$	,7960	0,7
$1,800 \cdot 10^{+01}$	,7678	1,2
$2,000 \cdot 10^{+01}$	,6787	1,3

Table D.9: Calculated responses $R_d(E_n) = R$ and their relative uncertainty $s(R)/R$ at energy E_n for the 10" Bonner sphere (BS).

E_n	$R_d(E_n)$	$s(R)/R$
MeV	cm^2	%
$1,000 \cdot 10^{-09}$	,0256	7,0
$3,160 \cdot 10^{-09}$	,0304	6,3
$1,000 \cdot 10^{-08}$	,0406	5,4
$3,160 \cdot 10^{-08}$	,0538	4,8
$5,000 \cdot 10^{-08}$	,0637	4,6
$1,000 \cdot 10^{-07}$	,0772	4,8
$3,160 \cdot 10^{-07}$	,1268	3,9
$1,000 \cdot 10^{-06}$	,1589	3,4
$3,160 \cdot 10^{-06}$	,1922	3,1
$1,000 \cdot 10^{-05}$	,2315	2,6
$3,160 \cdot 10^{-05}$	,2369	2,5
$1,000 \cdot 10^{-04}$	,2797	2,4
$5,000 \cdot 10^{-04}$	,3194	2,4
$1,200 \cdot 10^{-03}$	,3401	2,3
$3,160 \cdot 10^{-03}$	,3711	2,0
$8,150 \cdot 10^{-03}$	,3856	2,2
$2,740 \cdot 10^{-02}$	,4674	2,0
$7,100 \cdot 10^{-02}$	,5254	1,9
$1,000 \cdot 10^{-01}$	,5812	1,6
$1,440 \cdot 10^{-01}$	,6729	1,7
$2,500 \cdot 10^{-01}$	,8599	1,5
$4,000 \cdot 10^{-01}$	1,095	1,2
$4,250 \cdot 10^{-01}$	1,115	1,2
$5,650 \cdot 10^{-01}$	1,286	1,2
$8,000 \cdot 10^{-01}$	1,569	1,0
$1,000 \cdot 10^{+00}$	1,775	0,9
$1,200 \cdot 10^{+00}$	1,918	0,6
$1,500 \cdot 10^{+00}$	2,069	0,9
$2,000 \cdot 10^{+00}$	2,281	0,8
$2,500 \cdot 10^{+00}$	2,310	0,9
$3,000 \cdot 10^{+00}$	2,350	0,8
$3,500 \cdot 10^{+00}$	2,110	0,9
$5,000 \cdot 10^{+00}$	2,128	0,9
$7,500 \cdot 10^{+00}$	1,773	0,9
$1,000 \cdot 10^{+01}$	1,491	1,0

Table D.9 continued: ... for the 10" BS

E_n	$R_d(E_n)$	$s(R)/R$
MeV	cm^2	%
$1,480 \cdot 10^{+01}$	1,187	1,2
$1,800 \cdot 10^{+01}$	,9995	0,9
$2,000 \cdot 10^{+01}$	,9135	1,0

Table D.10: Calculated responses $R_d(E_n) = R$ and their relative uncertainty $s(R)/R$ at energy E_n for the 12" Bonner sphere (BS).

E_n	$R_d(E_n)$	$s(R)/R$
MeV	cm^2	%
$1,000 \cdot 10^{-09}$	,0110	16,2
$2,150 \cdot 10^{-09}$	,0101	8,0
$4,640 \cdot 10^{-09}$	,0122	7,7
$1,000 \cdot 10^{-08}$	,0137	7,8
$2,150 \cdot 10^{-08}$	,0173	7,8
$4,640 \cdot 10^{-08}$	,0215	7,7
$5,000 \cdot 10^{-08}$	,0238	8,5
$1,000 \cdot 10^{-07}$	,0328	8,7
$2,150 \cdot 10^{-07}$	,0416	7,8
$4,640 \cdot 10^{-07}$	,0507	6,9
$1,000 \cdot 10^{-06}$	,0568	2,6
$3,160 \cdot 10^{-06}$	,0701	6,8
$1,000 \cdot 10^{-05}$	,0820	5,9
$3,160 \cdot 10^{-05}$	,0886	5,7
$1,000 \cdot 10^{-04}$	,0928	5,3
$3,160 \cdot 10^{-04}$	,1175	4,9
$5,000 \cdot 10^{-04}$	,1205	4,6
$1,170 \cdot 10^{-03}$	,1218	4,7
$1,200 \cdot 10^{-03}$	,1276	4,6
$4,640 \cdot 10^{-03}$	,1371	4,3
$8,150 \cdot 10^{-03}$	,1464	4,6
$1,000 \cdot 10^{-02}$	,1430	4,4
$2,150 \cdot 10^{-02}$	,1689	4,1
$2,740 \cdot 10^{-02}$	,1630	4,1
$4,640 \cdot 10^{-02}$	,1726	4,0
$7,100 \cdot 10^{-02}$	,2068	3,6
$1,000 \cdot 10^{-01}$	,2361	3,6
$1,440 \cdot 10^{-01}$	,2510	3,2
$2,500 \cdot 10^{-01}$	,3431	2,8
$4,250 \cdot 10^{-01}$	,5065	1,4
$5,650 \cdot 10^{-01}$	,6572	2,0
$8,000 \cdot 10^{-01}$	,8396	1,6
$1,000 \cdot 10^{+00}$	1,040	1,6
$1,200 \cdot 10^{+00}$	1,173	0,9
$1,500 \cdot 10^{+00}$	1,381	1,4
$2,000 \cdot 10^{+00}$	1,624	1,3

Table D.10 continued: ... for the 12" BS

E_n MeV	$R_d(E_n)$ cm^2	$s(R)/R$ %
$2,050 \cdot 10^{+00}$	1,646	1,2
$2,072 \cdot 10^{+00}$	1,374	0,9
$2,077 \cdot 10^{+00}$	1,350	1,3
$2,082 \cdot 10^{+00}$	1,499	0,8
$2,086 \cdot 10^{+00}$	1,566	0,8
$2,110 \cdot 10^{+00}$	1,665	1,2
$2,120 \cdot 10^{+00}$	1,703	1,2
$2,200 \cdot 10^{+00}$	1,715	0,7
$2,300 \cdot 10^{+00}$	1,735	0,7
$2,400 \cdot 10^{+00}$	1,768	0,7
$2,500 \cdot 10^{+00}$	1,785	1,2
$2,600 \cdot 10^{+00}$	1,773	1,2
$2,700 \cdot 10^{+00}$	1,767	1,2
$2,800 \cdot 10^{+00}$	1,726	1,2
$2,815 \cdot 10^{+00}$	1,699	1,1
$2,830 \cdot 10^{+00}$	1,684	1,1
$2,900 \cdot 10^{+00}$	1,641	1,3
$2,944 \cdot 10^{+00}$	1,541	1,2
$2,980 \cdot 10^{+00}$	1,789	1,1
$3,000 \cdot 10^{+00}$	1,895	1,2
$3,010 \cdot 10^{+00}$	1,892	1,1
$3,100 \cdot 10^{+00}$	1,877	1,2
$3,200 \cdot 10^{+00}$	1,796	1,2
$3,300 \cdot 10^{+00}$	1,748	1,2
$3,400 \cdot 10^{+00}$	1,702	1,3
$3,460 \cdot 10^{+00}$	1,729	1,2
$3,500 \cdot 10^{+00}$	1,704	1,2
$3,600 \cdot 10^{+00}$	1,721	1,2
$3,700 \cdot 10^{+00}$	1,747	1,2
$3,800 \cdot 10^{+00}$	1,807	1,2
$3,900 \cdot 10^{+00}$	1,798	1,2
$4,000 \cdot 10^{+00}$	1,909	1,2
$4,100 \cdot 10^{+00}$	1,887	1,2
$4,130 \cdot 10^{+00}$	1,856	1,1
$4,200 \cdot 10^{+00}$	1,853	1,2
$4,270 \cdot 10^{+00}$	1,812	1,1
$4,300 \cdot 10^{+00}$	1,824	1,1
$4,400 \cdot 10^{+00}$	1,888	0,7
$4,500 \cdot 10^{+00}$	1,882	1,2
$4,600 \cdot 10^{+00}$	1,946	0,7
$4,700 \cdot 10^{+00}$	1,963	1,2
$4,800 \cdot 10^{+00}$	1,957	0,7
$4,900 \cdot 10^{+00}$	1,984	0,7
$4,937 \cdot 10^{+00}$	1,962	1,1
$5,000 \cdot 10^{+00}$	1,980	1,0
$5,100 \cdot 10^{+00}$	1,965	0,7

Table D.10 continued: ... for the 12" BS

E_n MeV	$R_d(E_n)$ cm^2	$s(R)/R$ %
$5,200 \cdot 10^{+00}$	1,961	1,2
$5,300 \cdot 10^{+00}$	1,961	0,7
$5,350 \cdot 10^{+00}$	1,940	1,1
$5,371 \cdot 10^{+00}$	1,856	1,1
$5,400 \cdot 10^{+00}$	1,926	1,2
$5,500 \cdot 10^{+00}$	1,989	0,7
$5,600 \cdot 10^{+00}$	1,962	1,2
$5,700 \cdot 10^{+00}$	1,985	0,7
$5,800 \cdot 10^{+00}$	1,981	1,2
$5,900 \cdot 10^{+00}$	1,988	0,7
$6,000 \cdot 10^{+00}$	1,984	0,7
$6,100 \cdot 10^{+00}$	1,992	1,2
$6,200 \cdot 10^{+00}$	1,965	1,1
$6,295 \cdot 10^{+00}$	1,854	1,1
$6,300 \cdot 10^{+00}$	1,860	1,2
$6,400 \cdot 10^{+00}$	2,004	1,2
$6,420 \cdot 10^{+00}$	1,954	1,1
$6,500 \cdot 10^{+00}$	1,959	0,7
$6,600 \cdot 10^{+00}$	1,989	1,2
$6,700 \cdot 10^{+00}$	1,970	0,7
$6,800 \cdot 10^{+00}$	1,986	1,2
$6,900 \cdot 10^{+00}$	1,979	0,7
$7,000 \cdot 10^{+00}$	2,021	1,2
$7,100 \cdot 10^{+00}$	1,967	1,1
$7,250 \cdot 10^{+00}$	1,892	1,1
$7,420 \cdot 10^{+00}$	1,826	1,1
$7,500 \cdot 10^{+00}$	1,805	1,2
$7,750 \cdot 10^{+00}$	1,699	1,1
$8,000 \cdot 10^{+00}$	1,714	1,2
$8,080 \cdot 10^{+00}$	1,692	1,1
$8,250 \cdot 10^{+00}$	1,753	0,7
$8,500 \cdot 10^{+00}$	1,755	1,2
$8,750 \cdot 10^{+00}$	1,712	0,7
$9,000 \cdot 10^{+00}$	1,720	1,2
$9,250 \cdot 10^{+00}$	1,641	0,7
$9,500 \cdot 10^{+00}$	1,620	0,7
$9,750 \cdot 10^{+00}$	1,605	0,7
$1,000 \cdot 10^{+01}$	1,603	1,3
$1,100 \cdot 10^{+01}$	1,534	0,7
$1,200 \cdot 10^{+01}$	1,463	1,3
$1,480 \cdot 10^{+01}$	1,329	1,1
$1,600 \cdot 10^{+01}$	1,257	1,4
$1,720 \cdot 10^{+01}$	1,183	0,8
$1,800 \cdot 10^{+01}$	1,122	1,5
$2,000 \cdot 10^{+01}$	1,049	1,1

Table D.11: Calculated responses $R_d(E_n) = R$ and their relative uncertainty $s(R)/R$ at energy E_n for the 15" Bonner sphere (BS).

E_n	$R_d(E_n)$	$s(R)/R$
MeV	cm^2	%
$1,000 \cdot 10^{-09}$	,0014	14,5
$1,000 \cdot 10^{-08}$	,0029	11,4
$5,000 \cdot 10^{-08}$	,0051	15,6
$1,000 \cdot 10^{-07}$	,0050	15,1
$1,000 \cdot 10^{-06}$	,0116	7,7
$3,160 \cdot 10^{-06}$	,0147	7,3
$1,000 \cdot 10^{-05}$	,0166	6,4
$3,160 \cdot 10^{-05}$	,0180	6,1
$1,000 \cdot 10^{-04}$	,0213	5,7
$5,000 \cdot 10^{-04}$	,0250	8,2
$1,200 \cdot 10^{-03}$	,0223	8,9
$8,150 \cdot 10^{-03}$	,0270	9,9
$2,740 \cdot 10^{-02}$	,0364	8,7
$7,100 \cdot 10^{-02}$	,0392	8,4
$1,440 \cdot 10^{-01}$	,0567	3,5
$2,500 \cdot 10^{-01}$	,0744	2,7
$4,250 \cdot 10^{-01}$	,1231	4,2
$5,650 \cdot 10^{-01}$	,1709	1,9
$8,000 \cdot 10^{-01}$	,2597	3,6
$1,200 \cdot 10^{+00}$	,4620	1,4
$2,000 \cdot 10^{+00}$	,8081	2,0
$2,050 \cdot 10^{+00}$	,8474	1,4
$2,072 \cdot 10^{+00}$	,6510	1,3
$2,077 \cdot 10^{+00}$	,6329	1,6
$2,082 \cdot 10^{+00}$	,7164	1,2
$2,086 \cdot 10^{+00}$	,8067	1,1
$2,110 \cdot 10^{+00}$	,8769	1,4
$2,120 \cdot 10^{+00}$	,8964	1,1
$2,200 \cdot 10^{+00}$	,9116	1,1
$2,300 \cdot 10^{+00}$	,9287	1,0
$2,400 \cdot 10^{+00}$	,9913	1,0
$2,500 \cdot 10^{+00}$	,9925	1,2
$2,600 \cdot 10^{+00}$	1,009	1,0
$2,700 \cdot 10^{+00}$	1,021	1,0
$2,800 \cdot 10^{+00}$	1,018	1,0
$2,815 \cdot 10^{+00}$	1,003	1,0
$2,830 \cdot 10^{+00}$	,9921	1,0
$2,900 \cdot 10^{+00}$	,9493	2,0
$2,944 \cdot 10^{+00}$	,8969	1,9
$2,980 \cdot 10^{+00}$	1,069	1,8
$3,000 \cdot 10^{+00}$	1,182	1,9
$3,010 \cdot 10^{+00}$	1,181	1,7
$3,100 \cdot 10^{+00}$	1,158	1,7
$3,200 \cdot 10^{+00}$	1,085	1,0

Table D.11 continued: ... for the 15" BS

E_n	$R_d(E_n)$	$s(R)/R$
MeV	cm^2	%
$3,300 \cdot 10^{+00}$	1,041	1,0
$3,400 \cdot 10^{+00}$	1,036	1,0
$3,460 \cdot 10^{+00}$	1,054	1,8
$3,500 \cdot 10^{+00}$	1,086	2,0
$3,600 \cdot 10^{+00}$	1,046	1,0
$3,700 \cdot 10^{+00}$	1,088	1,0
$3,800 \cdot 10^{+00}$	1,141	0,9
$3,900 \cdot 10^{+00}$	1,188	1,9
$4,000 \cdot 10^{+00}$	1,192	1,8
$4,100 \cdot 10^{+00}$	1,259	0,9
$4,130 \cdot 10^{+00}$	1,239	1,7
$4,200 \cdot 10^{+00}$	1,235	1,7
$4,270 \cdot 10^{+00}$	1,221	1,7
$4,300 \cdot 10^{+00}$	1,220	1,7
$4,400 \cdot 10^{+00}$	1,310	0,9
$4,500 \cdot 10^{+00}$	1,344	0,9
$4,600 \cdot 10^{+00}$	1,394	0,9
$4,700 \cdot 10^{+00}$	1,434	0,9
$4,800 \cdot 10^{+00}$	1,451	0,9
$4,900 \cdot 10^{+00}$	1,480	0,8
$4,937 \cdot 10^{+00}$	1,490	0,8
$5,000 \cdot 10^{+00}$	1,475	1,4
$5,100 \cdot 10^{+00}$	1,513	0,8
$5,200 \cdot 10^{+00}$	1,492	0,8
$5,300 \cdot 10^{+00}$	1,505	0,8
$5,350 \cdot 10^{+00}$	1,462	0,8
$5,371 \cdot 10^{+00}$	1,386	1,0
$5,400 \cdot 10^{+00}$	1,460	0,8
$5,500 \cdot 10^{+00}$	1,546	0,8
$5,600 \cdot 10^{+00}$	1,562	0,8
$5,700 \cdot 10^{+00}$	1,554	0,8
$5,800 \cdot 10^{+00}$	1,552	0,8
$5,900 \cdot 10^{+00}$	1,558	0,8
$6,000 \cdot 10^{+00}$	1,551	0,8
$6,100 \cdot 10^{+00}$	1,573	0,8
$6,200 \cdot 10^{+00}$	1,512	1,6
$6,295 \cdot 10^{+00}$	1,439	1,6
$6,300 \cdot 10^{+00}$	1,441	1,7
$6,400 \cdot 10^{+00}$	1,589	0,8
$6,420 \cdot 10^{+00}$	1,604	1,5
$6,500 \cdot 10^{+00}$	1,610	0,8
$6,600 \cdot 10^{+00}$	1,664	0,8
$6,700 \cdot 10^{+00}$	1,696	0,8
$6,800 \cdot 10^{+00}$	1,689	0,8
$6,900 \cdot 10^{+00}$	1,694	0,8
$7,000 \cdot 10^{+00}$	1,748	1,6

Table D.11 continued: ... for the 15" BS

E_n	$R_d(E_n)$	$s(R)/R$
MeV	cm^2	%
$7,100 \cdot 10^{+00}$	1,692	1,4
$7,250 \cdot 10^{+00}$	1,631	1,5
$7,420 \cdot 10^{+00}$	1,560	1,5
$7,500 \cdot 10^{+00}$	1,557	1,6
$7,750 \cdot 10^{+00}$	1,491	1,5
$8,000 \cdot 10^{+00}$	1,474	1,7
$8,080 \cdot 10^{+00}$	1,465	1,5
$8,250 \cdot 10^{+00}$	1,526	0,8
$8,500 \cdot 10^{+00}$	1,557	0,8
$8,750 \cdot 10^{+00}$	1,534	0,8
$9,000 \cdot 10^{+00}$	1,535	0,8
$9,250 \cdot 10^{+00}$	1,518	0,8
$9,500 \cdot 10^{+00}$	1,507	0,8
$9,750 \cdot 10^{+00}$	1,497	0,8
$1,000 \cdot 10^{+01}$	1,543	1,5
$1,100 \cdot 10^{+01}$	1,478	0,8
$1,200 \cdot 10^{+01}$	1,414	0,8
$1,480 \cdot 10^{+01}$	1,352	0,9
$1,600 \cdot 10^{+01}$	1,253	1,8
$1,720 \cdot 10^{+01}$	1,240	0,9
$1,800 \cdot 10^{+01}$	1,215	1,8
$2,000 \cdot 10^{+01}$	1,094	1,9

Table D.12: Calculated responses $R_d(E_n) = R$ and their relative uncertainty $s(R)/R$ at energy E_n for the 18" Bonner sphere (BS).

E_n	$R_d(E_n)$	$s(R)/R$
MeV	cm^2	%
$1,000 \cdot 10^{-09}$	,0005	32,9
$1,000 \cdot 10^{-08}$	,0005	26,8
$5,000 \cdot 10^{-08}$	,0011	44,5
$1,000 \cdot 10^{-07}$	,0012	17,0
$1,000 \cdot 10^{-06}$	,0015	21,9
$1,000 \cdot 10^{-05}$	,0022	15,6
$3,160 \cdot 10^{-05}$	,0045	15,2
$1,000 \cdot 10^{-04}$	,0039	13,7
$5,000 \cdot 10^{-04}$	,0034	22,7
$1,200 \cdot 10^{-03}$	,0041	16,2
$8,150 \cdot 10^{-03}$	,0056	14,8
$2,740 \cdot 10^{-02}$	,0073	13,8
$7,100 \cdot 10^{-02}$	,0078	10,9
$1,000 \cdot 10^{-01}$	,0087	15,2
$1,440 \cdot 10^{-01}$	,0103	12,5
$2,500 \cdot 10^{-01}$	,0151	19,4
$4,250 \cdot 10^{-01}$	.0298	11,0

Table D.12 continued: ... for the 18" BS

E_n	$R_d(E_n)$	$s(R)/R$
MeV	cm^2	%
$5,640 \cdot 10^{-01}$	,0383	8,1
$5,650 \cdot 10^{-01}$	,0399	8,0
$8,000 \cdot 10^{-01}$	,0678	5,3
$1,200 \cdot 10^{+00}$	,1483	2,9
$1,700 \cdot 10^{+00}$	,2801	3,7
$2,500 \cdot 10^{+00}$	,4902	1,6
$5,000 \cdot 10^{+00}$	1,006	1,2
$6,500 \cdot 10^{+00}$	1,195	1,7
$7,000 \cdot 10^{+00}$	1,325	1,7
$7,500 \cdot 10^{+00}$	1,186	1,7
$9,000 \cdot 10^{+00}$	1,287	2,1
$1,000 \cdot 10^{+01}$	1,279	1,7
$1,100 \cdot 10^{+01}$	1,238	1,7
$1,200 \cdot 10^{+01}$	1,236	1,7
$1,480 \cdot 10^{+01}$	1,204	1,0
$1,600 \cdot 10^{+01}$	1,196	1,6
$1,720 \cdot 10^{+01}$	1,175	1,6
$1,800 \cdot 10^{+01}$	1,140	1,6
$2,000 \cdot 10^{+01}$	1,088	1,6

E Calculated responses for the bare detector

Table E.1: Calculated responses $R_d(E_n) = R$ and their relative uncertainty $s(R)/R$ at energy E_n for the bare detector. Column 2 gives the responses for the values of ^{3}He gas pressure and angle of irradiation, $p^*_{He} = 200$ kPa and $\varphi = 90°$, respectively used in measurements [8].

p^*_{He} =	200 kPa		172 kPa		20 kPa		200 kPa	
φ =	90°		90°		90°		0°	
E_n	$R_d(E_n)$	$\frac{s(R)}{R}$	$R_d(E_n)$	$\frac{s(R)}{R}$	$R_d(E_n)$	$\frac{s(R)}{R}$	$R_d(E_n)$	$\frac{s(R)}{R}$
MeV	cm^2	%	cm^2	%	cm^2	%	cm^2	%
$1,000 \cdot 10^{-09}$	6,259	0,1	6,057	0,2	1,729	0,2	5,625	0,2
$1,469 \cdot 10^{-09}$	6,119	0,2	5,871	0,2			5,512	0,2
$2,154 \cdot 10^{-09}$	5,898	0,2	5,614	0,2	1,285	0,2	5,324	0,2
$3,162 \cdot 10^{-09}$	5,611	0,2	5,273	0,2			5,074	0,2
$4,641 \cdot 10^{-09}$	5,230	0,2	4,864	0,2	,9294	0,2	4,754	0,2
$6,813 \cdot 10^{-09}$	4,808	0,2	4,426	0,2			4,382	0,2
$1,000 \cdot 10^{-08}$	4,354	0,1	3,974	0,2	,6594	0,2	3,981	0,1
$1,469 \cdot 10^{-08}$	3,892	0,2	3,520	0,2			3,569	0,2
$2,154 \cdot 10^{-08}$	3,433	0,2	3,085	0,2	,4617	0,1	3,164	0,2
$3,162 \cdot 10^{-08}$	3,036	0,2	2,711	0,2			2,802	0,2
$4,642 \cdot 10^{-08}$	2,632	0,2	2,338	0,1	,3248	0,1	2,439	0,2
$6,813 \cdot 10^{-08}$	2,267	0,2	2,001	0,1			2,107	0,1
$1,000 \cdot 10^{-07}$	1,938	0,1	1,702	0,1	,2240	0,1	1,810	0,1
$1,469 \cdot 10^{-07}$	1,644	0,1	1,440	0,1			1,546	0,2
$2,154 \cdot 10^{-07}$	1,389	0,1	1,213	0,1	,1536	0,1	1,309	0,1
$3,162 \cdot 10^{-07}$	1,168	0,1	1,017	0,1			1,103	0,2
$4,641 \cdot 10^{-07}$	,9798	0,1	,8509	0,1	,1049	0,1	,9255	0,1
$6,813 \cdot 10^{-07}$	,8178	0,1	,7093	0,1			,7739	0,1
$1,000 \cdot 10^{-06}$	,6821	0,1	,5904	0,1	,0715	0,1	,6457	0,1
$1,580 \cdot 10^{-06}$	,5514	0,1	,4770	0,1			,5227	0,1
$2,510 \cdot 10^{-06}$	,4431	0,1	,3828	0,1	,0457	0,1	,4202	0,1
$3,160 \cdot 10^{-06}$	,3932	0,2					,3729	0,2
$3,980 \cdot 10^{-06}$	,3550	0,1	,3064	0,1			,3370	0,1
$6,310 \cdot 10^{-06}$	,2835	0,1	,2445	0,1	,0289	0,1	,2691	0,1
$1,000 \cdot 10^{-05}$	,2255	0,1	,1943	0,1	,0229	0,1	,2139	0,1
$2,150 \cdot 10^{-05}$	,1550	0,1	,1335	0,1	,0157	0,1	,1472	0,1
$3,160 \cdot 10^{-05}$	,1283	0,2					,1219	0,2
$4,640 \cdot 10^{-05}$	,1060	0,1	,0913	0,1	,0107	0,1	,1008	0,1
$1,000 \cdot 10^{-04}$	,0713	0,1	,0614	0,1	,0072	0,1	,0679	0,1
$2,150 \cdot 10^{-04}$	,0492	0,1	,0423	0,1	,0049	0,1	,0468	0,1
$3,160 \cdot 10^{-04}$	,0404	0,2					,0385	0,2
$4,640 \cdot 10^{-04}$	,0333	0,1	,0287	0,1	,0033	0,1	,0318	0,1
$1,000 \cdot 10^{-03}$	,0224	0,1	,0193	0,1	,0022	0,1	,0214	0,1

F Graphical comparison of calculations and measurements

This appendix shows the ratios $r_{d,E}$ of calculated responses to measured ones, defined in Equation (6.4), as a function of the sphere diameter d for all experimental energies E_x, Figures F.1 and F.2, and as a function of experimental energy E_x for all sphere diameters d, Figures F.3 and F.4.

In Figures F.1 and F.2:

- r_E is the weighted mean of $r_{d,E}$ for all spheres at a given energy E_x,
- f_E is the factor which for all spheres fits the calculations to the measurements at the given energy,
- χ^2_r is the reduced chi-square as given by Equation (A.17).
- The uncertainty bars represent:
  - left (thin): the contribution to the standard deviation of the ratio due to the uncertainty of uncorrelated quantities contributing to the measurements,
  - right (thick): the total uncertainty of the ratio, including the statistical contribution from the Monte Carlo calculations.
- The horizontal lines with uncertainty bars at both ends indicate the values of the mean ratio, r_E , and their standard deviations, excluding correlations (small, thin) and total (large, thick).

In Figures F.3 and F.4:

- r_d is the weighted mean of $r_{d,E}$ at all energies for a given sphere diameter,
- f_E is the factor which for all energies fits the calculations to the measurements for a given sphere diameter,
- χ^2_r is the reduced chi-square as given by Equation (A.17).
- The uncertainty bars represent:
  - left (thin): the contribution to the standard deviation of the ratio due to the total measurement uncertainty,
  - right (thick): the total uncertainty of the ratio, including the statistical contribution from Monte Carlo calculations.
- The horizontal lines with uncertainty bars at both ends indicate the values of the mean ratio, r_d, and their standard deviations.

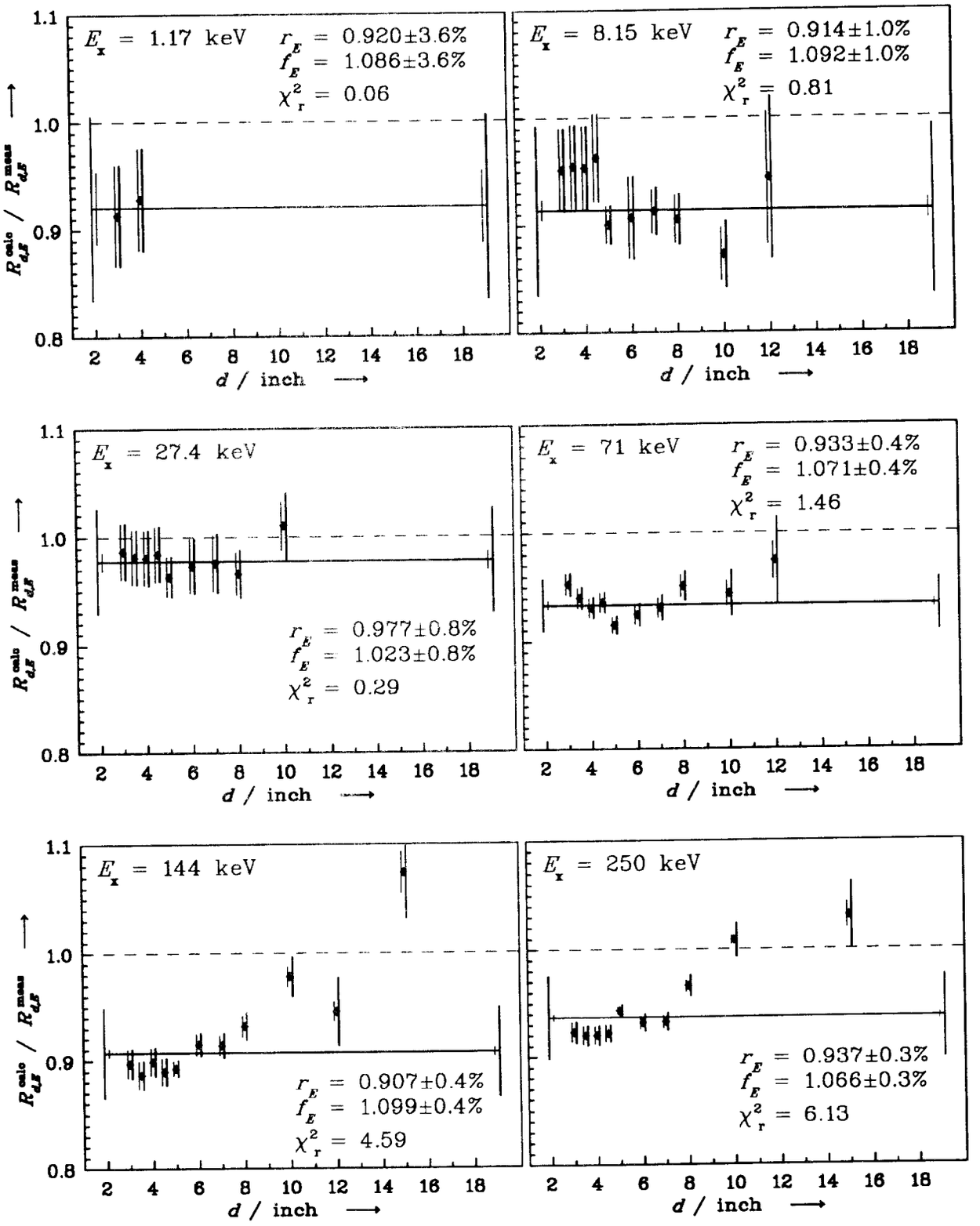

Figure F.1: Ratios $r_{d,E}$ of calculated responses to measured ones for energies E_x = 1,17 keV to 250 keV vs. sphere diameter d. The horizontal line represents the value of r_E. For more information see page 77.

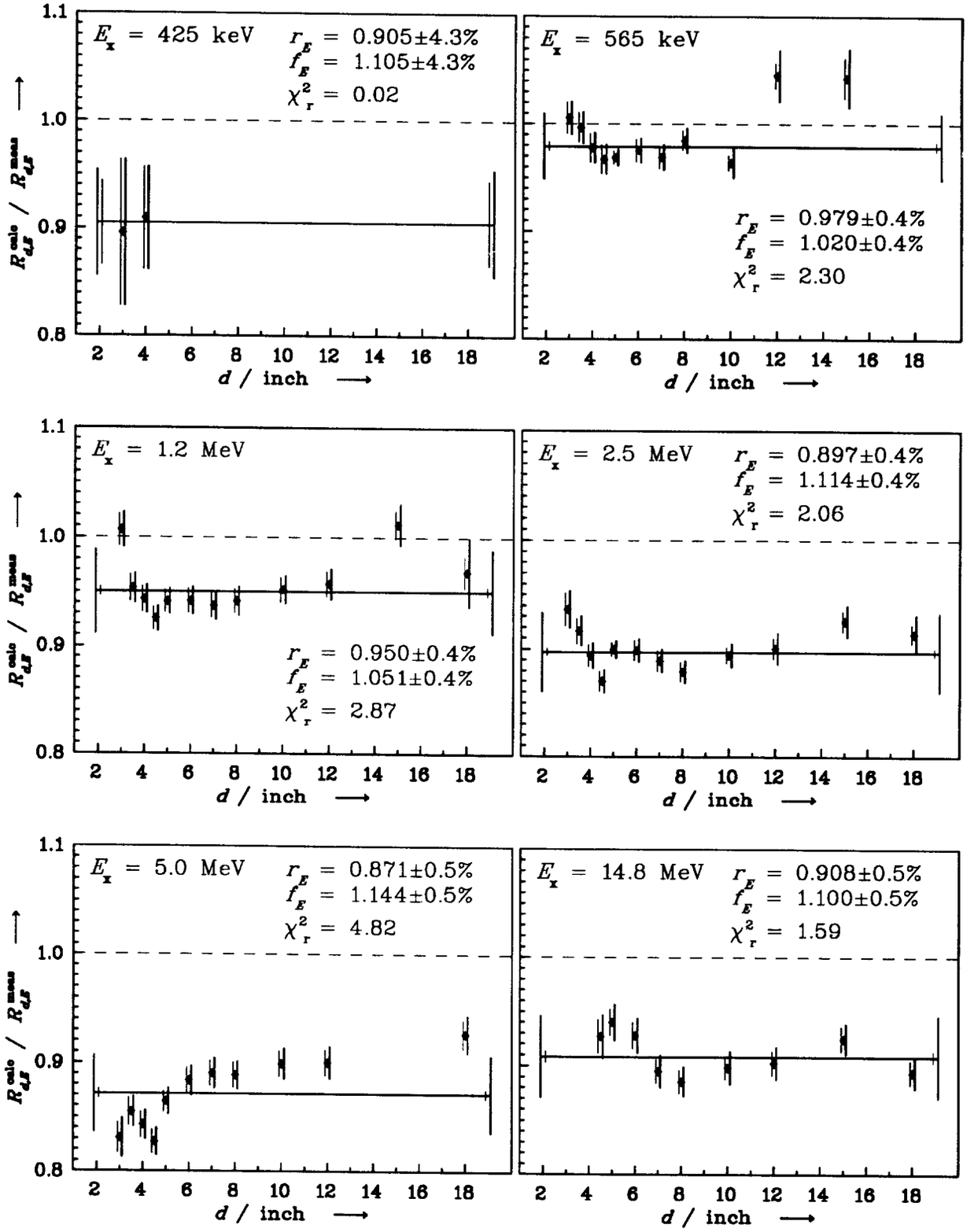

Figure F.2: Ratios $r_{d,E}$ of calculated responses to measured ones for energies E_x = 425 keV to 14,8 MeV vs. sphere diameter d. The horizontal line represents the value of r_E. For more information see page 77.

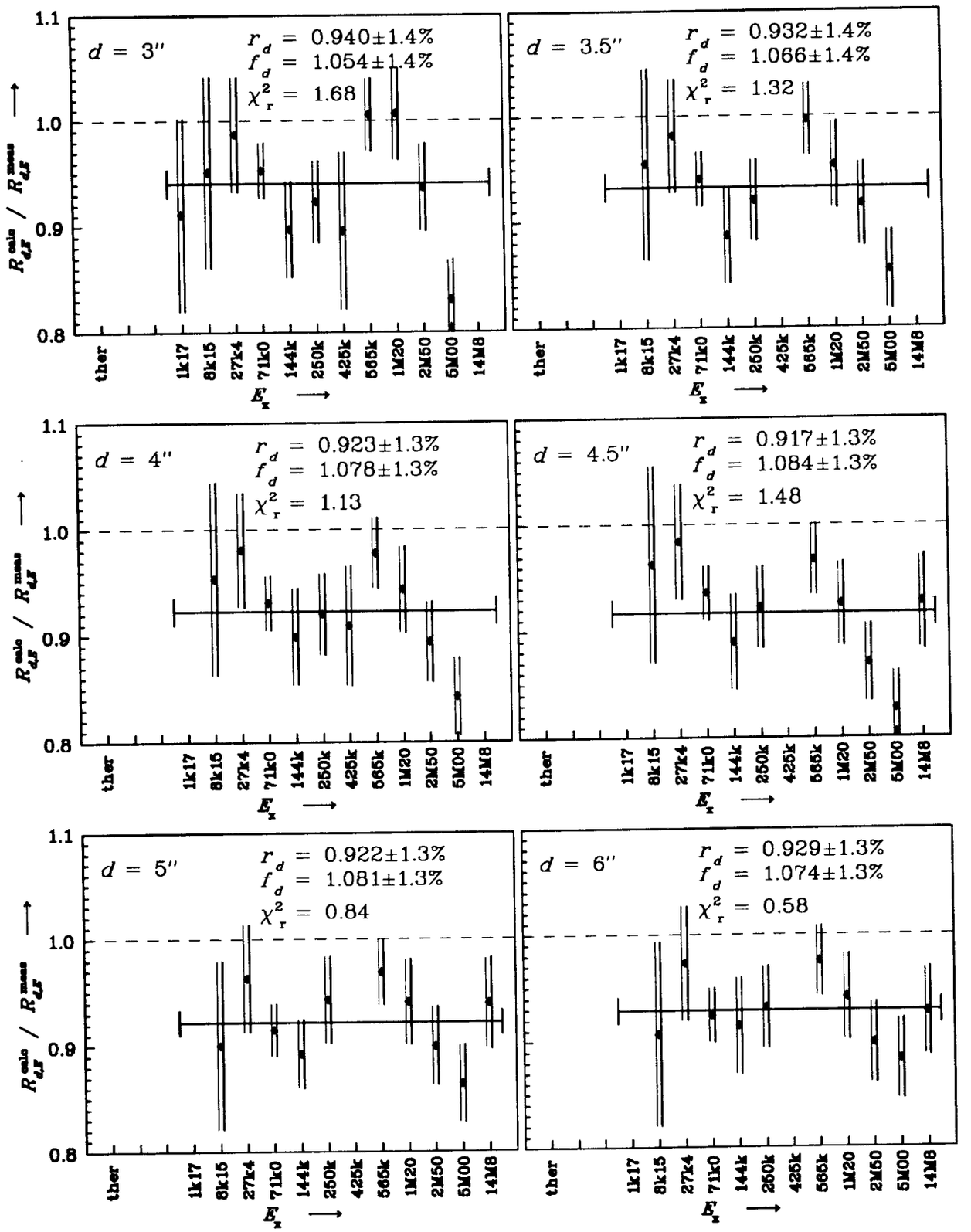

*Figure F.3: Ratios $r_{d,E}$ of calculated responses to measured ones of the 3" to 6" Bonner spheres vs. neutron energy E_x (*ther *means thermal region,* 1k17 *means 1,17 keV, etc.). The horizontal line represents the value of r_d, see also page 77.*

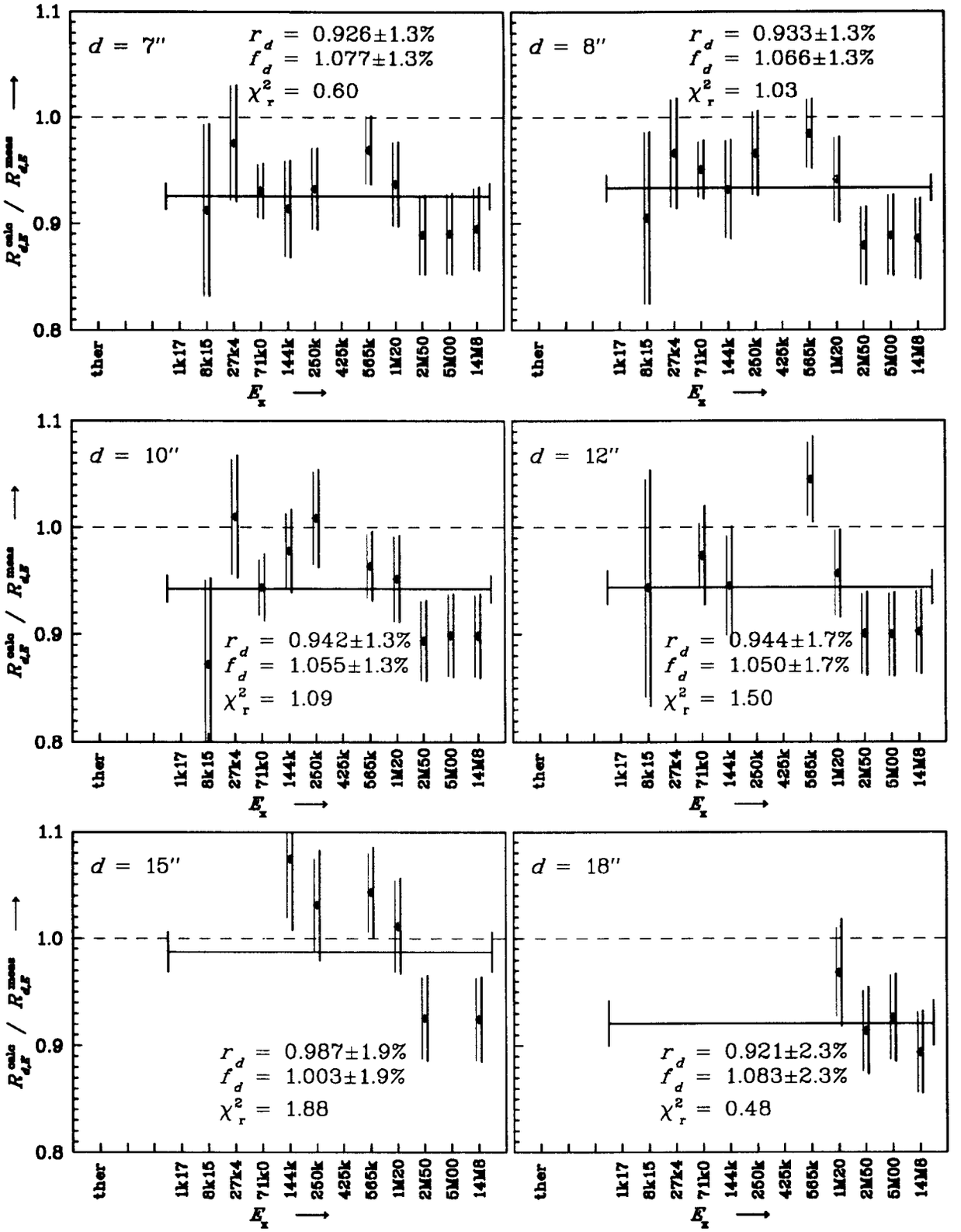

*Figure F.4: Ratios $r_{d,E}$ of calculated responses to measured ones of the 7" to 18" Bonner spheres vs. neutron energy E_x (*ther *means thermal region,* 1k17 *means 1,17 keV, etc.). The horizontal line represents the value of r_d, see also page 77.*

G Interpolated responses

Table G.1: Response matrix $\mathcal{R}$, 10 energies per decade (1 meV to 100 eV), responses in cm^2.

E_i/MeV	3"	3.5"	4"	4.5"	5"	6"	7"	8"	10"	12"	15"	18"
$1,000 \cdot 10^{-09}$	,5799	,4846	,4020	,3317	,2714	,1759	,1127	,0718	,0256	,0110	,0014	,0005
$1,259 \cdot 10^{-09}$	,5911	,4945	,4098	,3387	,2769	,1818	,1161	,0727	,0266	,0107	,0016	,0005
$1,585 \cdot 10^{-09}$	,6023	,5044	,4176	,3457	,2824	,1877	,1194	,0736	,0275	,0105	,0017	,0005
$1,995 \cdot 10^{-09}$	,6143	,5145	,4256	,3527	,2880	,1936	,1228	,0745	,0285	,0102	,0019	,0005
$2,512 \cdot 10^{-09}$	,6343	,5307	,4392	,3632	,2969	,1997	,1262	,0770	,0295	,0105	,0020	,0005
$3,162 \cdot 10^{-09}$	,6573	,5502	,4558	,3754	,3075	,2058	,1300	,0805	,0306	,0111	,0021	,0005
$3,981 \cdot 10^{-09}$	,6802	,5697	,4724	,3876	,3181	,2120	,1364	,0839	,0324	,0118	,0023	,0005
$5,012 \cdot 10^{-09}$	,7071	,5931	,4916	,4029	,3310	,2199	,1431	,0877	,0345	,0123	,0024	,0005
$6,310 \cdot 10^{-09}$	,7447	,6239	,5156	,4237	,3479	,2309	,1499	,0922	,0365	,0128	,0026	,0005
$7,943 \cdot 10^{-09}$	,7832	,6549	,5398	,4446	,3650	,2419	,1567	,0968	,0385	,0132	,0027	,0005
$1,000 \cdot 10^{-08}$	,8227	,6868	,5650	,4664	,3830	,2536	,1638	,1017	,0406	,0138	,0029	,0005
$1,259 \cdot 10^{-08}$	,8678	,7244	,5969	,4932	,4072	,2690	,1733	,1085	,0432	,0148	,0032	,0006
$1,585 \cdot 10^{-08}$	,9175	,7630	,6299	,5208	,4324	,2850	,1831	,1158	,0459	,0159	,0035	,0007
$1,995 \cdot 10^{-08}$	,9756	,8019	,6632	,5488	,4575	,3011	,1929	,1230	,0485	,0170	,0038	,0008
$2,512 \cdot 10^{-08}$	1,026	,8561	,7089	,5873	,4791	,3210	,2028	,1315	,0512	,0182	,0042	,0008
$3,162 \cdot 10^{-08}$	1,088	,9184	,7613	,6315	,5133	,3429	,2139	,1406	,0541	,0194	,0045	,0009
$3,981 \cdot 10^{-08}$	1,168	,9806	,8137	,6757	,5506	,3649	,2323	,1497	,0588	,0207	,0048	,0010
$5,012 \cdot 10^{-08}$	1,261	1,054	,8752	,7210	,5968	,3918	,2532	,1561	,0637	,0234	,0051	,0011
$6,310 \cdot 10^{-08}$	1,380	1,174	,9760	,8030	,6661	,4392	,2812	,1758	,0682	,0268	,0051	,0011
$7,943 \cdot 10^{-08}$	1,526	1,301	1,082	,8910	,7372	,4894	,3104	,1994	,0727	,0298	,0051	,0011
$1,000 \cdot 10^{-07}$	1,673	1,427	1,189	,9791	,8088	,5391	,3402	,2223	,0779	,0327	,0051	,0012
$1,259 \cdot 10^{-07}$	1,809	1,548	1,295	1,067	,8829	,5854	,3732	,2408	,0871	,0354	,0057	,0012
$1,585 \cdot 10^{-07}$	1,944	1,669	1,402	1,156	,9575	,6311	,4068	,2586	,0970	,0381	,0063	,0012
$1,995 \cdot 10^{-07}$	2,073	1,789	1,509	1,244	1,032	,6769	,4405	,2764	,1070	,0407	,0070	,0013
$2,512 \cdot 10^{-07}$	2,177	1,901	1,615	1,337	1,107	,7249	,4741	,2978	,1169	,0434	,0076	,0013
$3,162 \cdot 10^{-07}$	2,274	2,009	1,723	1,433	1,181	,7743	,5073	,3210	,1264	,0461	,0083	,0013
$3,981 \cdot 10^{-07}$	2,359	2,116	1,830	1,529	1,256	,8236	,5382	,3442	,1332	,0489	,0089	,0014
$5,012 \cdot 10^{-07}$	2,436	2,212	1,929	1,620	1,328	,8729	,5687	,3652	,1397	,0513	,0096	,0014
$6,310 \cdot 10^{-07}$	2,500	2,289	2,016	1,702	1,395	,9224	,5993	,3822	,1461	,0531	,0103	,0014
$7,943 \cdot 10^{-07}$	2,549	2,366	2,103	1,785	1,462	,9719	,6298	,3991	,1525	,0550	,0109	,0015
$1,000 \cdot 10^{-06}$	2,593	2,439	2,185	1,863	1,527	1,020	,6598	,4161	,1589	,0569	,0116	,0015
$1,259 \cdot 10^{-06}$	2,632	2,494	2,243	1,922	1,586	1,062	,6867	,4338	,1655	,0595	,0122	,0016
$1,585 \cdot 10^{-06}$	2,664	2,546	2,296	1,977	1,643	1,102	,7132	,4516	,1722	,0621	,0128	,0017
$1,995 \cdot 10^{-06}$	2,679	2,590	2,349	2,032	1,701	1,142	,7396	,4694	,1789	,0648	,0134	,0017
$2,512 \cdot 10^{-06}$	2,692	2,626	2,400	2,086	1,758	1,182	,7660	,4872	,1855	,0675	,0141	,0018
$3,162 \cdot 10^{-06}$	2,691	2,662	2,450	2,139	1,814	1,222	,7919	,5047	,1924	,0701	,0147	,0019
$3,981 \cdot 10^{-06}$	2,684	2,696	2,497	2,191	1,858	1,260	,8147	,5209	,2001	,0725	,0151	,0019
$5,012 \cdot 10^{-06}$	2,702	2,730	2,544	2,241	1,900	1,297	,8370	,5368	,2079	,0749	,0155	,0020
$6,310 \cdot 10^{-06}$	2,681	2,751	2,580	2,284	1,942	1,334	,8592	,5527	,2158	,0773	,0159	,0021
$7,943 \cdot 10^{-06}$	2,661	2,759	2,606	2,317	1,984	1,371	,8815	,5687	,2237	,0797	,0163	,0022
$1,000 \cdot 10^{-05}$	2,639	2,765	2,630	2,350	2,025	1,407	,9039	,5842	,2307	,0819	,0166	,0023
$1,259 \cdot 10^{-05}$	2,607	2,757	2,640	2,375	2,058	1,432	,9275	,5976	,2326	,0834	,0169	,0027
$1,585 \cdot 10^{-05}$	2,573	2,746	2,647	2,399	2,089	1,456	,9512	,6106	,2337	,0847	,0172	,0032
$1,995 \cdot 10^{-05}$	2,537	2,736	2,654	2,421	2,121	1,480	,9749	,6236	,2348	,0860	,0174	,0036
$2,512 \cdot 10^{-05}$	2,497	2,727	2,663	2,441	2,152	1,504	,9986	,6366	,2359	,0873	,0177	,0041
$3,162 \cdot 10^{-05}$	2,455	2,717	2,670	2,460	2,182	1,529	1,022	,6490	,2379	,0885	,0180	,0045
$3,981 \cdot 10^{-05}$	2,406	2,697	2,672	2,478	2,201	1,555	1,041	,6579	,2455	,0894	,0186	,0044
$5,012 \cdot 10^{-05}$	2,355	2,675	2,673	2,496	2,219	1,582	1,059	,6662	,2541	,0903	,0193	,0043
$6,310 \cdot 10^{-05}$	2,308	2,649	2,671	2,505	2,236	1,609	1,077	,6746	,2626	,0911	,0200	,0042
$7,943 \cdot 10^{-05}$	2,264	2,620	2,665	2,506	2,254	1,635	1,095	,6829	,2711	,0920	,0206	,0040
$1,000 \cdot 10^{-04}$	2,220	2,590	2,658	2,506	2,271	1,661	1,113	,6926	,2793	,0934	,0213	,0039

Table G.1 continued: ... (125,9 eV to 20 MeV), responses in cm^2.

E_i/MeV	3"	3.5"	4"	4.5"	5"	6"	7"	8"	10"	12"	15"	18"
$1,259 \cdot 10^{-04}$	2,173	2,555	2,643	2,510	2,284	1,679	1,131	,7107	,2854	,0978	,0218	,0038
$1,585 \cdot 10^{-04}$	2,126	2,518	2,627	2,513	2,296	1,695	1,149	,7302	,2910	,1027	,0224	,0038
$1,995 \cdot 10^{-04}$	2,079	2,482	2,611	2,517	2,309	1,712	1,167	,7506	,2967	,1076	,0229	,0037
$2,512 \cdot 10^{-04}$	2,033	2,446	2,595	2,521	2,320	1,728	1,185	,7718	,3024	,1126	,0234	,0036
$3,162 \cdot 10^{-04}$	1,987	2,413	2,581	2,527	2,326	1,745	1,203	,7856	,3081	,1171	,0240	,0035
$3,981 \cdot 10^{-04}$	1,943	2,381	2,566	2,533	2,331	1,762	1,221	,7983	,3138	,1190	,0245	,0035
$5,012 \cdot 10^{-04}$	1,898	2,348	2,550	2,536	2,336	1,779	1,238	,8111	,3194	,1204	,0249	,0034
$6,310 \cdot 10^{-04}$	1,849	2,314	2,527	2,526	2,342	1,801	1,254	,8241	,3249	,1208	,0243	,0036
$7,943 \cdot 10^{-04}$	1,799	2,280	2,503	2,513	2,349	1,824	1,268	,8372	,3304	,1212	,0236	,0038
$1,000 \cdot 10^{-03}$	1,749	2,246	2,479	2,501	2,356	1,846	1,283	,8502	,3358	,1216	,0229	,0040
$1,259 \cdot 10^{-03}$	1,705	2,209	2,455	2,488	2,362	1,866	1,299	,8637	,3417	,1266	,0225	,0042
$1,585 \cdot 10^{-03}$	1,660	2,169	2,429	2,473	2,362	1,876	1,318	,8784	,3490	,1296	,0230	,0043
$1,995 \cdot 10^{-03}$	1,614	2,128	2,403	2,459	2,363	1,886	1,336	,8926	,3564	,1312	,0235	,0045
$2,512 \cdot 10^{-03}$	1,573	2,087	2,377	2,453	2,363	1,895	1,355	,9036	,3637	,1328	,0241	,0047
$3,162 \cdot 10^{-03}$	1,532	2,047	2,352	2,447	2,362	1,905	1,373	,9141	,3706	,1344	,0246	,0048
$3,981 \cdot 10^{-03}$	1,492	2,010	2,326	2,433	2,355	1,912	1,388	,9251	,3746	,1360	,0252	,0050
$5,012 \cdot 10^{-03}$	1,451	1,973	2,300	2,418	2,346	1,919	1,402	,9362	,3782	,1384	,0258	,0052
$6,310 \cdot 10^{-03}$	1,410	1,937	2,275	2,402	2,337	1,926	1,417	,9473	,3817	,1421	,0263	,0054
$7,943 \cdot 10^{-03}$	1,370	1,900	2,249	2,387	2,329	1,934	1,432	,9594	,3861	,1454	,0270	,0055
$1,000 \cdot 10^{-02}$	1,333	1,864	2,223	2,374	2,330	1,953	1,453	,9819	,3994	,1445	,0285	,0059
$1,259 \cdot 10^{-02}$	1,295	1,829	2,196	2,362	2,333	1,974	1,475	1,007	,4149	,1508	,0303	,0062
$1,585 \cdot 10^{-02}$	1,257	1,793	2,170	2,350	2,337	1,996	1,497	1,032	,4305	,1586	,0321	,0065
$1,995 \cdot 10^{-02}$	1,220	1,758	2,143	2,338	2,340	2,018	1,520	1,057	,4460	,1661	,0339	,0069
$2,512 \cdot 10^{-02}$	1,185	1,725	2,117	2,327	2,343	2,040	1,542	1,075	,4615	,1652	,0357	,0072
$3,162 \cdot 10^{-02}$	1,151	1,695	2,094	2,320	2,353	2,071	1,570	1,100	,4761	,1656	,0368	,0074
$3,981 \cdot 10^{-02}$	1,114	1,663	2,073	2,313	2,366	2,108	1,602	1,144	,4901	,1698	,0375	,0075
$5,012 \cdot 10^{-02}$	1,077	1,630	2,053	2,307	2,379	2,144	1,644	1,188	,5042	,1790	,0382	,0077
$6,310 \cdot 10^{-02}$	1,040	1,597	2,032	2,300	2,392	2,181	1,704	1,232	,5182	,1973	,0389	,0078
$7,943 \cdot 10^{-02}$	,9994	1,558	2,006	2,292	2,407	2,228	1,770	1,287	,5437	,2164	,0420	,0081
$1,000 \cdot 10^{-01}$	,9548	1,512	1,973	2,282	2,424	2,284	1,843	1,355	,5838	,2348	,0477	,0087
$1,259 \cdot 10^{-01}$	,9112	1,467	1,940	2,273	2,440	2,341	1,916	1,422	,6391	,2455	,0534	,0097
$1,585 \cdot 10^{-01}$	,8625	1,415	1,903	2,258	2,455	2,403	2,001	1,509	,7055	,2672	,0598	,0112
$1,995 \cdot 10^{-01}$	,8065	1,354	1,860	2,238	2,468	2,472	2,104	1,622	,7835	,3054	,0672	,0131
$2,512 \cdot 10^{-01}$	,7497	1,291	1,813	2,213	2,476	2,540	2,212	1,739	,8666	,3483	,0764	,0157
$3,162 \cdot 10^{-01}$	,6885	1,215	1,741	2,163	2,458	2,601	2,345	1,879	,9774	,4154	,0960	,0216
$3,981 \cdot 10^{-01}$	,6266	1,137	1,664	2,109	2,430	2,649	2,477	2,020	1,089	,4875	,1175	,0280
$5,012 \cdot 10^{-01}$	,5611	1,046	1,566	2,029	2,376	2,681	2,560	2,156	1,214	,5938	,1508	,0347
$6,310 \cdot 10^{-01}$	,4947	,9473	1,450	1,921	2,291	2,688	2,628	2,290	1,376	,7151	,1991	,0487
$7,943 \cdot 10^{-01}$	,4292	,8477	1,324	1,796	2,168	2,644	2,685	2,415	1,566	,8455	,2641	,0703
$1,000 \cdot 10^{+00}$	,3659	,7478	1,198	1,667	2,046	2,576	2,707	2,520	1,771	1,035	,3711	,1121
$1,259 \cdot 10^{+00}$	,3152	,6490	1,070	1,511	1,908	2,488	2,703	2,617	1,949	1,220	,4963	,1683
$1,585 \cdot 10^{+00}$	,2668	,5587	,9349	1,343	1,727	2,345	2,635	2,669	2,110	1,427	,6505	,2543
$1,995 \cdot 10^{+00}$	,2183	,4689	,8000	1,168	1,544	2,163	2,528	2,594	2,262	1,595	,7986	,3673
$2,512 \cdot 10^{+00}$	,1724	,3829	,6693	1,007	1,359	1,957	2,354	2,486	2,313	1,757	,9871	,4991
$3,162 \cdot 10^{+00}$	,1402	,3172	,5624	,8345	1,171	1,691	2,145	2,259	2,253	1,754	1,059	,6652
$3,981 \cdot 10^{+00}$	,1102	,2547	,4591	,6950	,9812	1,467	1,895	2,085	2,116	1,820	1,185	,8366
$5,012 \cdot 10^{+00}$	,0820	,1967	,3628	,5653	,8025	1,267	1,673	1,951	2,100	1,956	1,467	1,007
$6,310 \cdot 10^{+00}$	,0647	,1643	,3062	,4680	,6848	1,061	1,439	1,772	1,925	1,976	1,600	1,188
$7,943 \cdot 10^{+00}$	,0491	,1360	,2560	,3495	,5769	,8736	1,199	1,450	1,716	1,770	1,544	1,237
$1,000 \cdot 10^{+01}$	,0348	,1078	,2059	,2682	,4690	,7335	,9637	1,198	1,497	1,600	1,510	1,269
$1,259 \cdot 10^{+01}$	,0281	,0795	,1557	,2254	,3612	,5957	,8079	1,021	1,312	1,434	1,404	1,228
$1,585 \cdot 10^{+01}$	,0228	,0562	,1124	,1819	,2677	,4660	,6631	,8500	1,120	1,261	1,286	1,191
$1,995 \cdot 10^{+01}$	,0177	,0427	,0840	,1401	,2046	,3540	,5258	,6806	,9156	1,051	1,097	1,089
$2,000 \cdot 10^{+01}$	,0177	,0426	,0837	,1397	,2039	,3528	,5244	,6789	,9134	1,049	1,095	1,088

PTB-Berichte der Serie N (Neutronenphysik)

N-1: G. Börker, R. Böttger, H. J. Brede, H. Klein u. a.:
Elastic and Inelastic Differential Neutron Scattering Cross Sections of Oxygen between 6 and 15 MeV.
120 S., 6 Abb., 57 Tab., ISBN 3-88314-906-3, 1989, DM 32,50

N-2: B. W. Bauer, W. G. Alberts, M. Luszig-Bhardra, B. R. L. Siebert:
Experimental Investigation into the Influence of Neutron Energy, Angle of Incidence and Phantom Shape on the Response of Individual Neutron Dosemeters: Detailed Analysis of Results for the Albedo Neutron Dosemeter in Use at the PTB.
54 S., 21 Abb., ISBN 3-89429-005-6, 1990, DM 20,50

N-3: H. Schumny:
Personal Computers for Data Acquisition and Measurement, Standards interfaces, State of the Art, Trends, Applications.
66 S., 24 Abb., 5 Tab., ISBN 3-89429-009-9, 1990, DM 23,50

N-4: D. R. Schlegel-Bickmann, H. J. Brede, S. Guldbakke u. a.:
Measurement of k_U-Values of Argon-Filled Magnesium Ionisation Chambers.
76 S., zahlr. Tab., ISBN 3-89429-063-3, 1990, DM 26,00

N-5: B. W. Bauer, B. R. L. Siebert, W. G. Alberts u. a.:
Experimental Investigation into the Influence of Neutron Energy, Angle of Incidence and Phantom Shape on the Response of Individual Neutron Dosemeters: Experimental Procedure and Summary of Results.
36 S., 5 Abb., 10 Tab., ISBN 3-89429-072-2, 1990, DM 17,00

N-6: B. R. L. Siebert, W. G. Alberts, B. W. Bauer:
Computational Study of Phantoms for Individual Neutron Dosimetry.
40 S., 20 Abb., 10 Tab., ISBN 3-89429-075-7, 1990, DM 17,50

N-7: D. Schmidt, R. Böttger, H. Klein, R. Nolte:
Investigation of the ^{9}Be(a, n) ^{12}C Reaction.
I: Experimental Procedure and Uncertainties.
42 S., 22 Abb., ISBN 3-89429-176-1, 1992, DM 20,00

N-8: D. Schmidt, R. Böttger, H. Klein, R. Nolte:
Investigation of the ^{9}Be(a, n) ^{12}C Reaction.
II. Differential Cross Sections for E_a = 7.02 - 15.70 MeV and $E_{ex}(^{12}C)$ = 0.0, 4.439, 7.654, 9.641, 10.84, 11.83 and 12.71 MeV.
96 S., 44 Abb., 3 Tab., ISBN 3-89429-177-X, 1992, DM 32,00

N-9: R. Nolte, H. Schuhmacher, H. J. Brede, U. J. Schrewe:
Neutron Spectrometry with Liquid Scintillation Detectors at Neutron Energies between 20 MeV and 70 MeV: A Status Report.
58 S., 17 Abb., ISBN 3-89429-328-4, 1993, DM 23,50

N-10: W. G. Alberts (Hrsg.):
Investigation of Individual Neutron Monitors on the Basis of Etched-track Detectors: The 1990 EURADOS-CENDOS Exercise.
136 S., ISBN 3-89429-198-2, 1992, DM 36,00

N-11: K. Weise, W. Wöger:
Eine Bayessche Theorie der Meßunsicherheit.
34 S., ISBN 3-89429-227-X, 1992, DM 18,50

N-12: R. A. Hollnagel:
Comparison of the Effective Dose, E, and the Effective Dose Equivalent, H_E, from Neutron Irradiation with Special Regard to the Dose from Induced Photons.
54 S., 15 Abb., ISBN 3-89429-261-X, 1992, DM 22,50

N-13: H. Schuhmacher, U. J. Schrewe:
Dose Equivalent Measurements on Board Civil Aircraft.
42 S., 14 Abb., 5 Tab., ISBN 3-89429-306-3, 1993, DM 20,00

N-14: D. Schmidt, B. R. L. Siebert:
Monte Carlo Simulation of Fast Neutron Scattering Experiments Including DD-Breakup Neutrons.
48 S., 34 Abb., ISBN 3-89429-332-2, 1993, DM 22,50

N-15: W. G. Alberts, H. Kluge:
PTB-Vergleichsmessungen an Personendosimetern für Neutronenstrahlung.
40 S., 28 Abb., 12 Tab., ISBN 3-89429-352-7, 1993, DM 20,50

N-16: M. Weyrauch, K. Weise:
Untersuchung der Unsicherheiten bei der Messung mit Thermolumineszenz-Dosimetern.
28 S., 3 Abb., ISBN 3-89429-374-8, 1993, DM 18,00

N-17: P. Mikula, V. Wagner, R. Scherm:
On the focusing in neutron diffraction by elastically bent perfect crystals.
34 S., 13 Abb., ISBN 3-89429-478-7, 1994, DM 19,50

N-18: D. Schmidt, Xia Haihong:
Neutron Production by Deuteron Breakup on ^{4}He.
ca. 39 S., 15 Abb., 2 Tab., ISBN 3-89429-536-8, 1994, ca. DM 20,50

N-19: M. Matzke:
Unfolding of Pulse Height Spectra: The HEPRO Program System.
ca. 73 S., ISBN 3-89429-543-0, 1994, ca. DM 28,00

N-20: D. Schmidt, W. Mannhart, H. Klein, R. Nolte:
Neutron Scattering on Natural Iron at Incident Energies between 9.4 and 15.2 MeV.
ca. 157 S., zahlr. Abb. und Tab., ISBN 3-89429-552-X, 1994, ca. DM 40,00

N-21: B. Wiegel, A. V. Alevra, B. R. L. Siebert:
Calculations of the Response Functions of Bonner Spheres with a Spherical ^{3}He Proportional Counter Using a Realistic Detector Model.
ca. 92 S., zahlr. Abb., ISBN 3-89429-563-5, 1994, ca. DM 31,00